Monitoring a Shallow Gasoline Release using GPR at CFB Borden

by

Cameron Hugh McNaughton

A thesis
presented to the University of Waterloo
in fulfillment of the
thesis requirement for the degree of
Master of Science
in
Earth Sciences

Waterloo, Ontario, Canada, 2011

Author's Declaration

I hereby declare that I am the sole author of this thesis. This is a true copy of the thesis, including any required final revisions, as accepted by my examiners.

I understand that my thesis may be made electronically available to the public.

Cameron H. McNaughton

Abstract

This hydrogeophysical field experiment evaluated the ability of high frequency (450 & 900 MHz) ground penetrating radar (GPR) to characterize the release of gasoline over an annual cycle of in situ conditions. In August 2008, 200 liters of E10 gasoline were released into the unconfined sand aquifer at CFB Borden. The 900 MHz profiling clearly shows the development of shallow (i.e., above 10 ns) high reflectivity in the vicinity of the trench immediately after the release. Additional lateral extension of high reflectivity zone was observed over the following 20 days until the seasonal water table low stand occurred, after which no further lateral movement was observed. Throughout the remainder of the monitoring, the 900 MHz profiling observed a long-term dimming of reflectivity at the periphery of the impacted zone.

While direct imaging of the shallow impacted zone by the 450 MHz antennas was significantly obscured by the superposition with the direct air-ground wave arrival; its improved depth of penetration allowed the measurement of a velocity "pull-up" of an underlying stratigraphic interface resulting from the displacement of low velocity water by high velocity gasoline. The maximum pull-up was observed during the water table low stand. The ongoing changes in the pull-up magnitude during the remainder of the observation period suggest the continued redistribution of fluids in the impacted zone.

Because of the shallow depth of the gasoline impacted zone, the effects of freezing during the winter period were observed in the GPR imaging. The presence of the gasoline impacted zone appears to have affected the depth of freezing, causing a depression of the frozen soil base. The dimming of the direct air-ground wave complex indicates that the contaminant phase brought to the surface by the water table fluctuations have impacted the nature of the near-surface freezing.

Acknowledgements

To all my friends and family, you have helped beyond measure. Hopefully I will be able to return the favour in some capacity in the future.

I would especially like to thank my supervisor Tony Endres for his guidance and support over the course of my master's studies and developing this thesis further. I would like to thank Jim Barker and Juliana Freitas for the opportunity to work on their fascinating project. Juliana, you were instrumental in organizing field work days and provided excellent insight for all the questions I threw at you! I would like to thank my committee members, Jim Barker and Jon Paul Jones, for their patience in completing this thesis and constructive comments.

The following people assisted with field work: Colby Steelman, Melissa Bunn, John Mosquera, Juliana Freitas, Jon Rigg, Cameron Toy, Daniel Gardner, Colin McCarter, Reynold Chow, Ben Doulatyari, Bobby Katanchi and Neelmoy Biswas. Special mentions to Adam Vasey, Colby Steelman, Melissa Bunn and Nick Bishop for help with edits and improving the various draft versions. Thanks to Sue Fisher and Trevor Clews for helping through the final stretch.

Any thesis from the Earth and Environmental Sciences would not be complete without thanking Bob Ingleton and Paul Johnson for all their help. They have assisted me throughout my graduate and undergraduate studies including constructing the shelter over the experimental cell for this project. I have learned a great deal from both of them throughout my time at Waterloo and have realized that their expertise and ingenuity is truly unparalleled.

To my parents Tom and Rena for their unwavering love and support throughout my entire life. To Colin and Krista, thanks for holding me to who I am. To Graham and Elisa for your kindness and encouragement in all my endeavours. Gemma, thank you for energizing me throughout the process! Of course, to my Grandma Vinke and Grandma Doris for a wonderful foundation from which to build.

To the real driving force behind everything that makes me who I am, Ilana, I am so fortunate that you found me and I am truly the lucky one.

Table of Contents

List of Figures

List of Tables

1.0 Introduction

Ground penetrating radar (GPR) can be utilized to characterize sites containing immiscible non-aqueous phase liquid (NAPL) contamination by detecting changes in traveltime and amplitude caused by the presence of the NAPL. NAPLs released into the environment are a well documented problem because of their potential impact on water resources. NAPL solubilities are generally considered low, but are still a concern given the minimal NAPL concentrations needed to impact water quality (e.g. 5 μg/L US EPA MCL for benzene a common gasoline component). Conventional hydrogeological site investigation techniques (e.g. well installations, soil/rock coring, water samples, soil samples, etc.) offer point measurements that are expensive, disruptive to existing site conditions and may re-mobilize contaminants. Further, the information obtained from these techniques can be problematic to infer subsurface properties across a site where the stratigraphy, heterogeneity, depth to water table or groundwater chemistry may change. In comparison, GPR can produce non-invasive high resolution images of the subsurface; hence, GPR is able to preserve subsurface conditions. Further, GPR surveys are relatively inexpensive compared to other techniques. This geophysical method has the capacity to provide high resolution, spatially continuous images of the subsurface over extensive spatial areas.

1.1 Motivation

The purpose of this research is to assess the ability of GPR to characterize light non-aqueous phase liquid (LNAPL) releases in the subsurface. GPR can be utilized to gather information on site stratigraphy and delineate LNAPL pool boundaries. Using GPR to delineate free phase LNAPL pools in the subsurface will enhance conventional monitoring techniques and remediation of LNAPL at contaminated sites by directing resources and monitoring efforts to impacted areas.

1.2 Objectives

The goal of this thesis is to assess the ability of high frequency (i.e., 450 MHz and 900 MHz) ground penetrating radar to characterize LNAPL releases in the very shallow subsurface. To

attain this goal, this thesis examines the use of GPR for monitoring a shallow LNAPL release at Canadian Forces Base (CFB) Borden. Figure 1.1 schematically illustrates the potential complexity of the fluid distributions in such a zone. It was anticipated that GPR would provide spatial and temporal information about the location and quantity of a NAPL in the subsurface. Specific objectives for this thesis are:

i) Observe spatial variabilty in GPR response during controlled LNAPL release to characterize lateral spreading of the LNAPL.

ii) Use traveltime data to estimate the thickness of gasoline impacted zone.

iii) Determine if amplitude changes during evolution of LNAPL release occur in a discernable or predictable pattern.

iv) Examine the effect of natural processes (i.e. water content variations due to fluctuating water table and winter freeze / spring thaw) on the GPR response from the free phase LNAPL.

1.3 Scope

Work presented in this thesis, concerning the use of GPR for monitoring LNAPL releases in the subsurface, is a part of a larger research project conducted by Freitas (2009) to study a near surface controlled gasoline release. GPR was used to identify the spatial and temporal effects on a controlled LNAPL release subjected to natural processes and natural hydraulic gradients. The motivation behind Freitas' (2009) research is based on the current North American transportation fuel distribution system (refineries, piping, storage tanks, refueling stations, etc.) which uses petroleum hydrocarbons (i.e. gasoline) as the main energy source. A portion of ethanol is blended with the gasoline in the distribution system, gasoline blended with < 5% ethanol was mandated in the province of Ontario, Canada, under Ontario Regulation 535/05 in 2007. Gasoline is amended with ethanol (oxygenate) to improve engine combustion and replace MTBE (oxygenate). MTBE is considerably more toxic compared to ethanol; both are highly mobile in the subsurface (Freitas 2009). Due to leaks and spills, gasoline can accumulate in the subsurface below distribution facilities which can pose a threat to groundwater aquifers with drinking water quality and impact environmental and human health.

If the existing petroleum hydrocarbon system is modified to contain higher blends of ethanol, subsequent leaks and spills will interact with existing petroleum hydrocarbons causing complicated issues with co-solvency and re-mobilization of contaminants (Freitas 2009).

The scope of this thesis is to monitor an initial controlled gasoline release using GPR. Further work is ongoing which investigates the effects of ethanol on the initial gasoline release.

1.4 Detection of Subsurface Immiscible Fluids by Geophysical Methods

Immiscible NAPLs are classified into two categories on the basis of their densities, Dense non-aqueous phase liquids (DNAPLs) have a densities greater than water (ρ_{water} = 1.0 g/cm^3) while light non-aqueous phase liquids (LNAPLs) have a densities less than water.

The relative densities of these two NAPL categories lead to contrasting behaviours when they are released into the subsurface. Specifically, DNAPLs sink through water saturated porous media while LNAPLs float on the water saturated zone due to buoyancy effects (Fetter 1993; Schwartz and Zhang 2003). Downward migrating DNAPL, below the water table, tends to pool on boundaries where a contrast in permeability exists. LNAPLs tend to migrate through the unsaturated zone downward until the saturated zone is reached and "float" on the water table. As the water table fluctuates, a 'smeared zone' is created where air, water, LNAPL and the LNAPL vapour are all potentially present within the pore space.

Because of the large contrast in the electrical and other physical properties between contaminants and water, a number of geophysical techniques respond to the presence of NAPLs when it displaces water. Ground penetrating radar (GPR), DC resistivity, self potential (SP), induced polarization (IP) and other electro-magnetic (EM) induction methods have all been used for the detection of NAPLs in the subsurface (Knight 2001; Che-Alota et al. 2009; Atekwana et al. 2000; Brewster et al. 1995; Abdel Aal et al. 2006; Naudet et al. 2004). GPR has the distinct advantage in that it is capable of providing high resolution spatial imaging of the subsurface.

1.5 Use of Ground Penetrating Radar to Detect Subsurface Immiscible Fluids

Brewster et al. (1995) demonstrated the ability of GPR to image DNAPL pools on lower hydraulic conductivity stratigraphic boundaries in the well known Borden 9 m x 9 m cell controlled DNAPL release experiment using 770 L of chlorinated solvent. Hwang et al. (2008) used GPR to detect a small volume release (50 L) of DNAPL injected in the unconfined aquifer at CFB Borden and observed the pool evolution over 5 years due to the natural groundwater flow regime. Reflectivity of the DNAPL was distinct and diminished with time due to dissolution of the DNAPL mass (Hwang 2006, Hwang et al. 2008).

There have been several controlled experiments in sand packed tanks to demonstrate the ability of GPR to detect the presence of LNAPL (Redman et al. 1994; DeRyck 1994; Daniels et al. 1995; Kim et al. 2000; Bano et al. 2009). Redman et al. (1994), DeRyck (1994) and Kim et al. (2000) observed a velocity increase in the GPR profile during a controlled tank experiments. In particular, DeRyck (1994) released LNAPL into a large polyethylene tank filled with Borden sand. Using a tank filled with sand and clean water, a reflection from the bottom of the tank was observed in the GPR profiling. After the LNAPL was released into the tank, the traveltime of this bottom reflection decreased as a result of the increased velocity. This effect is referred to as a "velocity pull-up". Daniels et al. (1995) examined changes in the reflection amplitude observed in GPR profiling to detect buried containers packed with mixtures of varying proportions of air, water, sand and LNAPL. Daniels et al. (1995) showed that GPR was able to detect containers filled with LNAPL better than containers filled with sand. Both DeRyck (1994) and Daniels et al. (1995) were able to estimate, in controlled settings, the LNAPL pooled thickness from GPR reflections.

Previous field studies where GPR was used to characterize LNAPL impacted zones under natural condition have been as a result of accidental releases (Bermejo et al. 1997; Sauck et al. 1998; Atekwana et al. 2000; Orlando 2002; Lopes de Castro and Branco 2003; Jordan et al. 2004). What sets this study apart is the design of the control structure that allows natural processes to influence the evolution of the released LNAPL. The cell is open on each end to permit groundwater flow through the cell under natural hydraulic gradient. In addition, the cell

temperature was allowed to naturally vary, which permitted the season freeze and thaw porecesses to occur. We anticipated that changes in the GPR signature of the LNAPL impacted zone would happen when subjected to these natural processes. Another unique component was the known mass of LNAPL; this is not the case with field studies covering accidental releases.

Recently, it has been well established that geoelectric properties of mature NAPL impacted zones change over time due to biodegradation (Atekwana and Atekwana, 2009; Atekwana and Slater, 2009). As such, mature LNAPL releases have a different GPR response compared to a fresh release (Bermejo et al. 1997; Sauck et al. 1998; Atekwana et al. 2000; Werkema et al. 2003; Cassidy 2007, Che-Alota et al. 2009;). For this thesis, the relatively recent release of LNAPL had not allowed microbial communities time to become established and to degrade a sufficient mass of hydrocarbons to alter the GPR response. While Freitas (2009) had observed ethanol biodegradation byproducts at the study site in low concentrations, the influence of LNAPL biodegradation effects on GPR has been considered negligible for this study.

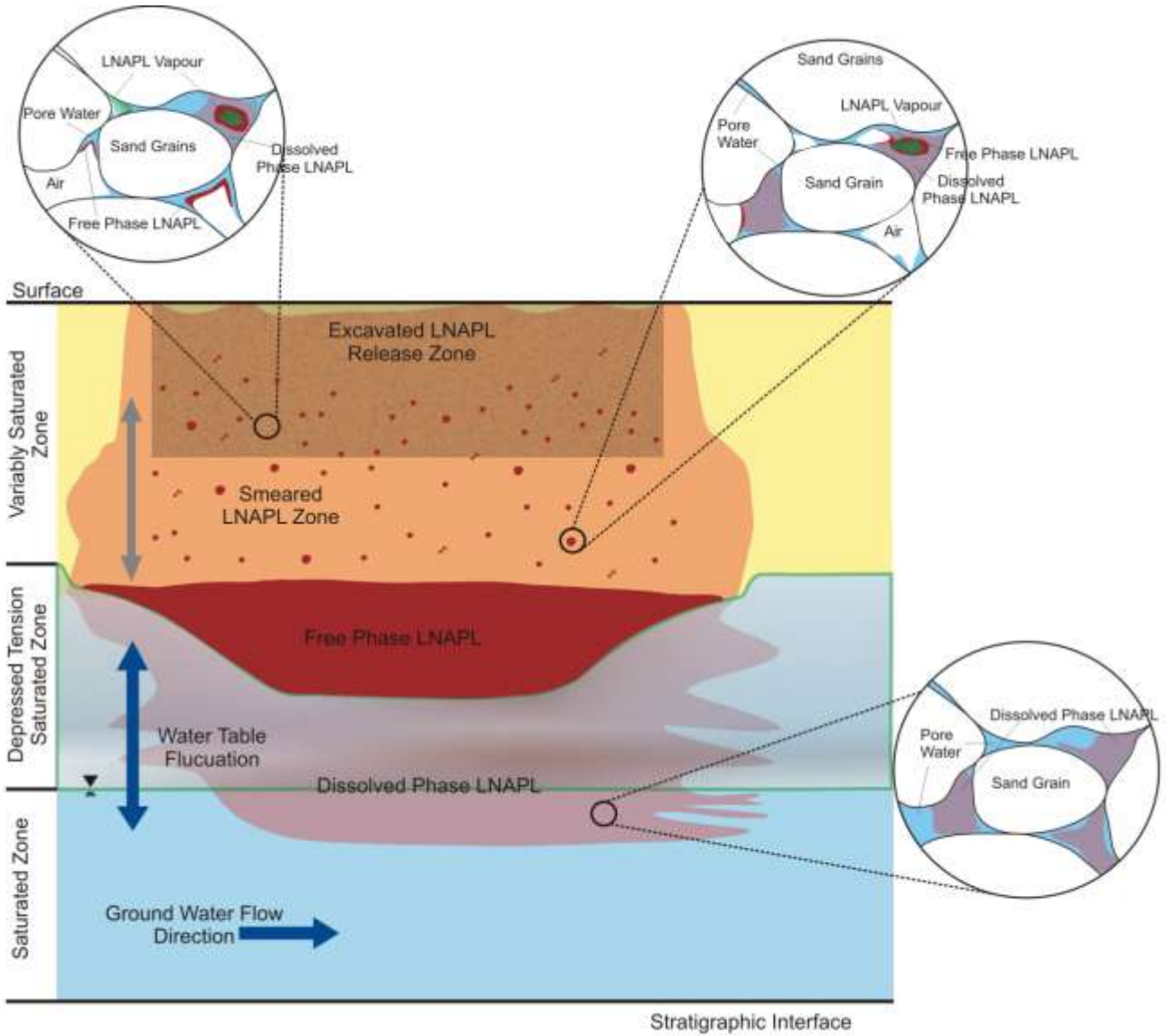

Figure 1.1– Schematic of LNAPL (gasoline) release at CFB Borden.

2.0 Ground Penetrating Radar and Associated Petrophysical Background

This section presents a brief introduction to the physical principles governing the use of GPR. Thorough discussions on GPR theory and applications are found in the following publications: Daniels (2004), Annan (2005a, 2005b and 2009). An overview of the use of GPR for contaminant detection is given by Redman (2009).

2.1 Ground Penetrating Radar Theory Fundamentals

Ground penetrating radar takes advantage of contrasts in electromagnetic (EM) wave propagation properties of subsurface porous media to produce high resolution images of the surveyed area. GPR emits a high frequency electromagnetic (EM) pulse that propagates into the subsurface from a transmitting antenna and reflected back to a receiving antenna where the signal is recorded. The propagation of this EM pulse is controlled by electrical properties (i.e., electrical conductivity, dielectric permittivity and magnetic permeability) of the subsurface. These propagation effects are manifested in two ways. First, the EM wave velocity is a function of the electrical properties, determining the traveltime for a pulse to propagate through a material. Second, the energy of an incident EM pulse is partitioned into reflected and transmitted pulses when it encounters at interface between materials with differing electrical properties; the magnitude of the electrical property contrast across this boundary controls the partitioning process.

The dielectric permittivity ε [units of Farads per metre (F/m)] of a medium describes its ability to polarize in the presence of an EM field. For convenience, the dielectric properties of geological materials are commonly expressed in terms a normalized quantity called relative dielectric permittivity κ defined as

$$\kappa = \frac{\varepsilon}{\varepsilon_0} \qquad (1)$$

where is the dielectric permittivity of a vacuum (= 8.85418 × 10^{-12} F/m). Typical κ values for geological materials can be found in Table 2.1.

The velocity of the GPR electromagnetic pulse is given by

—= (2)

where μ is the magnetic permittivity the medium in Henry per metre (H/m). The magnetic permittivity μ is generally assumed to be approximately equal in value to its value in free space (μ_O = 4 × 10^{-7} H/m) for most near surface applications due to the negligible amount of magnetic material present. Using this assumption, Equation (2) can be expressed as

—= (3)

where c = 0.3 m/ns is the EM wave velocity in a vacuum.

Given this assumption concerning magnetic permeability, contrasts in κ for adjacent materials at an interface determines the partitioning of energy during the reflection of an EM pulse. This partition is described by the reflection coefficient *R* which is the ratio between the amplitudes of the reflected and incident pulses (A_R and A_I, respectively):

— (4)

For this discussion, we will assume that the interface is horizontal and planar. In addition, we can assume that incident EM pulse is traveling toward the interface in medium #1 with

dielectric permittivity κ_1; medium #2 with dielectric permittivity κ_2 is below the interface (Figure 2.1). The value of R is also dependent on the direction of the EM pulse is propagating relative to the interface; this direction is described in terms of the incident angle . For the normal incidence case (i.e.,) where the pulse is traveling perpendicular to the interface, the reflection coefficient is given by

(5)

From this equation it can be seen that as the difference between κ values increases for adjoining materials the larger the amount of EM energy will be reflected.

For non-normal incidence pulses (i.e.,), the value of R is also dependent on the orientations of the electric and magnetic field components of the EM pulse. The following versions of R for differing electric and magnetic field orientation are given by Annan (2005a). The reflection coefficient perpendicular is given by

(6)

whereas the reflection coefficient parallel $R_{\parallel}$ is defined as

(7)

where and are the angle of the incident EM wave and the angle of the transmitted EM wave, respectively. These angles are related by Snell's Law:

(8)

where v_1 and v_2 are the EM wave velocities in Medium #1 and #2, respectively. The expressions for and $R_{\parallel}$ are commonly referred to as the Fresnel's equations.

From the Fresnel's equations, it can be seen that the amplitude of reflected waves are dependent on the incident angle and the contrasts in electrical properties between the two media (Baker 1998). A GPR technique that is based on these dependencies is called amplitude variation with offset (AVO). The AVO technique uses reflection coefficients to constrain properties of the media at a given interface and can potentially be used to discriminate NAPL in the subsurface from changes in stratigraphy. Discussion about the application of AVO technique to GPR data for NAPL detection can be found in Baker (1998), Jordan and Baker (2004) and Jordan et al. (2004).

2.1.1 Constant offset profiling

The most commonly used imaging technique is constant offset profiling; this technique is illustrated in Figure 2.2. The constant offset profiles are conducted with the transmitting antenna (transmitter) and the receiving antenna (receiver) fixed at a constant separation or offset distance. This transmitter-receiver array is moved along the profile line at a uniform step size between sounding locations. Each sounding is repeated multiple times and stacked in time in order to suppress random noise; this procedure produces a single composite trace for each sounding location.

Each time the transmitter and receiver are moved a new trace is recorded. All the traces plotted together produce an image of the subsurface. A trace is plotted as the two-way travel time (ns) for the EM pulse versus position (m) of the centre point of the transmitter-receiver array. Profile surveys are used to generate a 2D image of the subsurface showing locations of prominent reflecting interfaces. To determine the depth to these interfaces, a second survey type called a common mid-point sounding is used to obtain subsurface velocity information.

2.1.2 Common Mid-Point (CMP) Sounding

The common mid-point (CMP) sounding is a multi-offset survey that that is performed to obtain subsurface EM wave velocity information. A schematic diagram of this procedure is show in Figure 2.3. It is performed by placing the transmitter and the receiver in close proximity and then increasing the offset distance by simultaneously moving both antennae apart from a fixed midpoint position. This movement is done using a fixed step size, and a trace is obtained for each step.

CMP surveys gather information about subsurface EM wave velocity from the systematic variation in reflection event traveltimes as the offset distance changes. Velocity estimates are performed by a normal moveout (NMO) analysis of reflection events (Yilmaz 2001). NMO analysis is based on the hyperbolic nature of traveltime-offset relationship for reflection events which is given by

—— (9)

where = traveltime at offset distance x, = zero offset traveltime (i.e., $x = 0$) and = apparent (or NMO) velocity for the reflection.

It can be shown that is equivalent to the root-mean-square (RMS) average velocity of the material between the surface and the reflecting boundary. The NMO velocity is then used to estimate depths from two-way traveltime data.

For a CMP survey, the antennas may be oriented perpendicular or parallel to the survey line or strike of subsurface features (Figure 2.4). In the geophysical literature, the terms broadside or perpendicular broadside are used for perpendicular orientation (Figure 2.5) and the terms end-fire or parallel end-fire are used to describe parallel orientation (Baker and Jordan 2003, Baker et al. 2007). Each orientation corresponds to one of the polarizations used the Frensel

equations (i.e., perpendicular orientation corresponds to and parallel orientation corresponds to $R_{\parallel}$).

2.2 Ground Penetrating Radar Survey Considerations

When designing a GPR survey, there are three significant considerations for utilizing the GPR technique (Davis and Annan 1989; Knight 2001). The first is the amount of attenuation of the EM pulse that is given by Davis and Annan (1989) as

(10)

where α is the attenuation constant in dB/m and σ is the conductivity of the medium in mS/m. The value of α describes the ability of a medium to transmit an EM pulse. As the conductivity of an earth material increases the attenuation of the EM pulse grows. Clay is an electrically conductive material; hence, it is not well suited for GPR surveys. Knight (2001) states that GPR surveys are best conducted in sands and gravels with <5% clay. The Borden aquifer has a clay fraction of 0.4% (Mocanu 2007) which provides a medium with negligible attenuation due to clay and is well suited for GPR.

The second consideration is commonly known as the depth of investigation vs. resolution, as described by Davis and Annan (1989). Resolution is the ability to distinguish between two closely spaced objects, increasing the resolution of a GPR survey allows thinner layers to be detected. Two events are considered distinctly resolvable if the events are separated by half the EM wave's half width (Annan 2005a). The resolution criteria or Fresnel wavelength conditions for differentiating two wavelets is given by Annan (2005a) as

(11)

where Δr = range resolution length (m), W = ¼ of wavelength at half of maximum amplitude (m) and v =EM wave velocity of the subsurface.

To increase resolution, you must increase the frequency at which the EM pulse is generated. Higher frequency pulses have shorter wavelengths and can be image smaller subsurface features (e.g. finely interbedded sand and silt or a perched water table). However, attenuation mechanisms preferentially affect higher frequency components, causing high frequency EM pulses to be attenuated more rapidly in the near surface. To increase the depth of investigation longer wavelengths which correspond to lower frequency EM pulses are required. However, these longer duration pulses are unable to resolve the finer details of the subsurface. Given the shallow depth of investigation needed within the experimental cell (i.e., within the 2-3 metres nearest the surface), higher frequencies can be used to achieve high resolution and while maintaining sufficient depth of investigation.

The third consideration illustrated by Davis and Annan (1989) is the amount of noise generated by electrical transmission wires and other anthropogenic sources. The GPR system used in this investigation has shielded antennas which will eliminate or reduce potential noise. Given these three considerations, the shallow Borden aquifer is considered a suitable geological medium for GPR methods.

2.3 Dielectric Properties of Clean and Contaminated Aquifer Material

The electrical properties of near surface materials are dependent on electrical properties of their components (e.g., air, water and solid grains), as well as the relative abundance of these components in the system (e.g., porosity, degree of water saturation) (Davis and Annan 1989). Aquifer constituents have varying values of the relative dielectric permittivities, κ. Air has a $\kappa = 1$ which allows the GPR signal, EM pulse, to travel at near the speed of light in a vacuum. Clean sands, gravels and ice generally have low $\kappa \leq 8$ while silts and clays have intermediate κ values from 5 to 40. Water has a high $\kappa \approx 80$ which produces a low EM wave velocity. NAPL contaminants generally have low $\kappa \leq 5$; therefore, if NAPL is present in an aquifer and displaces water, there could be a significant increase in the EM wave velocity.

A wide spectrum of volumetric mixing formulae have been used to analyse the bulk dielectric properties of heterogeneous soils in terms of the volumetric content and dielectric permittivities of their distinct components (Brovelli and Cassiani 2008). A widely used version is the Complex Refractive Index (CRI) model (e.g., Roth et. al., 1990) which is based on the assumption the total traveltime for an EM pulse through a composite material is equivalent to the sum of traveltimes through each constituent. Hence, the CRI model for a three phase system of solids, water and air representing the uncontaminated aquifer material is given by

(12)

where = bulk dielectric permittivity, = dielectric permittivity of water, = dielectric permittivity of air, = dielectric permittivity of soild grains, = porosity [m^3 / m^3] and is the water saturation [m^3 / m^3]. For the gasoline impacted material, the CRI model is a four phase system of solids, water, air and NAPL describe as follows:

– (13)

where = dielectric permittivity of NAPL and = NAPL saturation [m^3 / m^3].

The values used to evaluate the CRI model are found in Table 2.2. Groundwater temperature at Borden within 1 – 2 mbgs fluctuates seasonally; therefore, = 82 was chosen to account for the temperature dependence on . The bulk dielectric permittivity from the CRI model is directly related to the relative dielectric permittivity introduced in Equation 2.

Using the principles that were used to obtain the CRI, a CRI based model can be derived for quantifying the NAPL present at the top of the variably-saturated zone. The total travel time *T* for a normal incidence GPR pulse to travel through a completely saturated sand aquifer composed of three phases; solids, water and NAPL depicted in Figure 2.6 as Zone 1 is

(14)

The total travel time $T^{'}$ for the clean two phase, sand and water, Zone 2 is

(15)

Therefore, the change in travel time between the contaminated Zone 1 and the clean Zone 2 is given by

(16)

Using physical parameters of the Borden aquifer in Table 2.2, Equation (3) is used to calculate the velocity for v_w and v_{NAPL}. Therefore, the weighted average based on the proportion of aquifer materials in the model yields

(17)

The average velocity can be multiplied by the estimated two-way traveltime through the pool of NAPL. Finally, the effective thickness of the gasoline in the variably-saturated zone can be approximated using

(18)

In Section 5.4, the CRI model described above is evaluated using Borden values and incorporating observed values from this study into the model.

Table 2.1 – Typical relative dielectric permittivity of materials.

Material	**Relative dielectric permittivity (κ)**	**Reference**
Air	1	Davis and Annan (1989)
Ice	3 – 4	Davis and Annan (1989)
Water (at 25^{o}C)	80	Davis and Annan (1989)
Water (at 0^{o}C)	88	van Loon et al. (1991)
Dry sand	3 – 5	Davis and Annan (1989)
Wet sand	20 – 30	Davis and Annan (1989)
Petroleum (LNAPL)	2.07 – 2.14	Telford et al. (1976)
Tetrachloroethylene (DNAPL)	2.3	Brewster and Annan (1994)

Table 2.2 – Borden sand and aquifer parameters used to evaluate CRIM.

Parameter	Value	Source
Dielectric permittivty of water,	82	Weast et al. (1985)
Dielectric permittivty of dry sand,	5	Weast et al. (1985)
Complex Refractive Index Model fitting parameter,	0.5	Brovelli and Cassiani (2008)
Porosity of Borden Sand,	0.33	MacKay et al. (1986)
Layer 1 – Borden sand + LNAPL		
Dielectric permittivty of gasoline (LNAPL),	2.1	Telford et al. (1976)
Residual water saturation of Borden sand,	0.06	Nwankwor (1985)
Layer 2 – Clean Borden sand		
Dielectric permittivty of air,	1	Weast et al. (1985)
Complete water saturation of Borden sand,	0.33	MacKay et al. (1986)

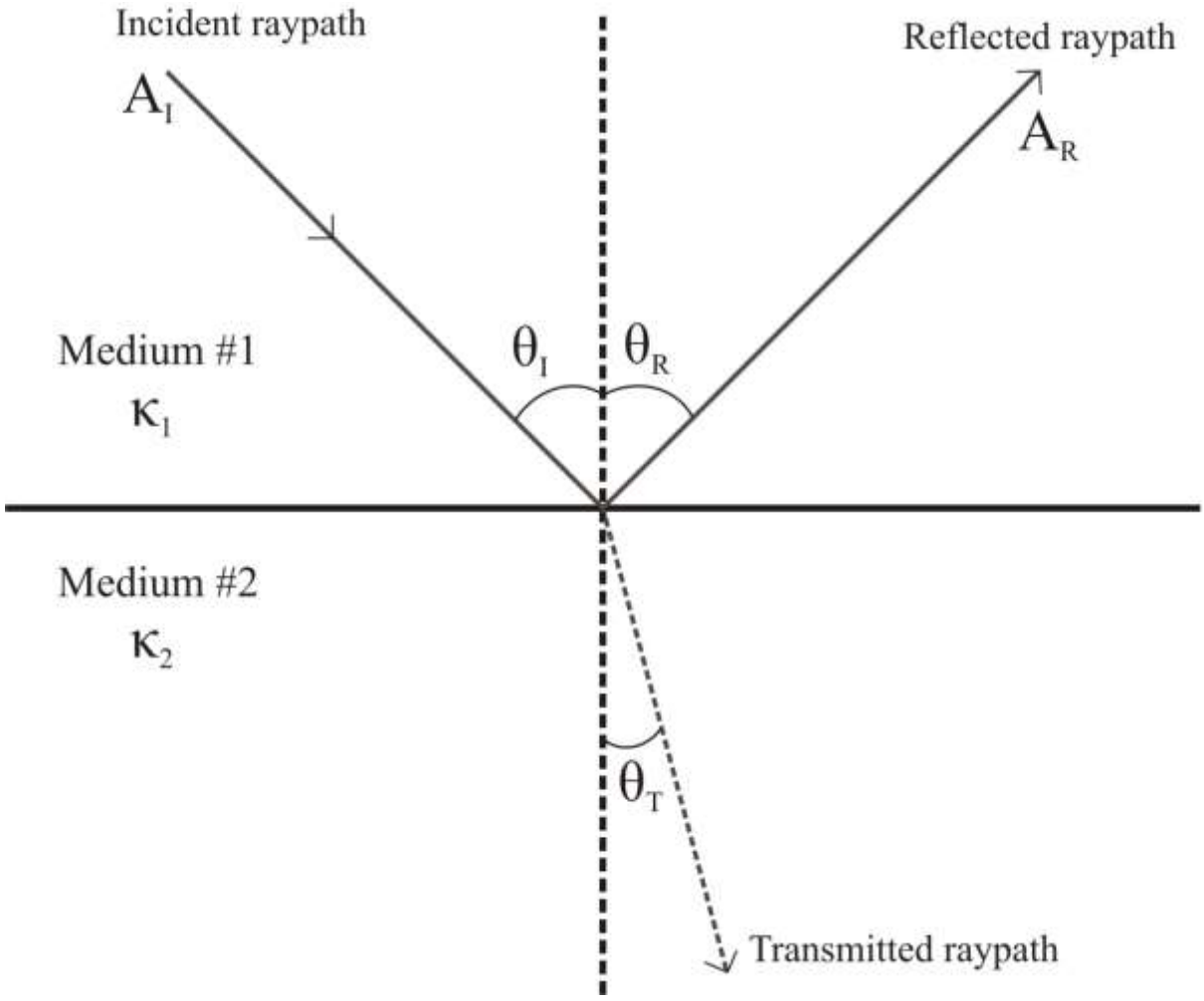

Figure 2.1 – Schematic diagram illustrating reflection and transmission for a two media system separated by a horizontal interface.

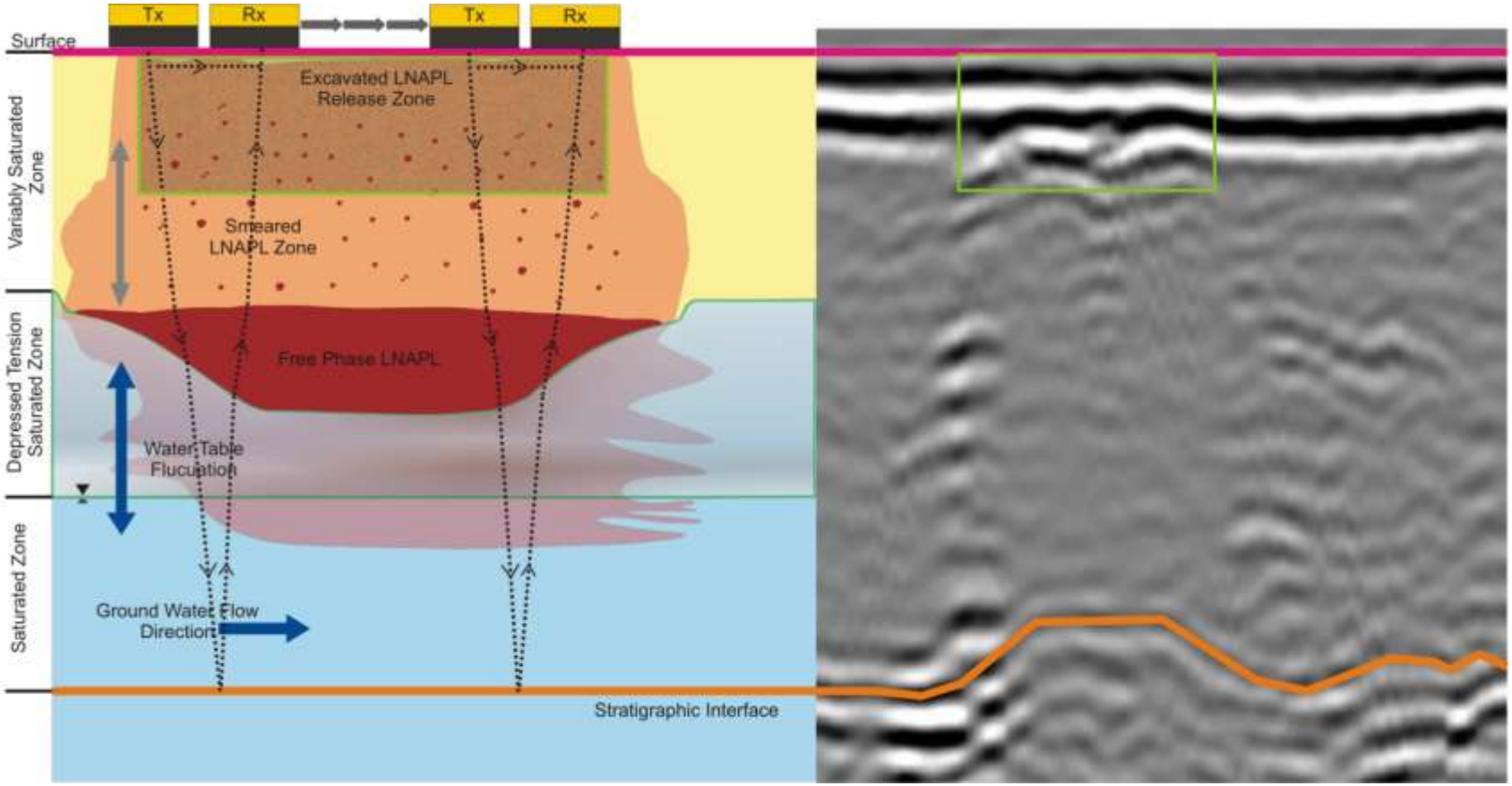

Figure 2.2 – Constant offset reflection profiling over the LNAPL release zone. Each sounding produces a trace along the profile of the line. White indicates negative amplitude, black positive amplitude.

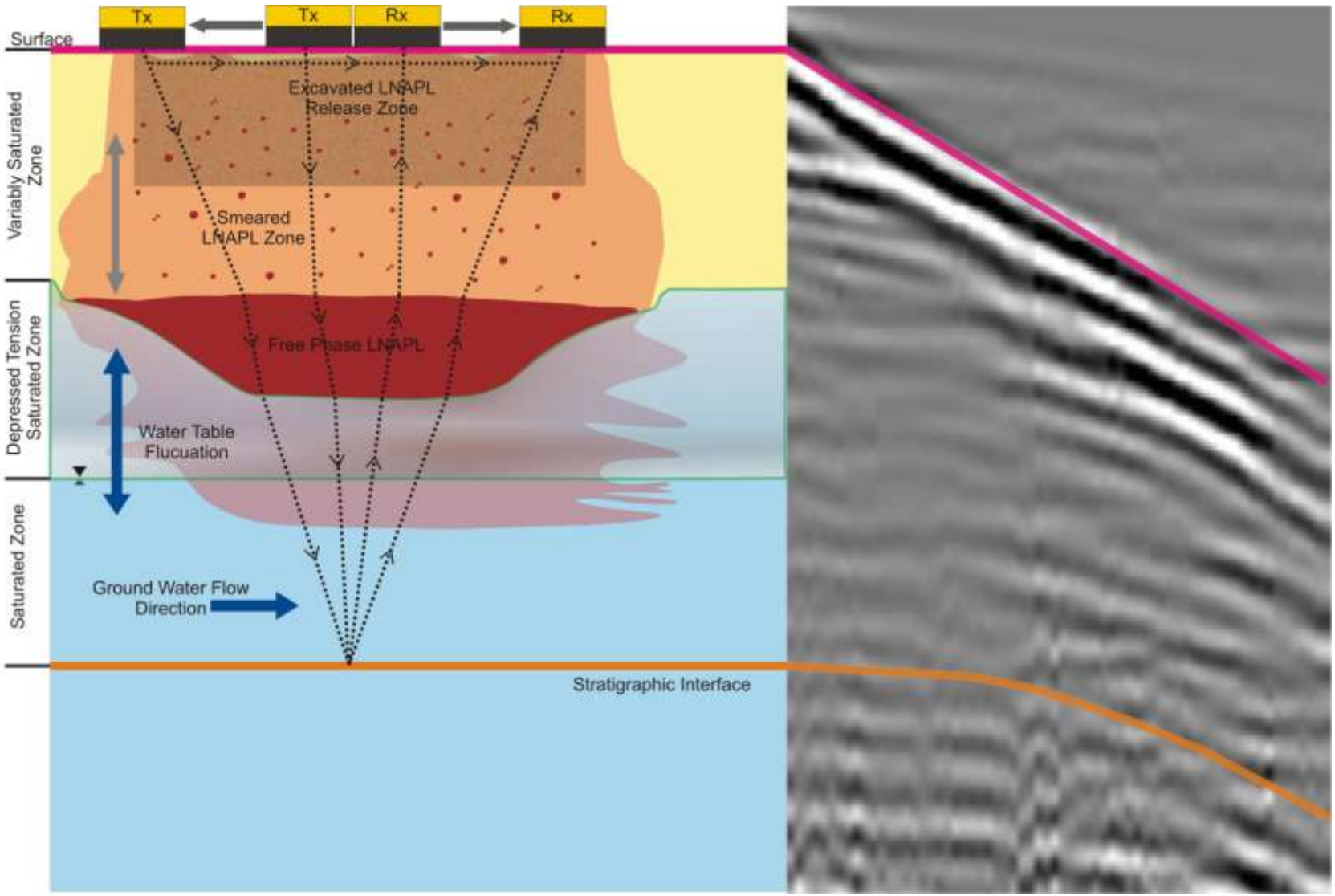

Figure 2.3 – Multi-offset CMP sounding over the LNAPL release zone. Each sounding produces a trace about a central point. White indicates negative amplitude, black positive amplitude.

Figure 2.4 – GPR antennas positioned in the perpendicular orientation.

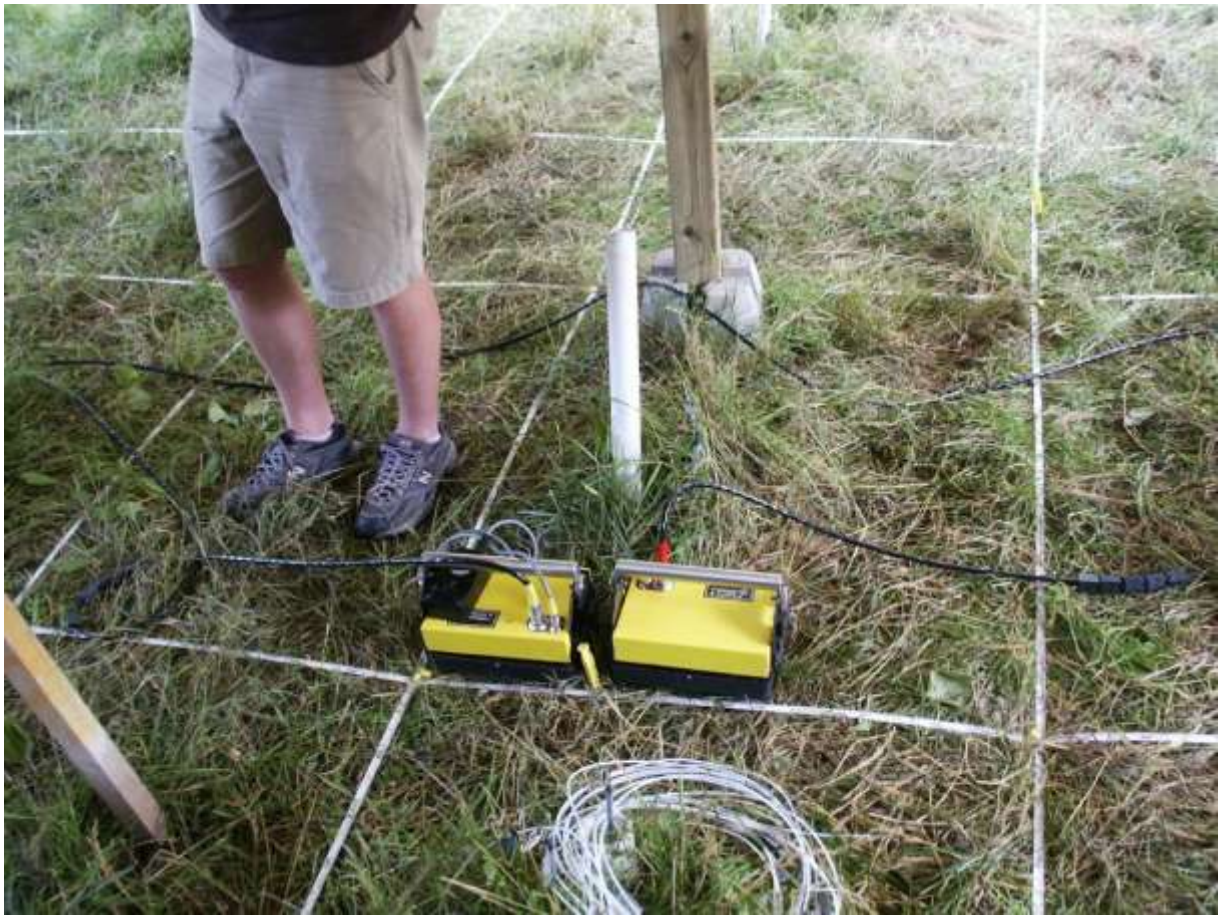

Figure 2.5 – GPR antennas positioned in the parallell orientation.

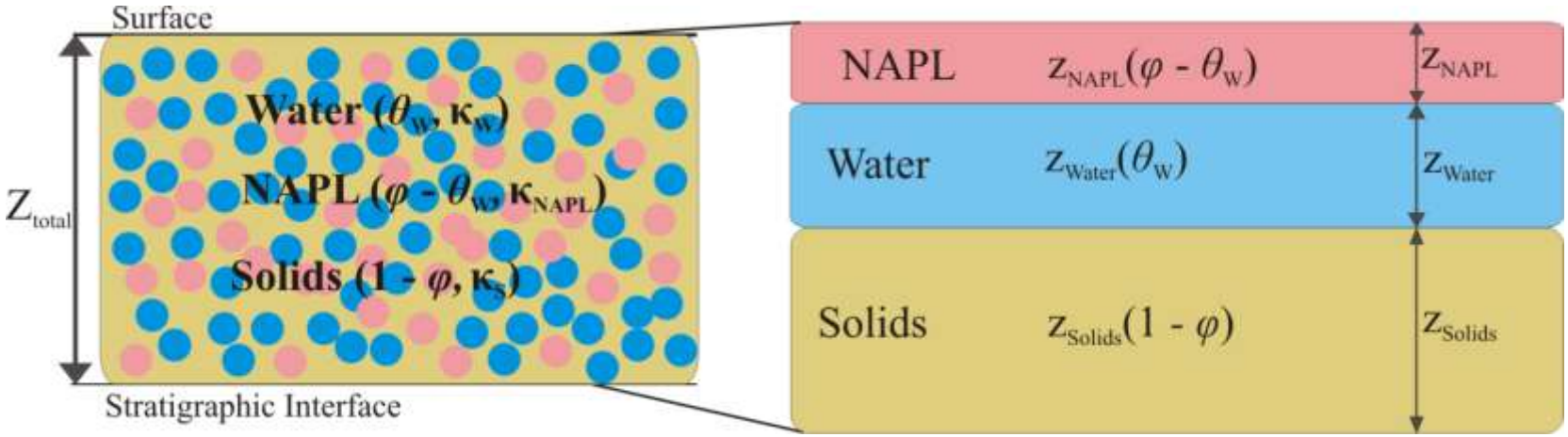

Figure 2.6 – Left: Three phase system of solids (yellow), water (blue) and NAPL (pink). Right: Three phase mathematical model representing effective layered media for CRI model.

3.0 Experiment Methodology and Background

Chapter 3 provides an overview of the methodology used to collect data over the gasoline (LNAPL) release, outlines the field site, field observations and details the procedure used to release the gasoline. The background considerations of the study, data collection and other methods of investigation are also summarized.

3.1 Field Site Description

The field site for the experiment is located at Canadian Forces Base (CFB) Borden in a former sand pit, 130 km northeast of the University of Waterloo and 90km northwest of Toronto (Figure 3.1). Research has been conducted by the University of Waterloo at Canadian Forces Base (CFB) Borden since the early 1980's and has produced a large number of significant hydrogeological studies (e.g., MacFarlane et al., 1983; Nwankwor et al., 1984, 1992; MacKay et al., 1986; Sudicky, 1986). It is also the site of important studies in hydrogeophysics that are listed in Table 3.1. Further, a hydrogeophysical lab experiment was performed by Vakili (2008) on a large-scale column which evaluated geophysical techniques to detect LNAPL within variable saturated conditions using Borden sand.

The unconfined sand aquifer at Borden was deposited within a foreshore prograding glaciolacustrine sequence from Lake Algonquin approximately 12,000 years before present (Bolha 1986). Sudicky (1986) describes the aquifer as "comprised of primarily horizontal, discontinuous lenses of medium-grained, fine-grained and silty fine-grained sand". Heterogeneity in the aquifer is in the form of "thin laminations, 0.01 to 0.1 metres thick, that are typically continuous over lengths of 2 to 5 metres". The aquifer is considered relatively homogeneous, mildly anisotropic at the field scale. The aquifer materials in the sand pit have porosity (φ) of 0.33, and hydraulic conductivity estimates within the pit range between 4.0 x 10^{-5} to 1.05 x 10^{-4} m/s (Laukonen 2001). Yang (2008) determined the hydraulic conductivity of the E10 cell, which is located 15 m from the cell used in this study, to be 7.85 x 10^{-5} m/s. The aquifer is 7 - 8 m thick below the sandpit and is underlain by a clayey-silt aquitard.

3.1.1 Experimental Cell Description

The most recent hydrocarbon experiments in the Borden aquifer are being conducted in cells that are hydraulically connected to the aquifer but contain released contaminants (Mocanu 2007; Lambert 2008; Molson et al. 2008; Freitas 2009). There are currently three cells, or gates, installed within the sandpit site; for this study, we are using Cell #3 also known as the E10 gate. A plan view of this cell is given in Figure 3.2. The cell walls are constructed of steel sheet piling which has been sealed with grout at each joint. The cell walls are 7 m deep and end near the top of the aquitard, this design prevents contamination from experiments in adjacent cells and contains the outflow (Lambert, 2008). Each cell is 21.0 m long and 7.5 m wide, the ends are open to allow groundwater under the natural hydraulic gradient to flow through the cell. The cell walls were installed in a northerly direction with the intent to allow groundwater to flow parallel to the walls. However, observations show that groundwater flow direction can fluctuate yearly from approximately N11^{o}W to N50^{o}E and may enter the cells at a slight angle (Lambert, 2008). The average flow direction is N21^{o}E (Mocanu 2007). The downgradient side of the cells are covered by a gravel pad and an enclosed shelter.

The downgradient end of cell #3 contains a pump and treat system. Water leaving the cell is pumped to a tank where it is air-sparged to remove remaining hydrocarbons. The air-sparged water is pumped to a larger holding tank where it is evaluated for hydrocarbon content. Once hydrocarbon concentrations in the holding tank are below a set detection level, the water is released back into aquifer outside the cell via the gravel pad. In July 2008, a temporary shelter was constructed extending 7.7 m upgradient from the main shelter to eliminate infiltration effects due to precipitation on the gasoline release. Cell #3 has been outfitted with several rows of soil vapour extraction nests, monitoring wells for water table measurements and multilevel sampling wells equipped with porous suction samplers for sampling within the variably saturated zone (Freitas and Barker 2008; Freitas 2009).

3.2 Gasoline Release

This gasoline release is the first field component of a multi-phase project examining the effects of ethanol on an existing subsurface gasoline source zone (Freitas 2009). An important consideration in the timing of the gasoline release was that it had to occur above the tension

saturated zone. Previous laboratory work (Nwankwor et al. 1984, Akindunni and Gillham 1992) and field observations (Nwankwor et al. 1992; Bevan et al. 2005) have found that tension saturated zone in the Borden aquifer extends approximately 0.30 m above the water table. Further, additional height above the tension saturated zone was necessary to account for to the collapse of the tension saturated zone after the introduction of gasoline (Yu et al. 2009). Given that the excavated trench in which the gasoline was released had a depth of 0.2 m and the tension saturated zone thickness of 0.3 m, a minimum depth of 0.5 m to the water table below ground surface was desired in order to release the gasoline.

To release the gasoline, a 1.5 m (length) by 0.8 m (height) by 0.2 m (depth) trench was excavated the day prior to the release (August 20, 2008). The sides of the excavation were supported with a four sided steel box and the bottom was lined with a 0.5 mm plastic sheet. On the day of the release (August 21, 2008), 180 L of mixed API gasoline (171 L) and MTBE (9 L) were blended with 20 L of pure ethanol within the lined trench to produce a ten percent ethanol blend, commonly referred to as E10. The gasoline used in this mixture was an API (American Petroleum Institute) standard 91-01 with no additives. In addition, 0.1 g/L of Oil-Red-O dye was added to make the mixture visible in soil cores. More details about the chemical and physical properties of the gasoline ethanol mixture are available in Freitas (2009). Samples were taken of the mixture and the plastic liner was removed so that the E10 mixture infiltrated into the subsurface. The excavation was covered to limit volatilization of the E10 mixture. Infiltration of the E10 into the soil took 5 hours; afterwards, the trench was repacked in lifts of 5 cm with the excavated sand and sod.

3.3 GPR Equipment and Data Aquisition

This section details the equipment, field site organization and data acquisition methods used to gather GPR data.

3.3.1 Ground Penetrating Radar Equipment

The GPR system used to collect data was a pulseEKKO 1000 manufactured by Sensors & Software of Mississauga, ON. The pulseEKKO 1000 has shielded antennas that allow its use near or in structures which may reflect GPR signal back to the antennas.

There are a number of acquisition parameters that need to be selected; Table 3.2 contains the values of these parameters used in this project. The time window is the time period, in nanoseconds (ns), for which the unit records arriving events at the receiving antenna and must be long enough to include all events of interest. The sampling interval is the time period in picoseconds (ps) between signal measurements within the time window; its value must consider acquisition effort and the potential of temporal aliasing. The stack is the number of times each trace is composited to improve the signal to noise ratio of the GPR data. Antenna separation, in metres, is a constant offset distance between the antennas during the reflection profiling. While any value can be used, the pulseEKKO 1000 has a bracket system to maintain a recommended constant antenna offset; these brackets were used for profiling during this work. The step size is the how far the antennas are moved for each trace, in metres. For reflection profiling, the step size is the distance the antenna array is moved between soundings, while step size for the CMP sounding is the incremental increase in the antenna offset distance as traces are collected. The choice of the step size must consider acquisition effort and the potential of spatial aliasing.

3.3.2 Profile Line and CMP Locations

The GPR profiling grid consists of 6 lines. Figure 3.2 shows the experimental cell in plan view. Lines 2, 3 and 4 were placed perpendicular to the cell wall and Lines A, B and C, were parallel to the cell wall. These lines were chosen to characterize both the release zone and un-impacted areas of the cell (Figure 3.2). It is important to make comparisons between the impacted and un-impacted areas as the LNAPL release was monitored, in order to differential geophysical changes due to the LNAPL from those induced by the naturally changing site conditions (i.e., water table fluctuations and freeze-thaw cycle).

Four CMP sites were selected to monitor the variations in subsurface velocity during the LNAPL release (Figure 3.2). A CMP site was originally centered at 1.0 m on line C, it was anticipated that this up gradient location would be unimpacted during the release. When the temporary shelter was constructed, its location was moved to 1.75 m on line C in order to remain within the shelter. A second CMP site was centred at 3.2 m on line C, immediately adjacent to the west side of the release zone, this location was selected to observe lateral spreading from the release zone. A third CMP site was centred at 3.2 m on Line A, off the

release zone, to observe if LNAPL spread laterally towards the east. The fourth site was centered at 3.6 m on Line 4 to observe the changes due to potential down-gradient gasoline migration.

On September 11, 2008, surveying of the GPR grid was completed for spatial distribution and digitization. The permanent wooden stakes located at the end of each line were surveyed in addition to each metre mark on every line, the intersections of the lines, and the four corners of the gasoline release trench. The data collected from the total station survey was compiled with data collected previously for other hydrogeological installations in the cell.

A list of all GPR monitoring dates can be found in Table 3.3. On each monitoring day, six reflection profiles and four CMP soundings were collected for each antenna frequency. In addition, individual CMP soundings were done for both antenna orientations (i.e., parallel and perpendicular) for each frequency at all locations. In total, 28 individual GPR data sets were collected per field day, for a grand total of 560 GPR data sets over the 308 day monitoring period.

3.3.3 Trench Signature Experiment

A trench signature experiment was started on September 28, 2008 to assess the potential overprint of the trenching process on the GPR response. The objective of this experiment was to determine whether our trench has a GPR response that significantly interferes with LNAPL effects. This experiment will ensure that when comparing between pre-release and post-release data any changes observed in the GPR reflections are due to effects of the gasoline and not a result of disturbing the sand. A similar experiment was conducted using antenna frequencies of 450 MHz, 225 MHz and 200 MHz in the very early planning stages of the overall project and negligible effects were noted (Freitas and Piggott, 2006). Site conditions may have changed over the intervening period and data for this work was acquired with 450 and 900 MHz antennas; hence, it was felt that an additional evaluation of trench effects was prudent.

The test trench was excavated within 10 m of the experimental cell within the floor of the abandoned sandpit. Two background perpendicular profile lines, denoted as Lines Y and Z, were collected on September 28, 2008. Line Y was positioned across the front of the trench

and Line Z bisected this line through the middle of the trench. This configuration was set up to simulate Line 3 and Line B, respectively, that were used to monitor the gasoline release. After the background GPR data were collected a test trench was dug to the same dimensions as the trench used in the gasoline release (1.5 m $\times$ 0.8 m $\times$ 0.2 m). Further, the trench was left open for 5 hours, then refilled with sand, repacked and sod relaid. After repacking the trench the GPR lines were recollected. After nine days (on October 7, 2008), the profile lines were monitored again to see if there had been any changes in the GPR reflections caused by disturbance of the sand profile. These results are discussed in Section 4.1.

3.4 Processing GPR Data

Following data acquisition, the GPR data must be processed in order to enhance subsurface reflection events and suppress random noise and unwanted coherent events. Background data and post-release data for profiles and CMP were processed using the same procedure described above in order to compare changes relative to the background. Table 3.4 lists the parameter values for the processing sequence.

The transfer software WINPXFER (Sensors & Software Inc.) was used to export the field data from the GPR system to a desktop computer. Initial processing of the GPR data was done in Sensors & Software Inc. software package EKKOview Deluxe version 1.2. Each profile and CMP file were inspected to assure that start position, end position, step size and number of traces were correct. The data sets were also checked for blank traces that are very infrequently inserted. EKKOview was utilized to interpolate the data between adjacent traces to fill in these blank traces.

Once these basic data quality issues were addressed, zero time adjustments were applied to the reflection profiling data. EKKOview estimates zero time using an amplitude threshold criterion to adjust each trace in a file. This criterion can be user defined or default values can be selected. Several threshold values were tried but the default of +/- 5% provided the most consistent zero time adjustment for both the 900 MHz and 450 MHz profile data. After adjusting the zero time, the time window was truncated to -5 ns to 40 ns for 900 MHz and -5 ns – 65 ns for 450 MHz. Data recorded prior to the zero time (i.e. negative time) was eliminated

as this contains no physical information. Late-time data were also eliminated as it is significantly contaminated by noise and does not contain useful reflection events.

Described below is the processing routine used for this particular set of data. For more information on processing of GPR data, please refer to Daniels (2004), Annan (2005a) and Cassidy (2009); background information about the general principle of processing theory is found in Yilmaz (2001). Two different processing streams were performed on the reflection profiles. The first stream was designed to produce well defined images of the shallow LNAPL impacted zone. The second stream focused on the imaging a much deeper stratigraphic reflection underlying the LNAPL impacted zone; changes in the image of this stratigraphic reflection can be use to characterize the LNAPL impacted zone.

Figure 3.3 displays typical results for selected sequential processing steps as described below. The processing focused on shallow LNAPL impacted zone was performed in EKKOview Deluxe. First, a dewow of the data was performed which removes low frequency signal saturation, referred to as a "wow" effect, from each trace. The dewow filter has parameters that are automatically selected by the software. Secondly, a frequency bandpass filter was applied to each trace to remove low and high frequency noise that lies outside the frequency band of the reflection signals. The frequency bandpass filtering requires four values (in MHz) corresponding to the i) low cut frequency, ii) lower plateau, iii) upper plateau and iv) high cut frequency. These four values can be selected from an average amplitude spectrum plot like the example shown in Figure 3.4. Values below the low cut frequency and above the high cut frequency are set to zero. The lower plateau and upper plateau are used to set the cosine-window, which suppresses unwanted reverberations in the data. Lastly, an SEC (spreading and exponential compensation) gain function is used to compensate for spherical spreading losses and exponential ohmic dissipation to the signal's energy by applying a mathematical function to multiply or 'gain' the signal. The SEC preserves relative amplitude information in the GPR signal, allowing for comparison of interface reflection strength. The SEC has three input parameters: attenuation exponent, start value and maximum gain.

GPR data processed to highlight deeper stratigraphic reflection were performed in the ReflexW version 5.0 software package developed by Sandmeier Software. Five processing steps are performed using ReflexW for each reflection profile data set: Dewow, bandpass filtering, gain

function, running average spatial filtering and mean filter. The dewow and bandpass filter in this package are comparable processes to those in EKKOview. The gain function in ReflexW is similar to the SEC in EkkoView; however, a additional linear gain parameter needs to be specified.

Following processing of the data by application of the gain function, a 2-D running average filter was used where a user-defined number of adjacent traces are averaged into a central trace. The running average filter suppresses noise and dipping events (e.g., diffraction tails), smoothes the trace and enhances 'coherent horizontal energy' contained in reflection events. Next, a 1-D mean filter was used where a user defined number of points above and below a given point is averaged, at the centre point. Each point comprising the trace is averaged by the 1-D Mean filter to smooth each trace individually.

CMP data were processed using the steps described above for deep stratigraphic reflectors, with the exception of the last two steps (2-D running average and 1-D mean filter). This processing stream was used since deep continuous reflectors can be used to estimate overlying media velocity. The CMP image was left unsmoothed in order to preserve the offset dependent normal moveout of reflection events.

3.4.1 Complex Attributes Processing

In addition to the standard data processing describe above, complex attributes processing was performed on the reflection profiles using ReflexW. This process involves the application of the Hilbert-transformation to each GPR trace to construct a complex-valued version of the trace. This process produces a set of complex attributes, also known as instantaneous attributes; these attributes are the envelope (also referred to as amplitude), phase and frequency. A more comprehensive discussion on instantaneous attributes is found in the Barnes (2007) tutorial on complex trace analyses.

Orlando (2002) demonstrated the use of complex attributes for the detection of LNAPL floating on the water table. Orlando (2002) was able to delineate the extent of LNAPL contamination floating on the water saturated zone at a field site in Italy by using spatial variations in real and complex attributes. Hence, it was anticipated that the used of complex

trace analysis would enhance our monitoring of the LNAPL impacted beyond what was possible using standard data processing techniques.

Table 3.1 – Hydrogeophysical investigations of the unconfined sand aquifer at CFB Borden.

Reference	Focus	Geophysical Technique
Bauman (1989)	Stratigraphic and hydrogeologic characteristics	Various including GPR
Schneider and Greenhouse (1992)	Controlled DNAPL detection	Resistivity and nuclear logging
Greenhouse et al. (1993)	Controlled DNAPL detection	Various including GPR
Brewster and Annan (1994)	Controlled DNAPL detection	GPR
Brewster et al. (1995)	Controlled DNAPL detection	Various including GPR
Endres and Greenhouse (1996)	Controlled DNAPL detection	Thermal Neutron Logging
Endres et al. (2000)	Water Table Detection during Pumping Test	GPR
Bevan et al. (2003)	Water Table Detection during Pumping Test	GPR and Neutron moisture content probe
Tomlinson et al. (2003)	Air saturation Detection during Air Sparging	Surface and Borehole GPR
Hwang et al. (2008)	Natural gradient DNAPL detection	GPR

Table 3.2 – GPR acquisition parameters for the pulseEKKO 1000 system.

Parameter	**900 MHz Antenna**	**450 MHz Antenna**
Time Window [ns]	50 ns	80 ns
Sampling Interval [ps]	100 ps	200 ps
Stack [-]	64	64
Antenna Separation [m]	0.17 m	0.25 m
Profile Survey Step-size [m]	0.02 m	0.05 m
CMP Survey Step-size [m]	0.02 m	0.02 m

Table 3.3 – List of GPR monitoring dates

	Date	**Days after Release**	**Label**
Background	20-August-2008	-1	Background
Monitoring # 1	21-August-2008	0	M1Aug21
Monitoring# 2	22-August-2008	1	M2Aug22
Monitoring# 3	25-August-2008	3	M3Aug25
Monitoring# 4	27-August-2008	5	M4Aug27
Monitoring# 5	29-August-2008	7	M5Aug29
Monitoring# 6	02-September-2008	11	M6Sep02
Monitoring# 7	04-September-2008	13	M7Sep04
Monitoring# 8	11-September-2008	20	M8Sep11
Monitoring# 9	17-September-2008	26	M9Sep17
Monitoring# 10	28-September-2008	37	M10Sep28
Monitoring# 11	07-October-2008	46	M11Oct07
Monitoring# 12	21-October-2008	60	M12Oct21
Monitoring# 13	03-November-2008	73	M13Nov03
Monitoring# 14	25-November-2008	97	M14Nov25
Monitoring# 15	04-December-2008	104	M15Dec04
Monitoring# 16	16-December-2008	116	M16Dec16
Monitoring# 17	22-January-2009	153	M17Jan22
Monitoring# 18	25-February-2009	187	M18Feb25
Monitoring# 19	26-June-2009	308	M19Jun26

Table 3.4 – GPR processing parameters for the pulseEKKO 1000 system.

Parameters for Profile Surveys in EKKOview	**900 MHz Antenna**	**450 MHz Antenna**
Dewow	Automatic	Automatic
Frequency Bandpass (MHz)	100 / 200 / 1600 / 2000	50 / 100 / 1250 / 1550
SEC Gain ([dB/m]/ ns /[-])	(0.5 / 1 / 200)	(0.5 / 1 / 200)
Parameters for Profile and CMP Surveys in ReflexW	**900 MHz Antenna**	**450 MHz Antenna**
1D subtract mean - Dewow	5	3
Frequency Bandpass (MHz)	100 / 200 / 1600 / 2000	50 / 100 / 1250 / 1550
Gain function (ns/[1/pulsewidth]/[dB/m]/[-])	0 / 0.8 / 11 / 800	0 / 0 / 10 / 1000
Parameters for filtering Profile Surveys in ReflexW	**900 MHz Antenna**	**450 MHz Antenna**
2D horizontal smoothing - Running Average (# of traces)	3	3
1D low pass - Mean Filter (# of sample points)	5	8

Figure 3.1 – Location of CFB Borden and the field site. Cell for experiment is located within the yellow box on the 75 m scale satellite image provided by Google Earth (Accessed December 17th, 2009). The clearing to the south side of the covered structure is where the cells are located. Cell #3 is the eastern most cell.

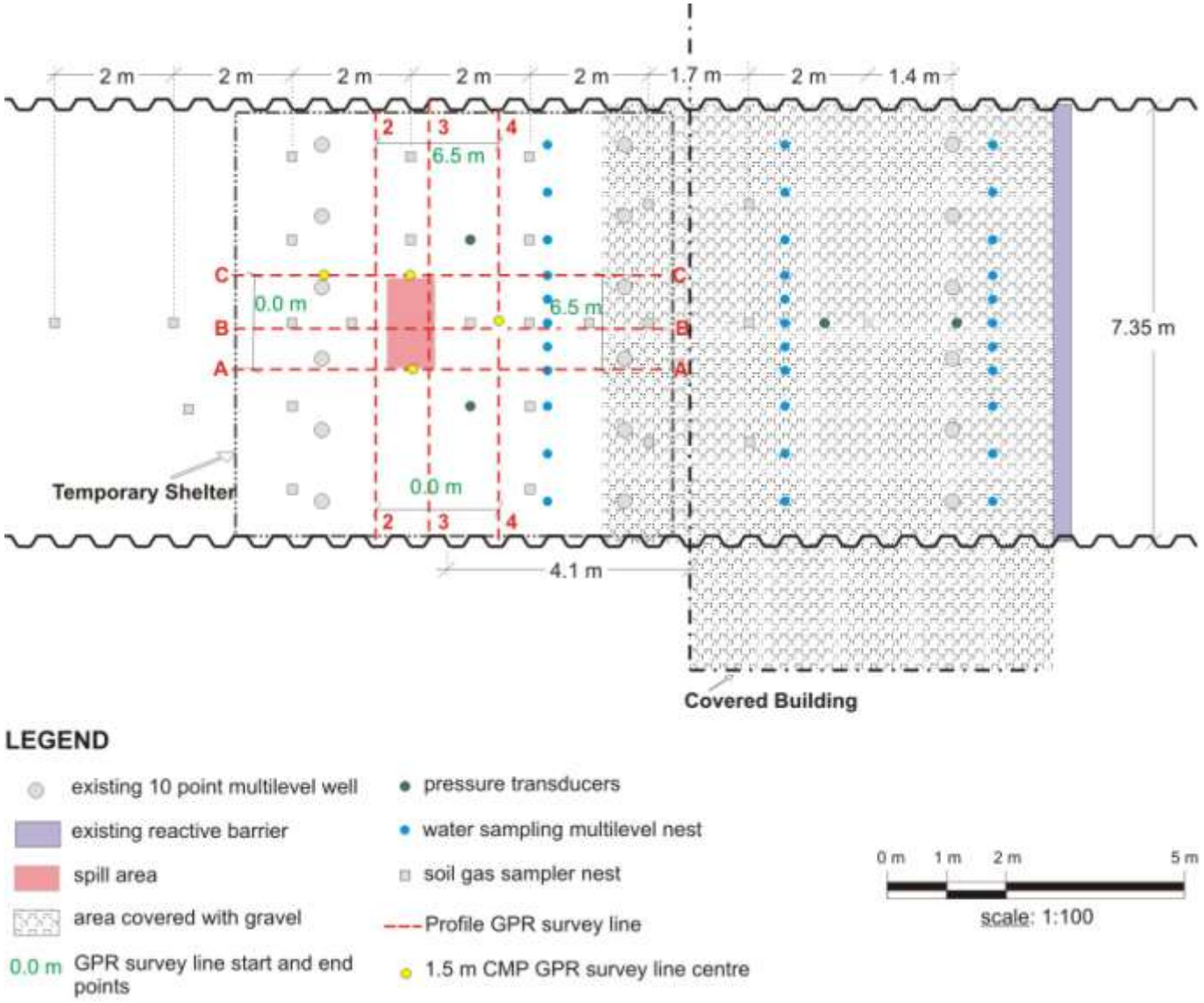

Figure 3.2 – Plan view of cell #3 at CFB Borden. (Modified after Freitas, 2009).

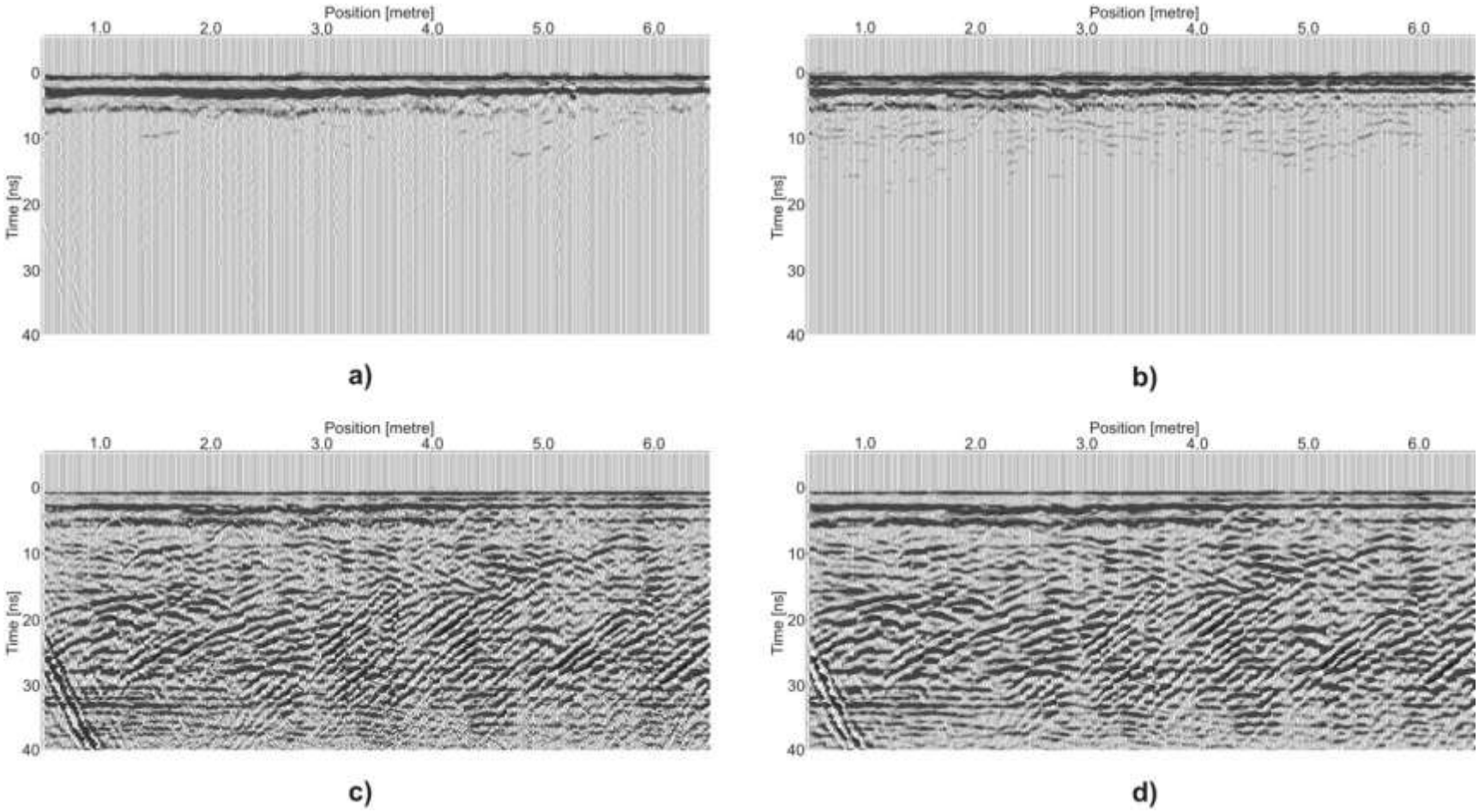

Figure 3.3 – Example showing the results of the processing steps using EKKOview for Line 3 900 MHz Background data set: a) Raw data, b) Dewowed, c) Gained and d) Filtered.

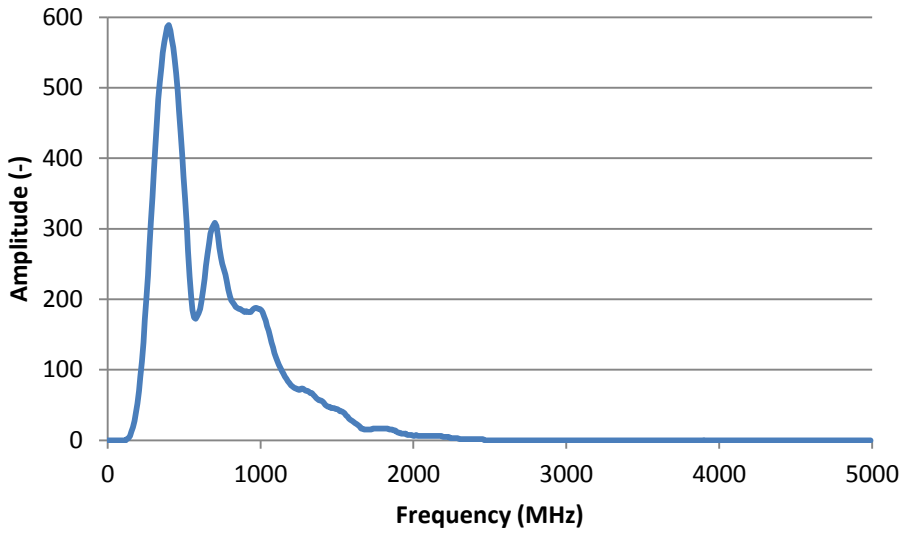

Figure 3.4 – Average amplitude spectrum plot for Line A 900 MHz Background August 20, 2008 data. This spectrum plot is used to determine the frequency bandpass filter values.

4.0 Experimental Results and Data Analysis

Figures 4.1 and 4.2 show the water table fluctuation data for the field site superimposed with the coring and monitoring dates, respectively. After a wet spring in 2008, CFB Borden experienced several large precipitation events that maintained saturated conditions near the ground surface during the following summer. The water table responded to these precipitation events with a substantial rise. The most dramatic rise occurred on August 5, 2008 when the water table rose from 0.55 metres below ground surface (mbgs) to 0.10 mbgs within a 6 hour period. Water table fluctuations between 0.70 mbgs to 0.15 metres above ground surface were observed within the experiment cell from July 2008 until June 2009. In the later part of August 2008, the water table lowered to below 0.5 mbgs and the gasoline was released on August 21, 2008.

Throughout the monitoring period, the release was subjected to seasonal changes in water table and temperature. In mid-September 2008, water table fluctuations caused by several large precipitation events forced the dyed LNAPL to the surface. The lateral extent of the LNAPL impacted zone as inferred by the red dye staining of vegetation and sand at the surface of the cell is shown in Figure 4.3 taken from Freitas (2009). The surface pattern showed an unexpected up gradient movement of the LNAPL after the release. In addition, Freitas (2009) reported that free phase LNAPL was extracted from a soil vapour monitoring point approximately 0.5 m on the west side of the 1.0 m mark of Line C, up gradient from the release zone during regular sampling after this water table fluctuation.

From late December to January, frost developed in the ground and persisted for the remainder of the 2008-2009 winter season. These frozen conditions drastically altered the GPR response and provided unique datasets from January and February which are discussed later in this chapter. From March until May 2009, the cell was flooded or saturated to ground surface. The GPR unit is not designed to work in these conditions; hence, the last monitoring day for this study was in June 2009. Another Masters student (John Mosquera) working with Professor Endres has continued the monitoring of the release with GPR through the summer of 2009 and is working on the second portion of the experiment where ethanol has been released.

4.1 Trench Signature Experiment

In addition to the GPR monitoring experiment, the trench signature experiment described in Section 3.3.3 examined the effects of trench excavation and fill technique used to release the gasoline mixture on the GPR data. The results from this signature experiment for the 450 and 900 MHz profiling are presented in Figures 4.4 and 4.5, respectively. The location of the trench excavation has been denoted in orange on both figures. For both antenna frequencies, there is negligible change of the GPR signal at or below the repacked trench location.

4.2 Constant-Offset Reflection Profiling Results

Of the six lines collected, the discussion herein focuses on Lines B, 3 and 4. Lines B and 3, which have the most distinctive GPR response to the release, are perpendicular in orientation and traversed the middle of the release zone (Figure 3.2). Line 4 is unique in that it is the only GPR line not impacted by free phase gasoline by the end of the study. Hence, Line 4 provides GPR data for unimpacted conditions to compare with the impacted lines.

Selected lines are shown to highlight the development of the GPR response for both frequencies throughout the monitoring period. The background data from August 20, 2008 show the profiles unaffected by the LNAPL release. August 25 data is shown to examine early time effects of the LNAPL. September 17 data was chosen since it shows the maximum reflectivity within the impacted zone. December 16 data is presented because it shows evolution of the GPR response before the ground is frozen. January 22 data is given to show the GPR response during frozen conditions. June 26 data is shown since it is the latest dataset in the monitoring period and the first dataset collected after frozen conditions.

4.2.1 900 MHz Profiles

The selected 900 MHz reflection profiles for Lines B, 3 and 4 are show in Figures 4.6-4.8, respectively. The background data (Figures 4.6a-4.8a) are similar. They show a clear, coherent, continuous direct ground wave between 0 ns – 7 ns with relatively low-medium amplitude stratigraphic reflections below. On Line B and Line 4 diffraction hyperbola originating from soil vapour installations and water sampling installations can be seen. On Line 3 and 4 there is a distinct reflection off the east side wall.

On both Line B and Line 3 high amplitude reflection events develop in the shallow subsurface (i.e., above 10 – 12 ns) below the release trench immediately after the release (Figures 4.6b and 4.7b); these events persisted throughout the entire monitoring period during unfrozen conditions. In addition, deeper (i.e., below 10 – 12 ns) high amplitude events are initially observed under the release trench and diminish significantly with time. The nature of these later arrivals is uncertain, it is conjectured that they could be scattering and reverberation of the signal. This may be due to a high degree of initial heterogeneity and the occurrence of interfacies with strong dielectric contrast, which probably was a result of the rapid release of the LNAPL and subsequent mixing within the near surface. It is probable that these heterogeneities dissipate as the gasoline phase is re-distributed within the aquifer.

Lateral extent of the shallow high amplitude reflections gradually increased until September 17, 2008 (Figures 4.6c and 4.7c) during which time the seasonal water table low stand occurred. Throughout the remainder of the monitoring during unfrozen conditions (Figures 4.6d,f and 4.7 d,f), no additional lateral extension of the these reflections were observed. Instead, GPR profiling found a long-term dimming of reflectivity in these events at their periphery. In addition, some variation in reflectivity were seen in the vicinity of the release trench. It is probable that the amplitude variations are influenced by fluctuations in the water table. Changes in water table depth affect the moisture content in the near surface which, in turn, changes the dielectric permittivity in this zone. These processes would cause variations in the dielectric contrast between clean and LNAPL impacted zones and result in reflectivity variations.

In contrast to Lines B and 3, the down gradient Line 4 exhibits little, if any, reflectivity variation during unfrozen conditions (Figure 4.8 b-d,f) relative to the background profile (Figure 4.8 a). It can be inferred from these results that the free phase LNAPL did not reach Line 4.

Frozen ground conditions were encountered during the January 22 and February 26 monitoring dates. A strong, continuous reflection event that was not present during unfrozen conditions can be seen extending across all of the profiles on these two dates (Figures 4.6e, 4.7e and 4.8e). Further, this event appears to advance deeper (i.e. greater traveltime) during monitoring on February 26. This behavior and the results from the CMP surveys presented in Section 4.3

support the interpretation that this event is the reflection from the interface between the overlying frozen soil and the underlying unfrozen aquifer.

Profiling along Line 4 indicates that was some degree of variation in the depth to this interface within the unimpacted region (Figure 4.8e). In contrast, profiling along both Lines B and 3 show the freezing process has been significant affected in the gasoline impacted areas (Figure 4.6e and 4.7e). Here, the traveltime of the freeze front is significantly increased. In addition, the waveform of the direct wave arrivals (i.e., the first event) varies over the impacted regions, indicating impact on freezing due to the presence of LNAPL extends upwards to very shallow depths, possibly to the surface.

4.2.2 450 MHz Profiles

The selected 450 MHz reflection profiles for Lines B, 3 and 4 are show in Figures 4.9, 4.10 and 4.11, respectively. The background data (Figures 4.9a, 10a and 11a) for Lines B, 3 and 4 are similar, which show the direct ground wave event a with continuous stratigraphic reflection event at 45 ns – 50 ns.

Due to the shallow depth of the gasoline impacted zone, it is not as well imaged using this antenna frequency due to its superposition with the direct air-ground wave arrival. A more diagnostic attribute of the gasoline impacted zone for this frequency on Lines B and 3 is the velocity pull-up due to the displacement of low velocity water by high velocity gasoline. The velocity pull-up of the continuous stratigraphic reflection is clearly seen by comparing the pre-release profiles (Figures 4.9a and 10a) with the post-release profiles obtained during unfrozen conditions (Figures 4.9b-d,f and 10 b-d,f). In particular, this stratigraphic event is distorted by the velocity pull-up beneath the release trench on the post-release profile. The magnitude of the pull-up is larger on the profiling to September 17 (Figures 4.9b-c and 10b-c) and appears to be less during the remainder of the unfrozen monitor period (Figures 4.9d,f and 10d,f).

Analogous to the 900 MHz results, the down gradient Line 4 exhibits no velocity pull-up during unfrozen conditions (Figure 4.11 b-d,f) relative to the background profile (Figure 4.11 a). Again, this behavior is consistent with the interpretation that the free phase LNAPL did not reach Line 4.

During frozen conditions (Figures 4.9d, 10d and 11d), the lower resolving power of the 450 MHZ and the resulting interference between the direct wave and the very shallow reflection events produce a less well defined image of the direct effects of the winter freezing process on the near surface region. Further, it can be seen that the development on the frozen soil and its associated velocity effects impacts the expression of the velocity pull-up.

4.3 Multi-offset CMP Results

In this section discussion will focus on the following two CMP soundings: centered at position 3.2 m on Line C- and centered at position 3.6 m on Line 4. The use of these two soundings give a comparison between the gasoline impacted zone and the unimpacted soil, respectively, for the CMP velocity analysis.

4.3.1 CMP Surveys

The CMP surveys for the same selected monitoring dates as shown above for the reflection profiling are show in Figures 4.12-15. On all of these CMP surveys, the direct ground wave and reflection events are present. On the CMPs, the direct wave appears as a first arrival, linear event that goes through zero time at the zero offset distance between antennas. In comparison, the reflection events appear as later arriving hyperbolae with their apex at the zero offset distance.

For the CMP surveys at the release location, the nature of shallow reflections (above 10-12 ns at 0.2 meters offset) in the 900 MHz data (Figure 4.12) varied throughout the experiment as a result of the introduction of the gasoline and its subsequent evolution. The quality of the deeper stratigraphic reflection (between 45-50 ns at 0.2 meters offset) in the 450 MHz data also varies at the contaminated location after the release (Figure 4.13). In comparison, both the shallow reflections in the 900 MHz data and the deeper stratigraphic reflection in the 450 MHz data remain relatively unchanged at the unimpacted location (Figure 4.14 and 4.15, respectively).

4.3.2 NMO Velocity Analysis Results

The x^2-t^2 method was used to perform the NMO velocity analysis of the reflection events found in the CMP soundings. These NMO velocity values represent a root-mean-square

(RMS) average of the EM wave velocities of the material between the surface and reflecting interface. Because of the limited depth of penetration of the 900 MHz, shallow reflections were used for this analysis. In the case of the 450 MHz data, the deeper stratigraphic reflection previously noted was used.

In addition to the reflections, velocity information can be obtained from the direct ground wave. This signal travels just below the surface and give its velocity is govern by conditions within the first few decimeters of the soil. Due to its linear traveltime-offset relationship, an x-t line fitting is performed to obtain its velocity.

The velocities obtained from the analyses of the CMP soundings are given in Figure 4.16-4.19. During the Fall 2008, the results for both 900 MHz CMPs (Figure 4.16-4.17) indicate comparable velocities for both the direct ground wave and shallow reflections. These results suggest relatively uniform shallow conditions at both sites. However, the velocity values at gasoline impacted location (Figure 4.16) are faster than the clean site (Figure 4.17). These higher velocities are consistent the displacement of water by gasoline. The higher velocities during the winter period are due to the transformation of water ($\kappa \sim 80$) in ice ($\kappa = 3.2$) during the freezing process.

The use of the deeper stratigraphic reflection for the 450 MHz velocities (Figure 4.18-4.19) means their average velocity incorporates the effect of the water saturated aquifer below the level of the gasoline impacted zone at both sites. The comparable direct ground wave and reflection velocities at the clean site (Figure 4.19) during the Fall 2008 show that uniform conditions extend to depth. At the impacted location during this period, the direct wave and reflection velocities diverge, showing the presence of vertical velocities changes. The faster direct wave velocities values compared to the reflection again indicate the displacement of water by gasoline in the shallow subsurface. As with the 900 MHz results; higher velocities during the winter period are a result of the formation of frost in the near surface.

The final results for the June 26, 2009 monitoring date are difficult to interpret in a simple manner. This situation is most like due to the complicated history of water level variations and the effects of the freeze-thaw cycle. The additional monitoring that occurred as part of the next segment of this experiment may clarify these results.

4.4 Complex Attributes

Orlando (2002) used complex trace attributes to delineate hydrocarbon contamination and determine gasoline thickness. These findings were the motivation to investigate the use of complex (or instantaneous) trace attributes on our data set. The complex attribute processing for Line B for background conditions on August 20 and Day 26 (September 17) after the release are shown for the 450 MHz (Figures 4.20 and 4.21, respectively) and for the 900 MHz (Figure 4.22 and 4.23, respectively).

Each of the complex attribute panels has the reflection profile overlay included to provide correlation between these attributes and the direct wave and reflection events. The instantaneous amplitude results appear to provide little additional information about the location or movement of the free phase gasoline beyond what was previous observed from the reflection profiling. The instantaneous frequency does not show any coherent features in either frequency. The instantaneous phase responds to high amplitude events and the results are similar to the instantaneous amplitude. Hence, processing data for complex attributes did not significantly change the conclusions obtained from the use of the reflection profiling alone.

It is important to note that Orlando (2002) was able to use complex attributes to identify LNAPL due to favourable site conditions, the plume Orlando (2002) investigated was at sufficient depth (i.e., 1.8 mbgs) to avoid interference from the direct wave arrival. The shallow LNAPL impacted zone (i.e. < 0.5 mbgs) encounter in this work results in a situation where the arrival time of reflections from the LNAPL release are in are superimposed to some degree by the ground wave arrival. The very high amplitude of the ground wave complicates this analysis of the LNAPL related reflections. If the water table were lower during the monitoring period of this experiment, complex attribute processing may be more beneficial in characterizing the LNAPL impacted zone.

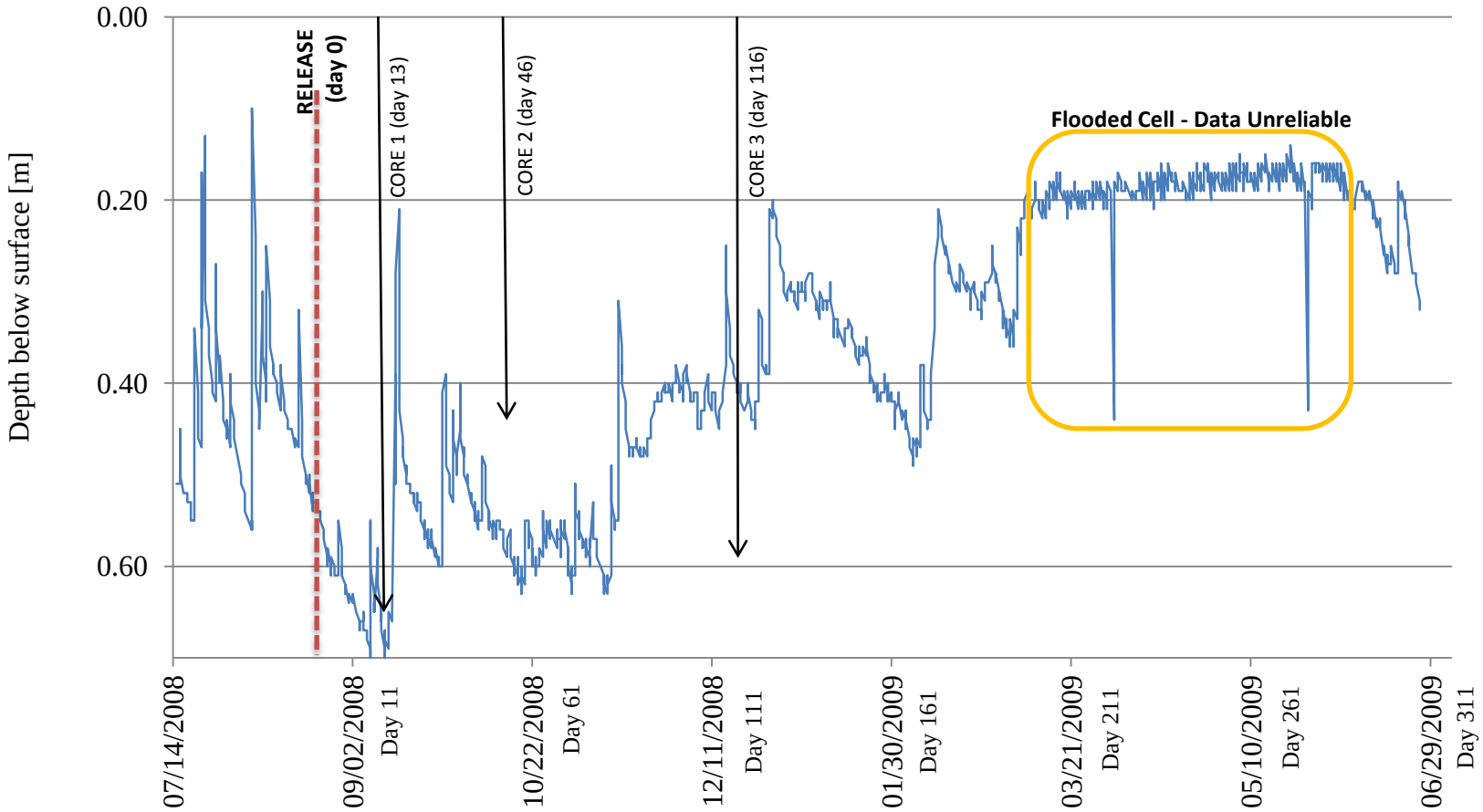

Figure 4.1 – Water table fluctuations throughout GPR monitoring period with the coring dates indicated. (Modified from Freitas, 2009).

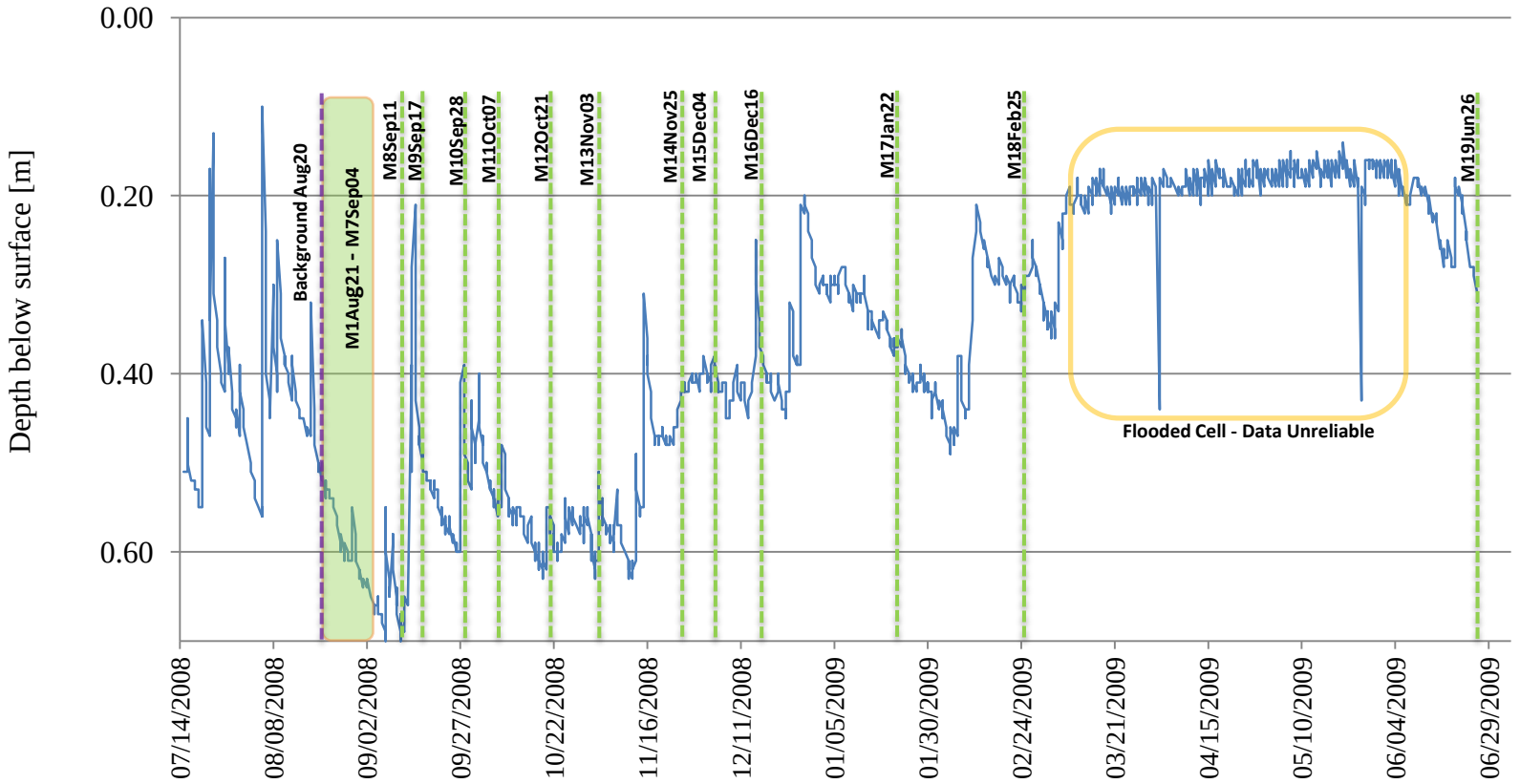

Figure 4.2 – Water table fluctuations throughout GPR monitoring period with monitoring dates shown. Purple line indicates pre-release monitoring while green lines and green shaded area indicate post-release monitoring.

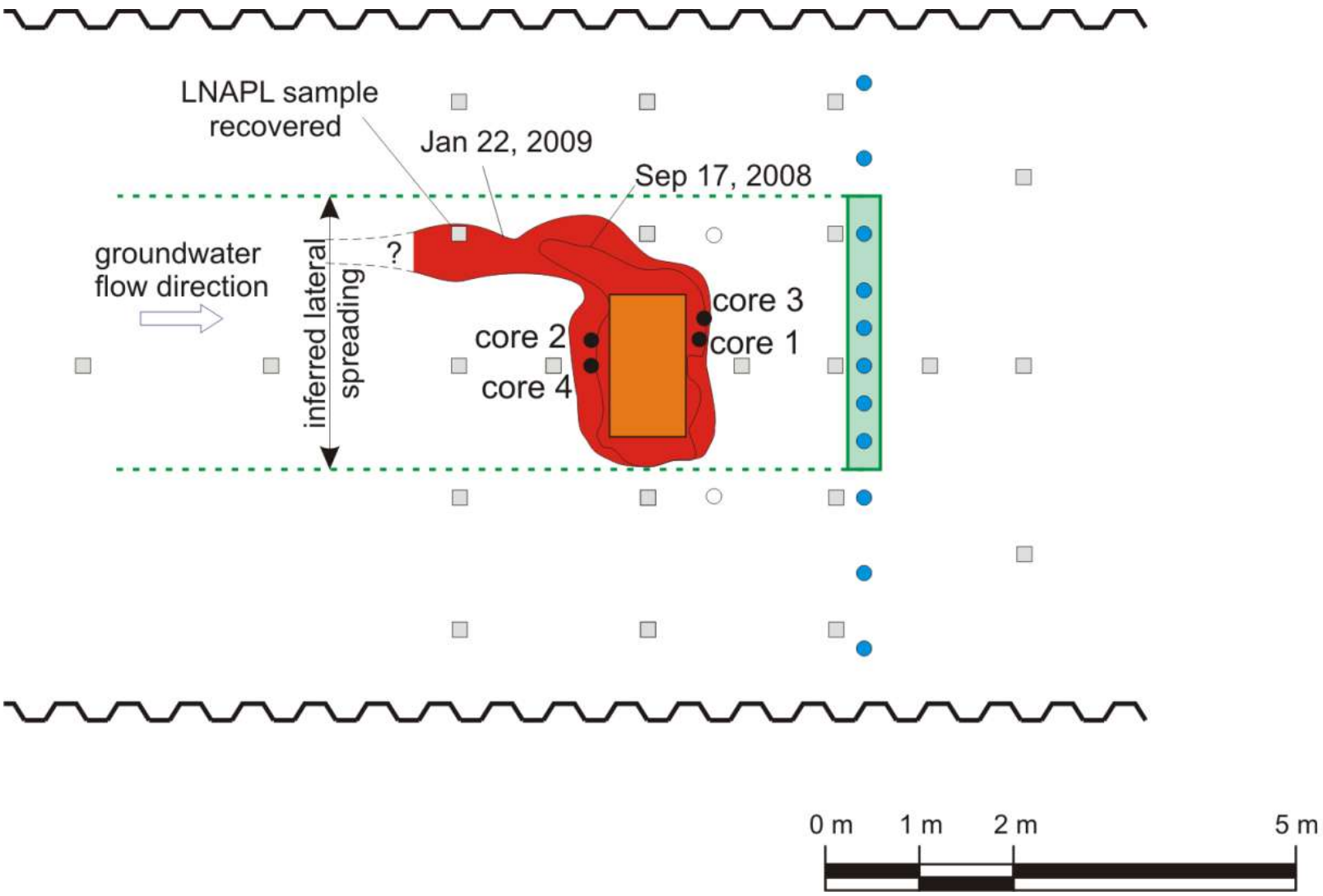

Figure 4.3 – Surface pattern of staining due to dyed LNAPL within cell (Modified from Freitas, 2009). Orange rectangle is the release zone. Red outlines staining observed staining on January 22 while the extent of mid September staining associated with the rapid water table rise is defined within this region by a solid line.

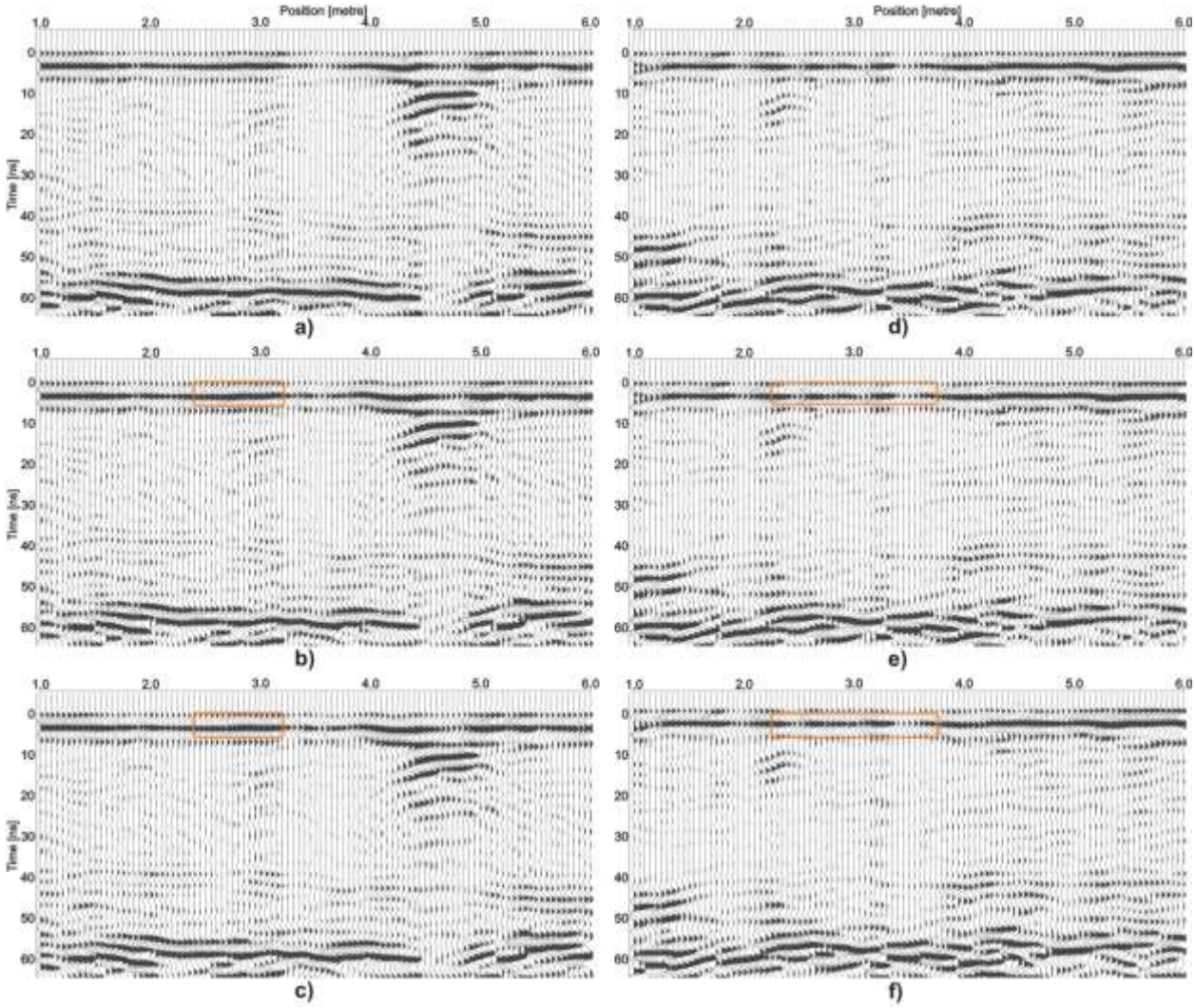

Figure 4.4 – 450 MHz profiles for simultaneous trenching experiment. Orange box denotes location of test excavation. Profiling dates: Background (28-Sep-2008), Monitoring 1 (28-Sep-2008) and Monitoring 2 (07-Oct-2008). a) Line Z-Background, b) Line Z-Monitoring 1, c) Line Z-Monitoring 2, d) Line Y-Background, e) Line Y-Monitoring 1 and f) Line Y-Monitoring 2.

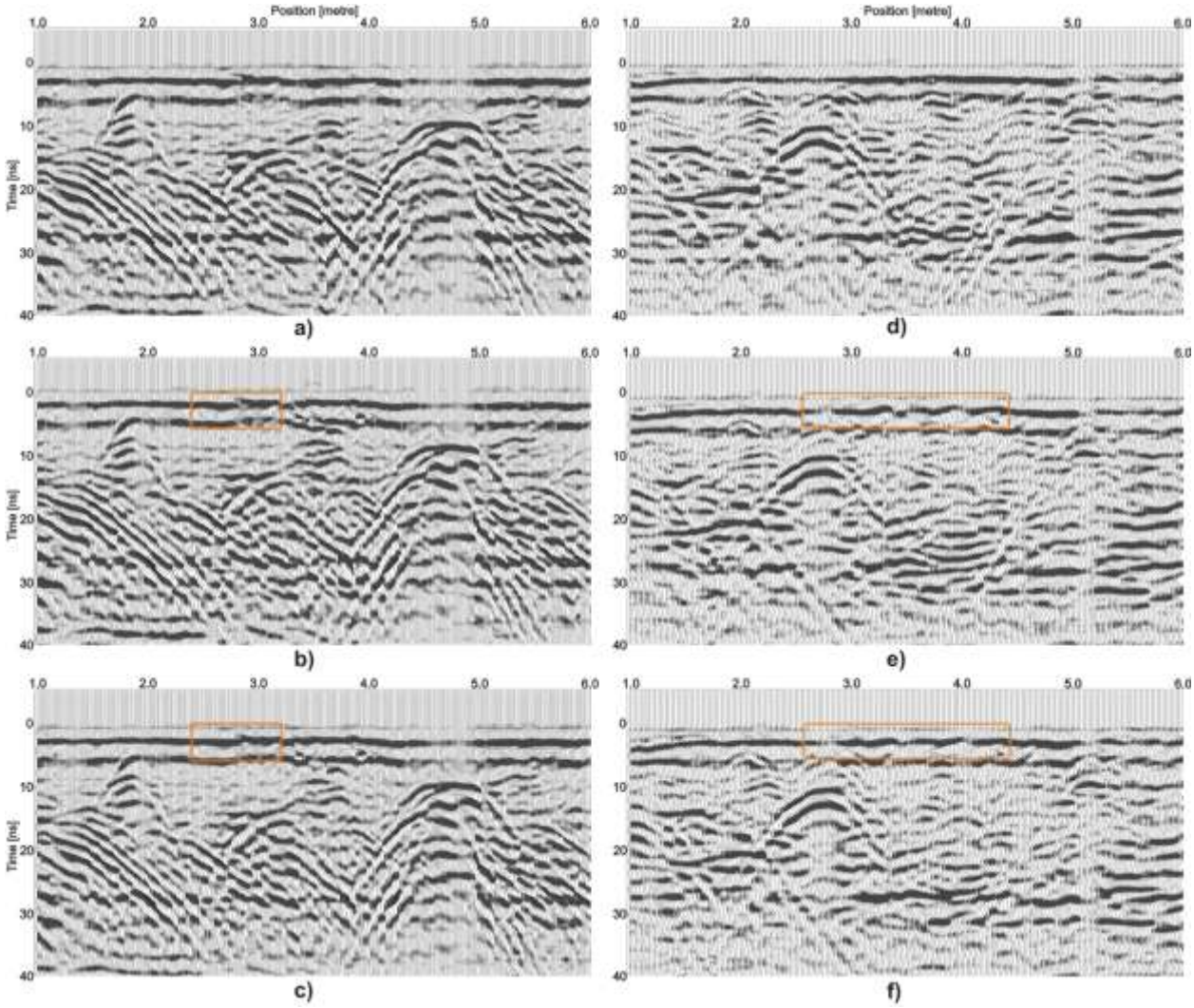

Figure 4.5 – 900 MHz profiles for simultaneous trenching experiment. Orange box denotes location of test excavation. Profiling dates: Background (28-Sep-2008), Monitoring 1 (28-Sep-2008) and Monitoring 2 (07-Oct-2008). a) Line Z-Background, b) Line Z-Monitoring 1, c) Line Z-Monitoring 2, d) Line Y-Background, e) Line Y-Monitoring 1 and f) Line Y-Monitoring 2.

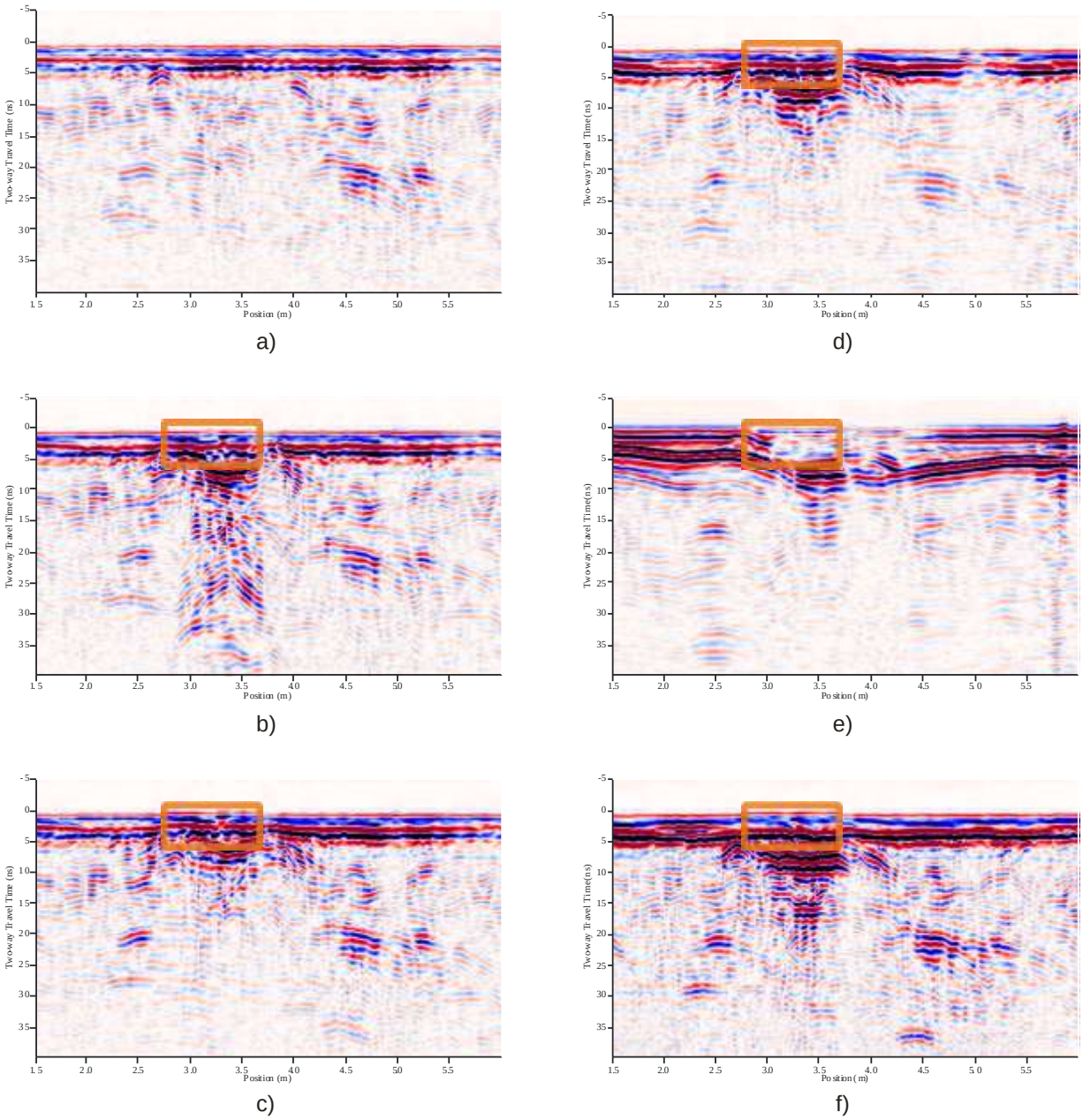

Figure 4.6 – Line B 900 MHz Profile: a) Background-August 20; b) Day -3August 25; c) Day 26-Septmeber 17; d) Day 116-December 16; e) Day 153–January 22; f) Day 308-June 26. Orange box outlines the location of the release zone.

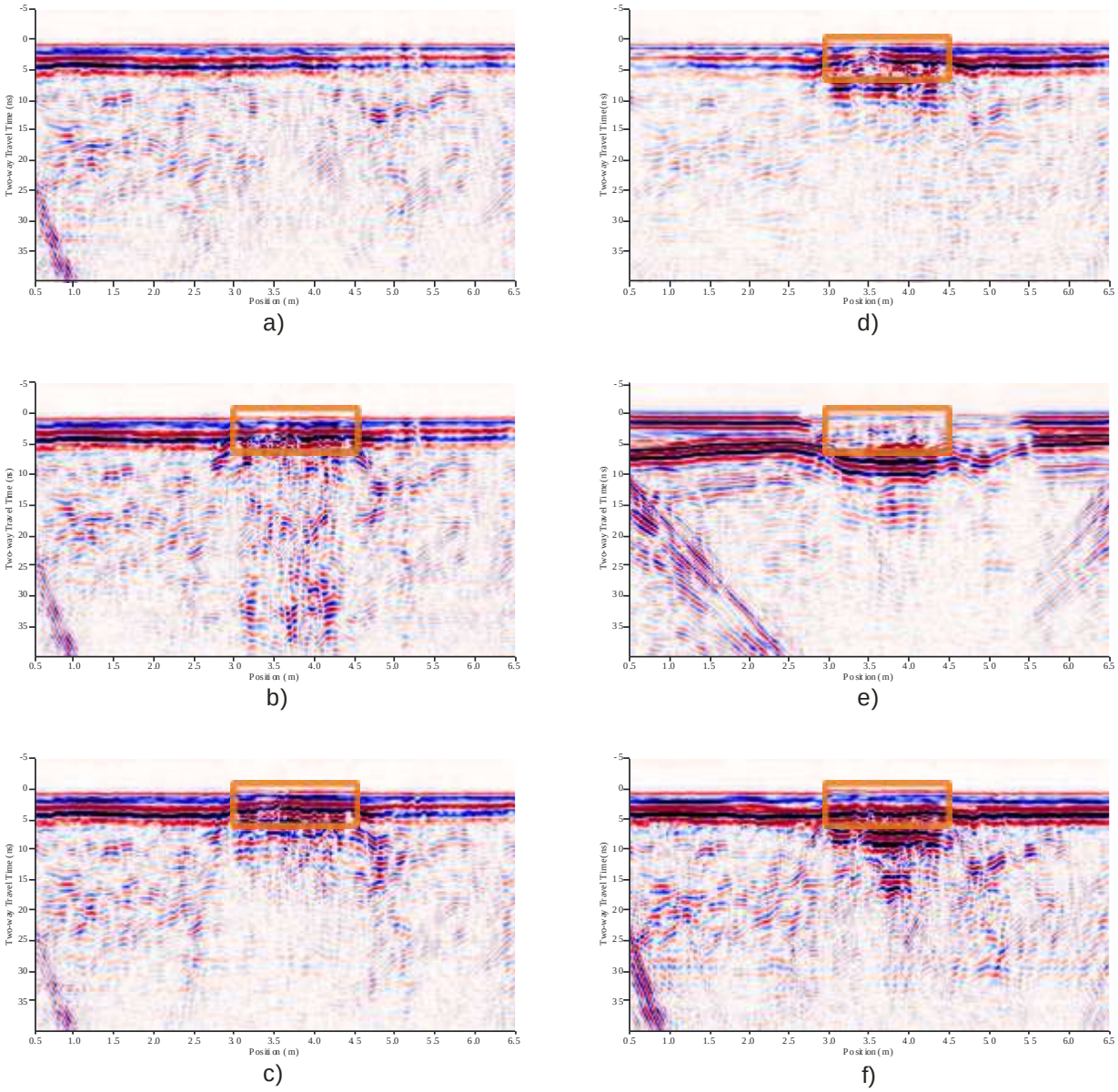

Figure 4.7 – Line 3 900 MHz Profile: a) Background-August 20; b) Day -3August 25; c) Day 26-Septmeber 17; d) Day 116-December 16; e) Day 153–January 22; f) Day 308-June 26. Orange box outlines the location of the release zone.

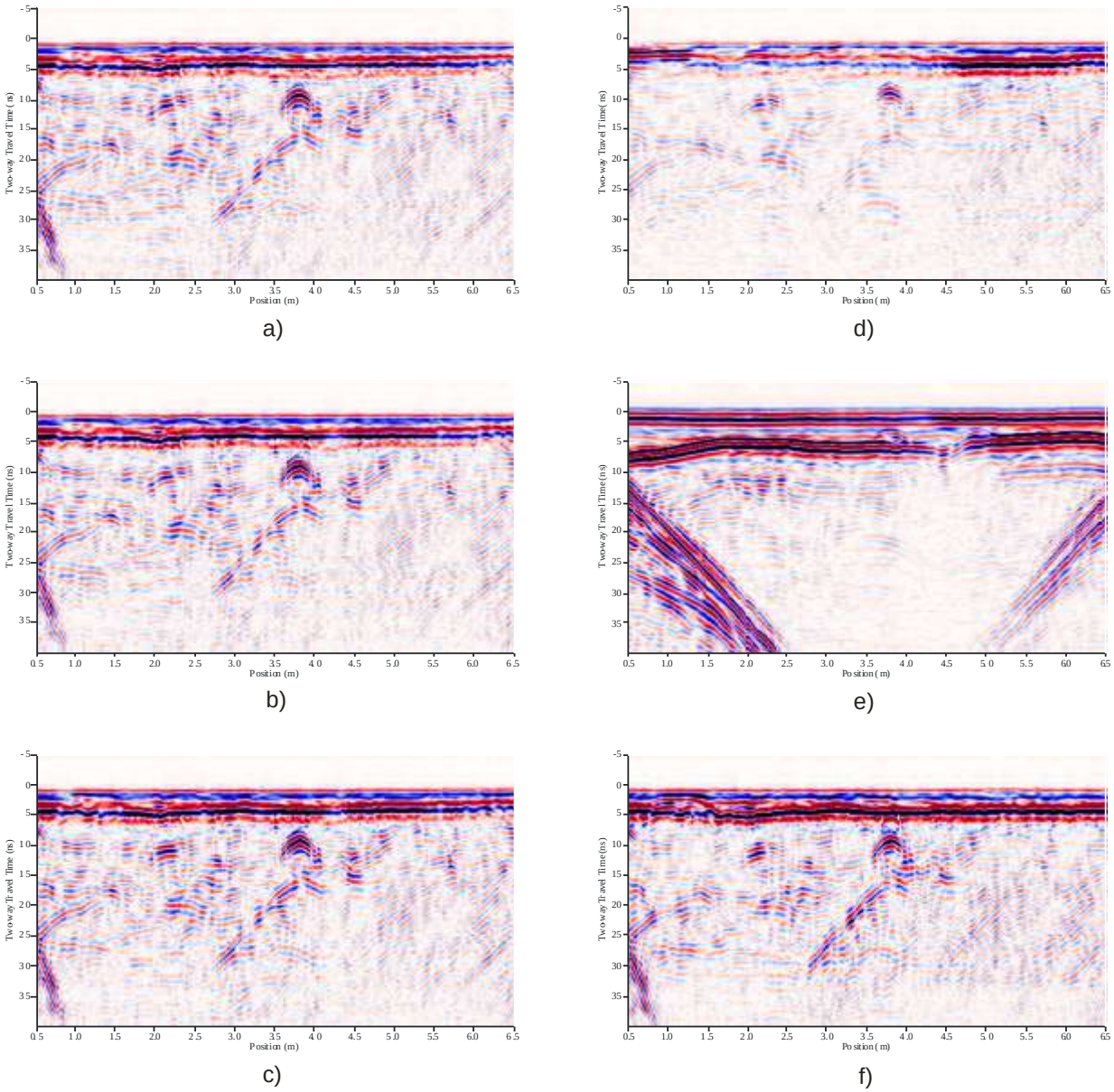

Figure 4.8 – Line 4 900 MHz Profile: a) Background-August 20; b) Day -3August 25; c) Day 26-Septmeber 17; d) Day 116-December 16; e) Day 153–January 22; f) Day 308-June 26.

.

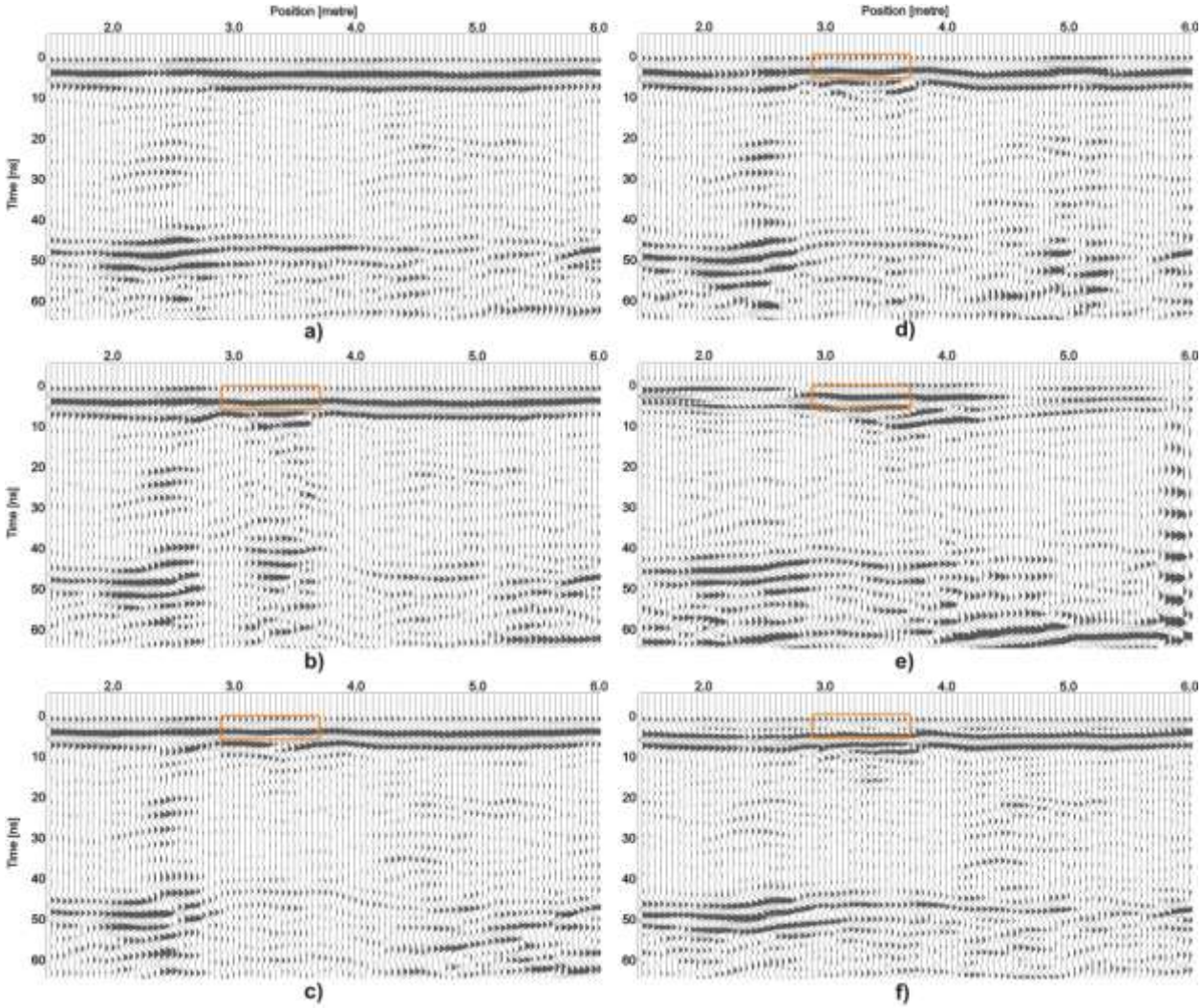

Figure 4.9 – Line B 450 MHz Profile: a) Background-August 20; b) Day -3August 25; c) Day 26-Septmeber 17; d) Day 116-December 16; e) Day 153–January 22; f) Day 308-June 26. Orange box outlines the location of the release zone.

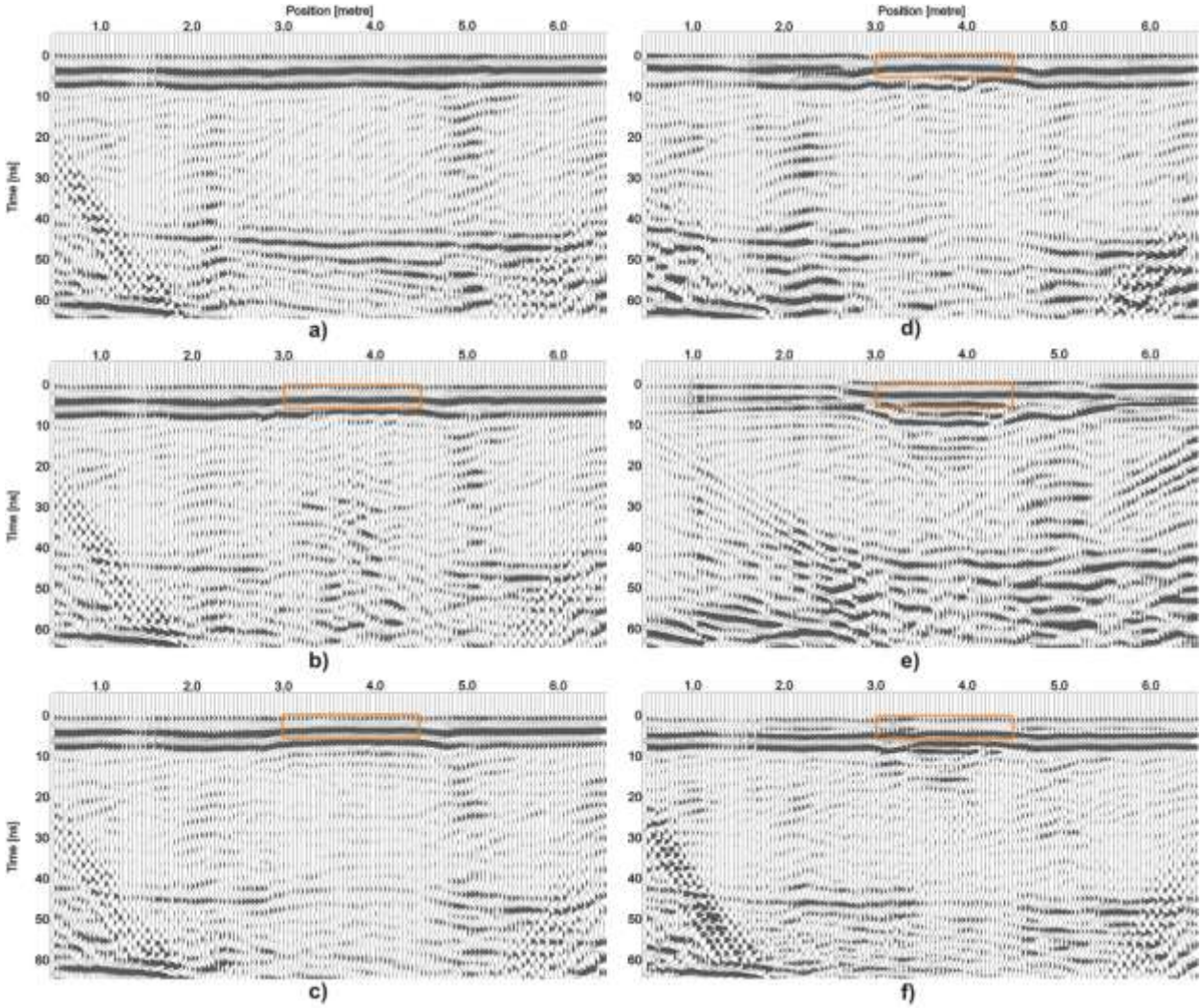

Figure 4.10 – Line 3 450 MHz Profile: a) Background-August 20; b) Day -3August 25; c) Day 26-Septmeber 17; d) Day 116-December 16; e) Day 153–January 22; f) Day 308-June 26. Orange box outlines the location of the release zone.

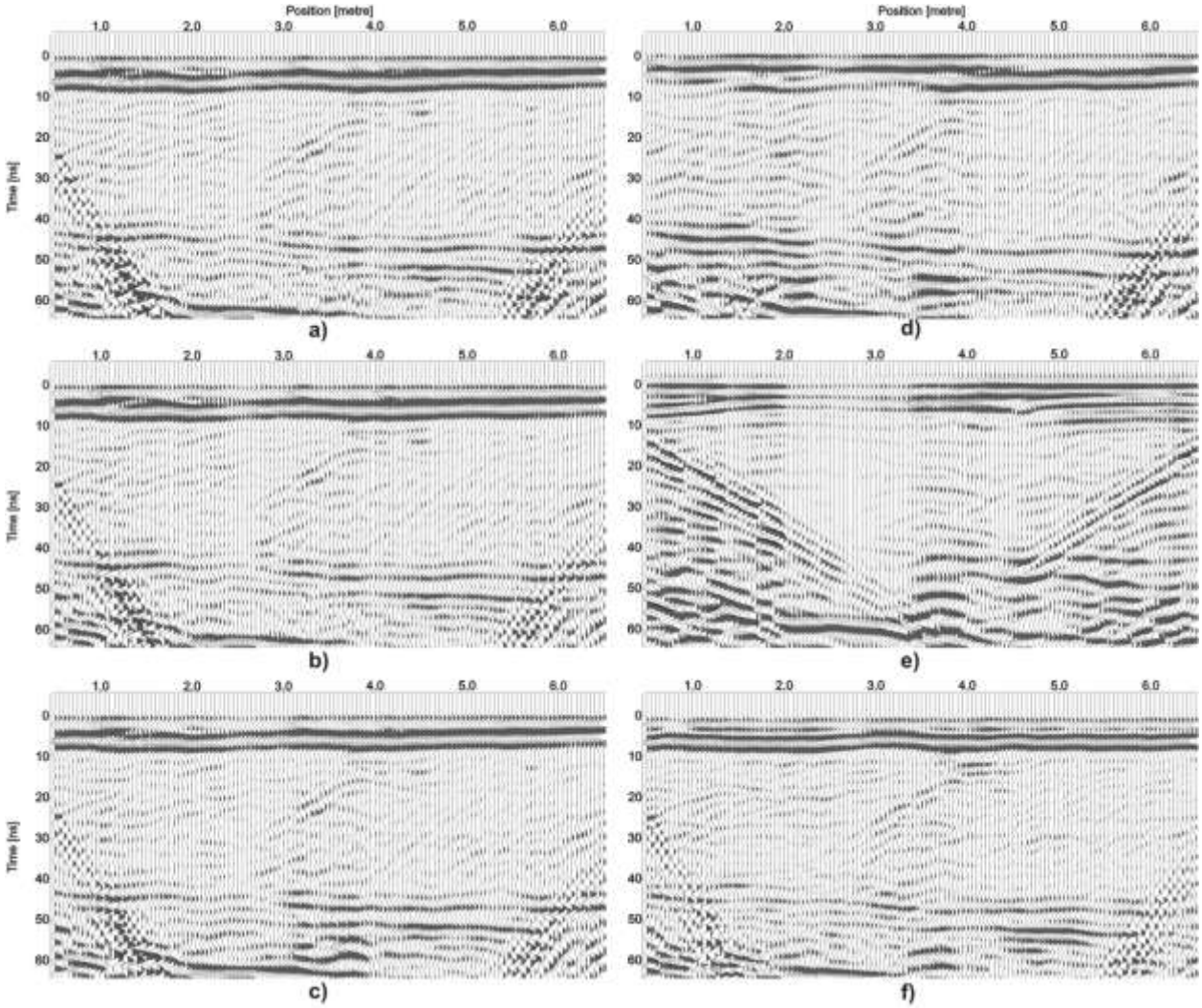

Figure 4.11 – Line 4 450 MHz Profile: a) Background-August 20; b) Day -3August 25; c) Day 26-Septmeber 17; d) Day 116-December 16; e) Day 153–January 22; f) Day 308-June 26.

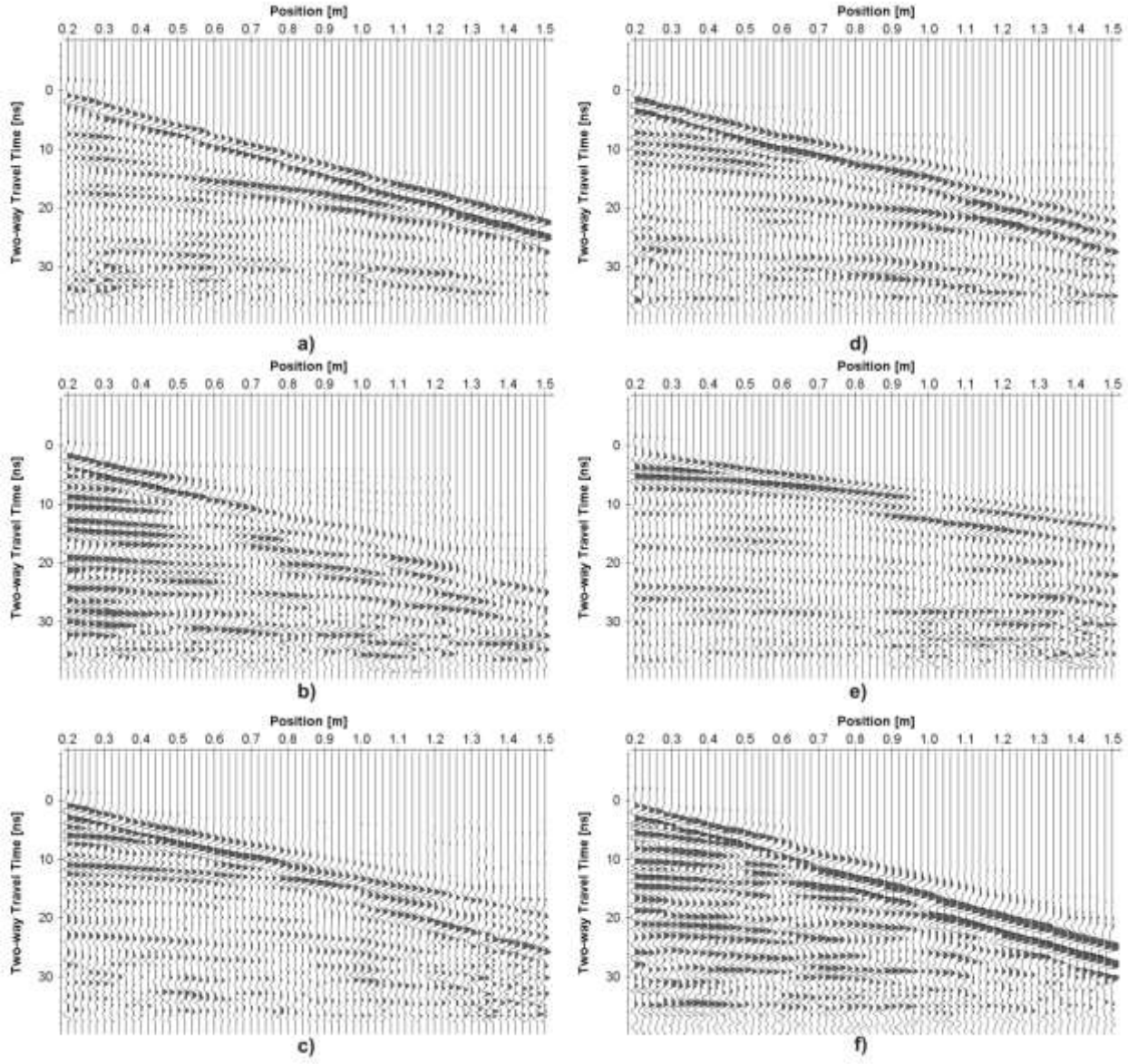

Figure 4.12 – Line C 900 MHz CMP centred at 3.2 m: a) Background-August 20; b) Day -3August 25; c) Day 26-Septmeber 17; d) Day 116-December 16; e) Day 153–January 22; f) Day 308-June 26.

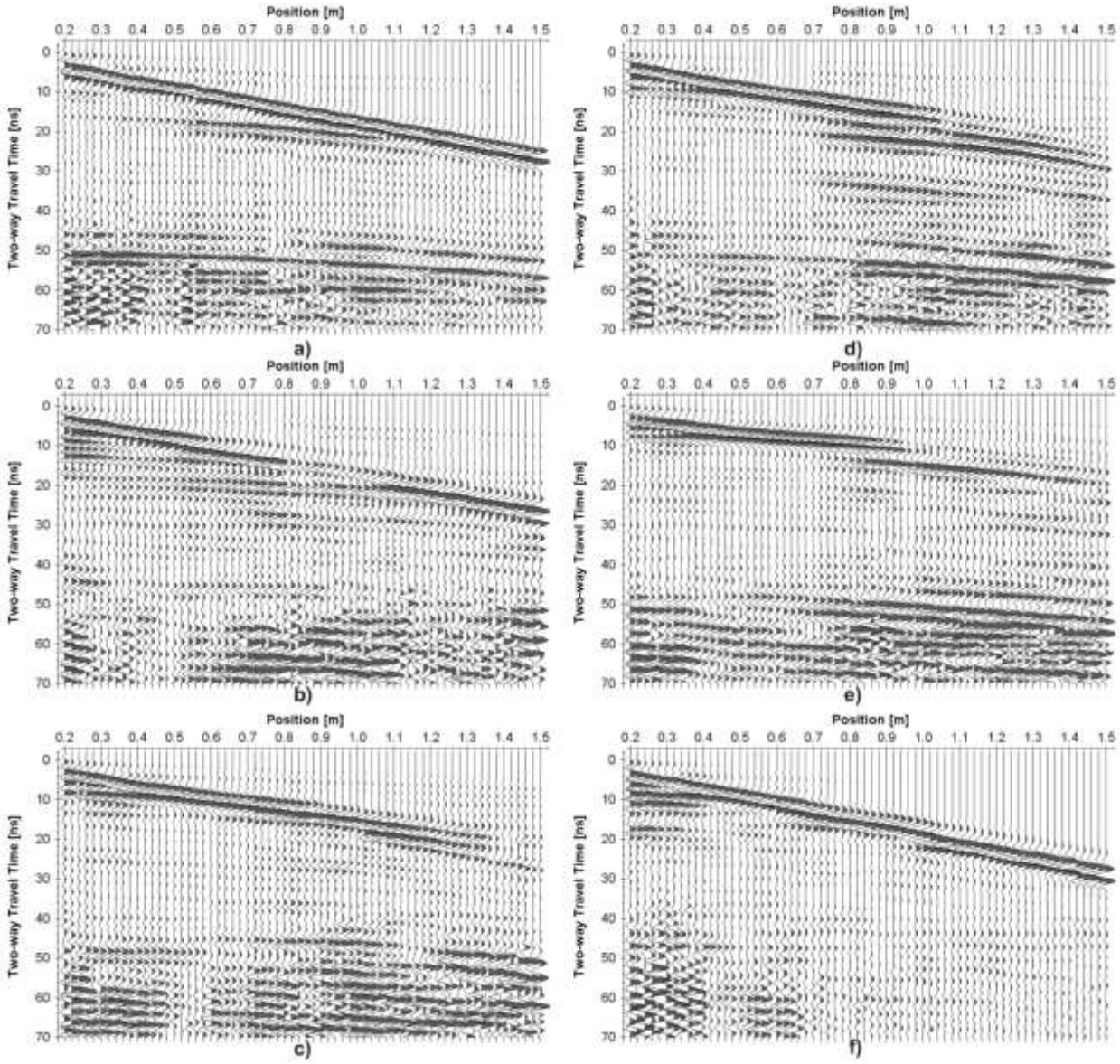

Figure 4.13 – Line C 450 MHz CMP centred at 3.2 m: a) Background-August 20; b) Day - 3August 25; c) Day 26-Septmeber 17; d) Day 116-December 16; e) Day 153–January 22; f) Day 308-June 26.

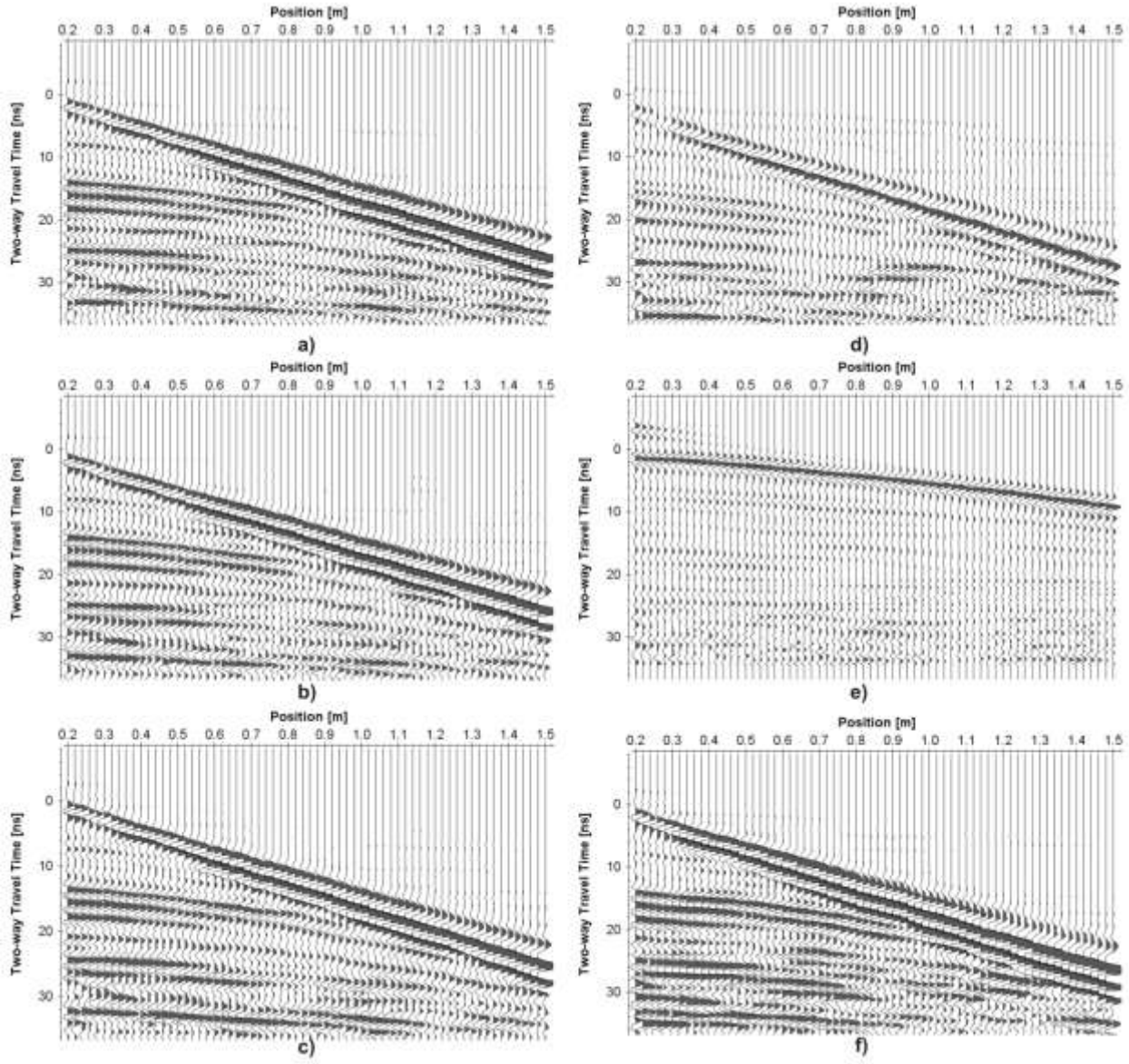

Figure 4.14 – Line 4 900 MHz CMP centred at 3.6 m: a) Background-August 20; b) Day -3August 25; c) Day 26-Septmeber 17; d) Day 116-December 16; e) Day 153–January 22; f) Day 308-June 26.

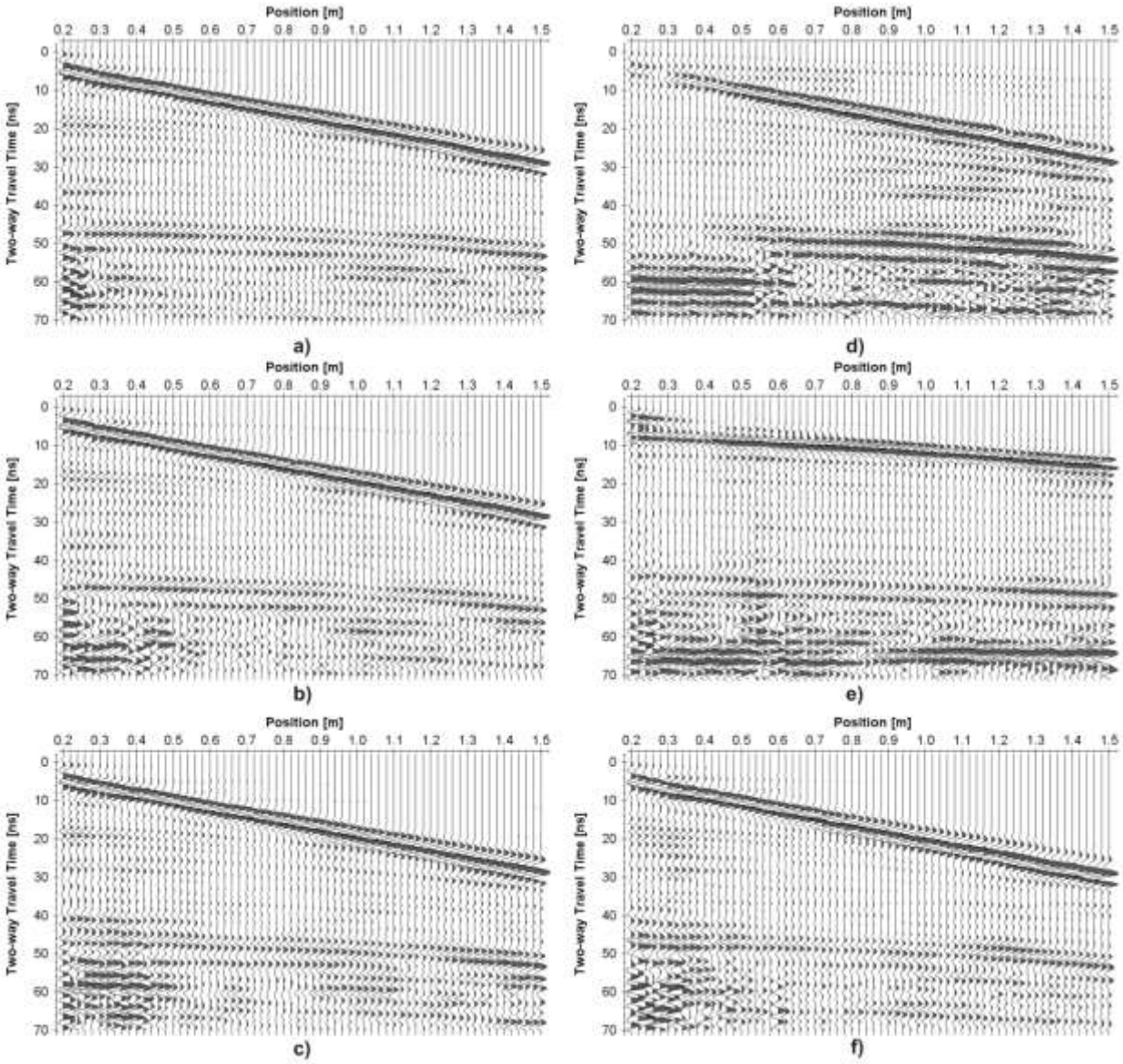

Figure 4.15 – Line 4 450 MHz CMP centred at 3.6 m: a) Background-August 20; b) Day -3August 25; c) Day 26-Septmeber 17; d) Day 116-December 16; e) Day 153–January 22; f) Day 308-June 26.

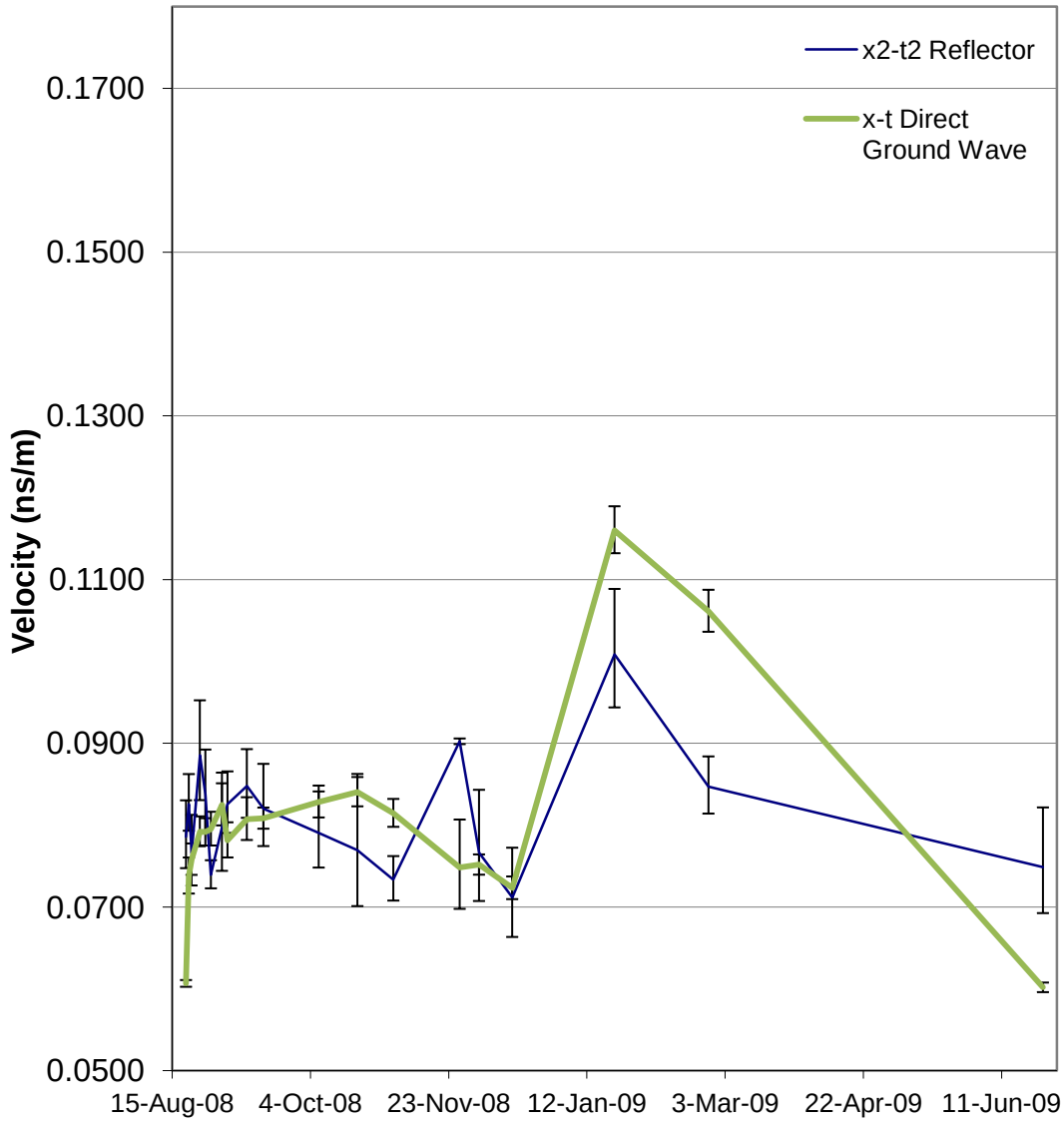

Figure 4.16 – Line C 900 MHz centered at 3.2 m velocity estimates for monitoring period.

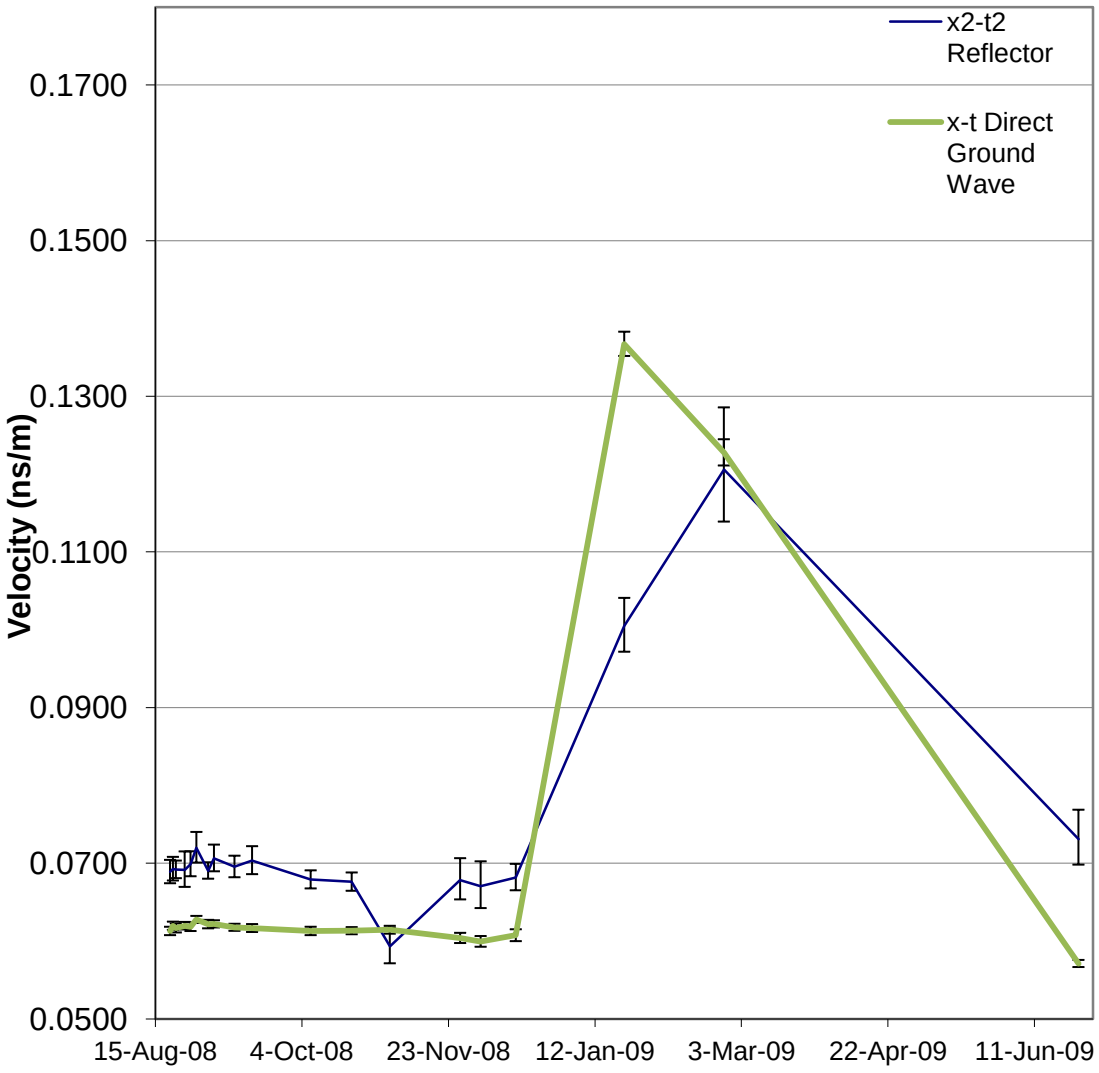

Figure 4.17 – Line 4 900 MHz centred at 3.6 m velocity estimates for monitoring period.

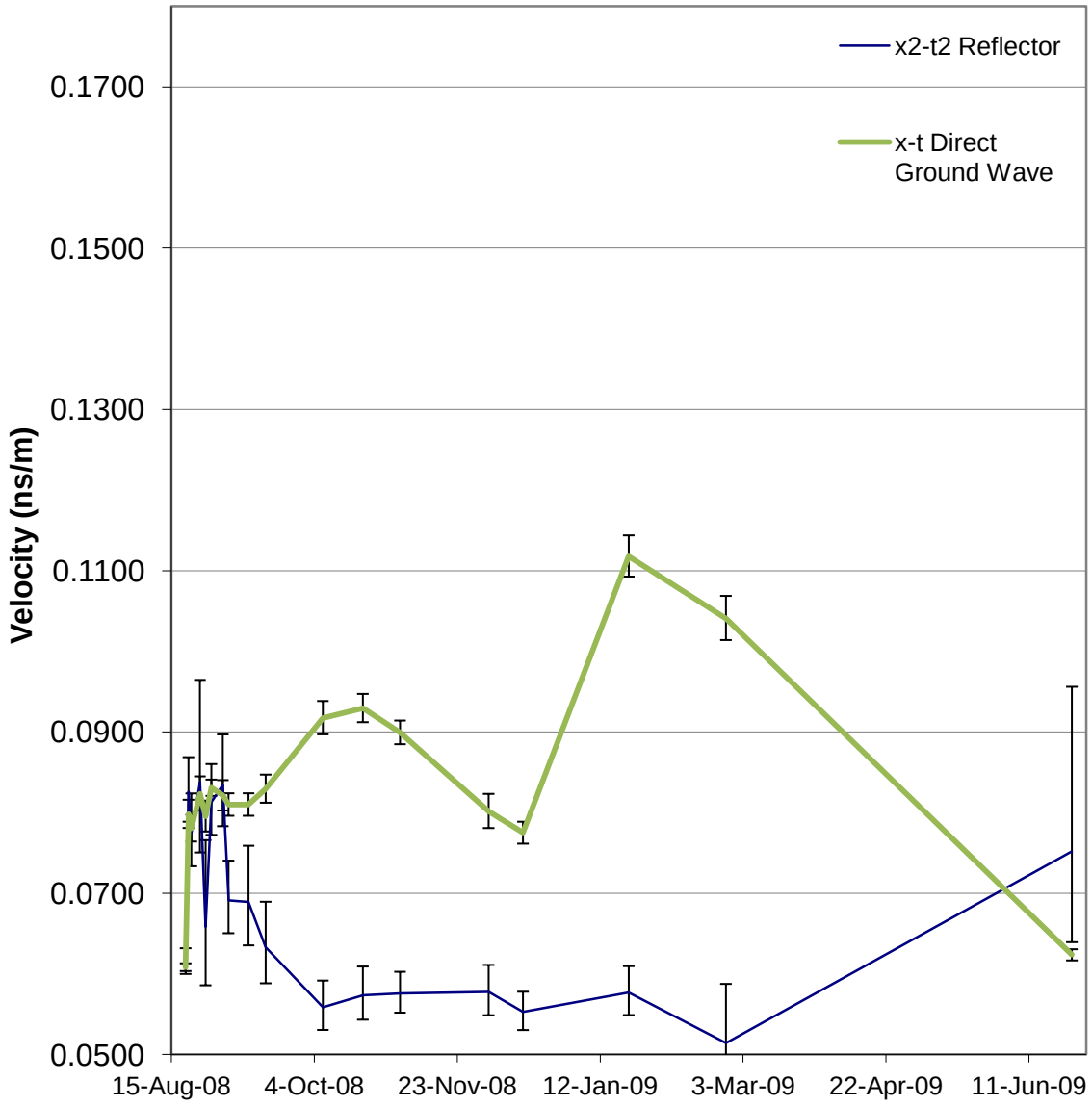

Figure 4.18 – Line C 450 MHz centered at 3.2 m velocity estimates for monitoring period.

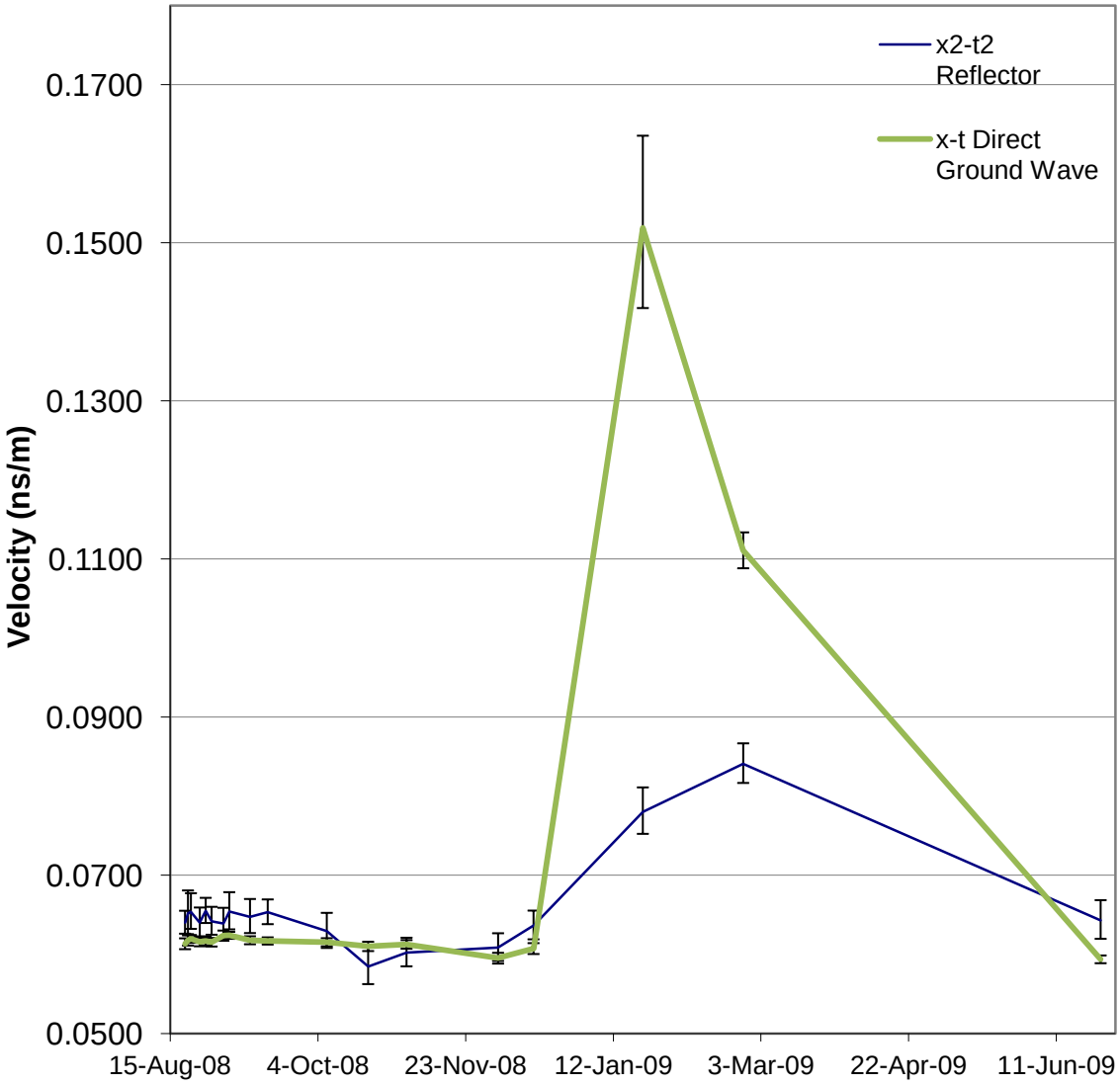

Figure 4.19 – Line 4 450 MHz centred at 3.6 m velocity estimates for monitoring period.

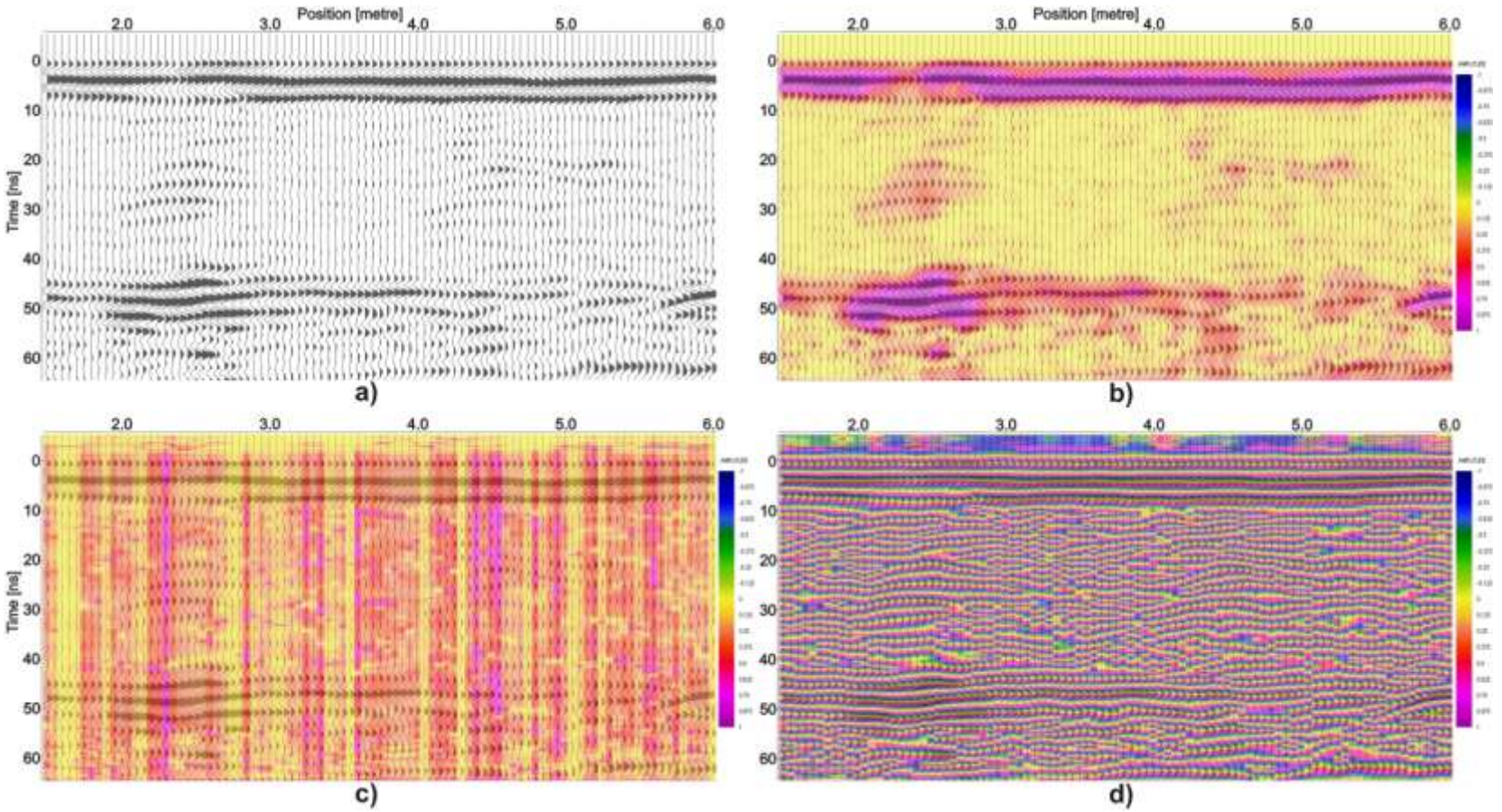

Figure 4.20 – Instantaneous attributes for Line B (Background-August 20) 450 MHz profile: a) Reflection profile, b) Instantaneous amplitude, c) Instantaneous frequency and d) Instantaneous phase. All of the instantaneous attribute results have a reflection profile overlay.

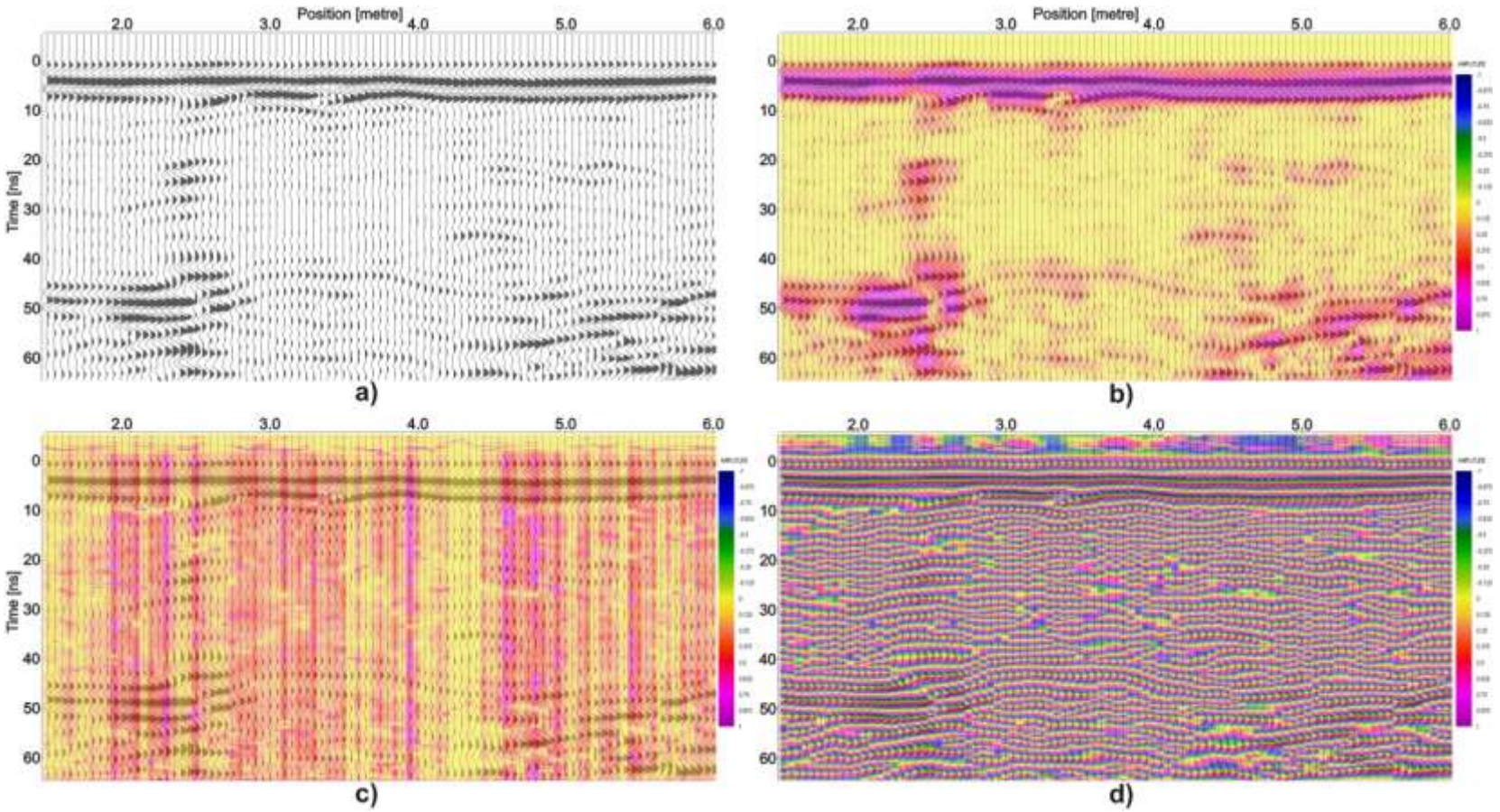

Figure 4.21 – Instantaneous attributes for Line B (Day 26-Septmeber 17) 450 MHz profile: a) Reflection profile, b) Instantaneous amplitude, c) Instantaneous frequency and d) Instantaneous phase. All of the instantaneous attribute results have a reflection profile overlay.

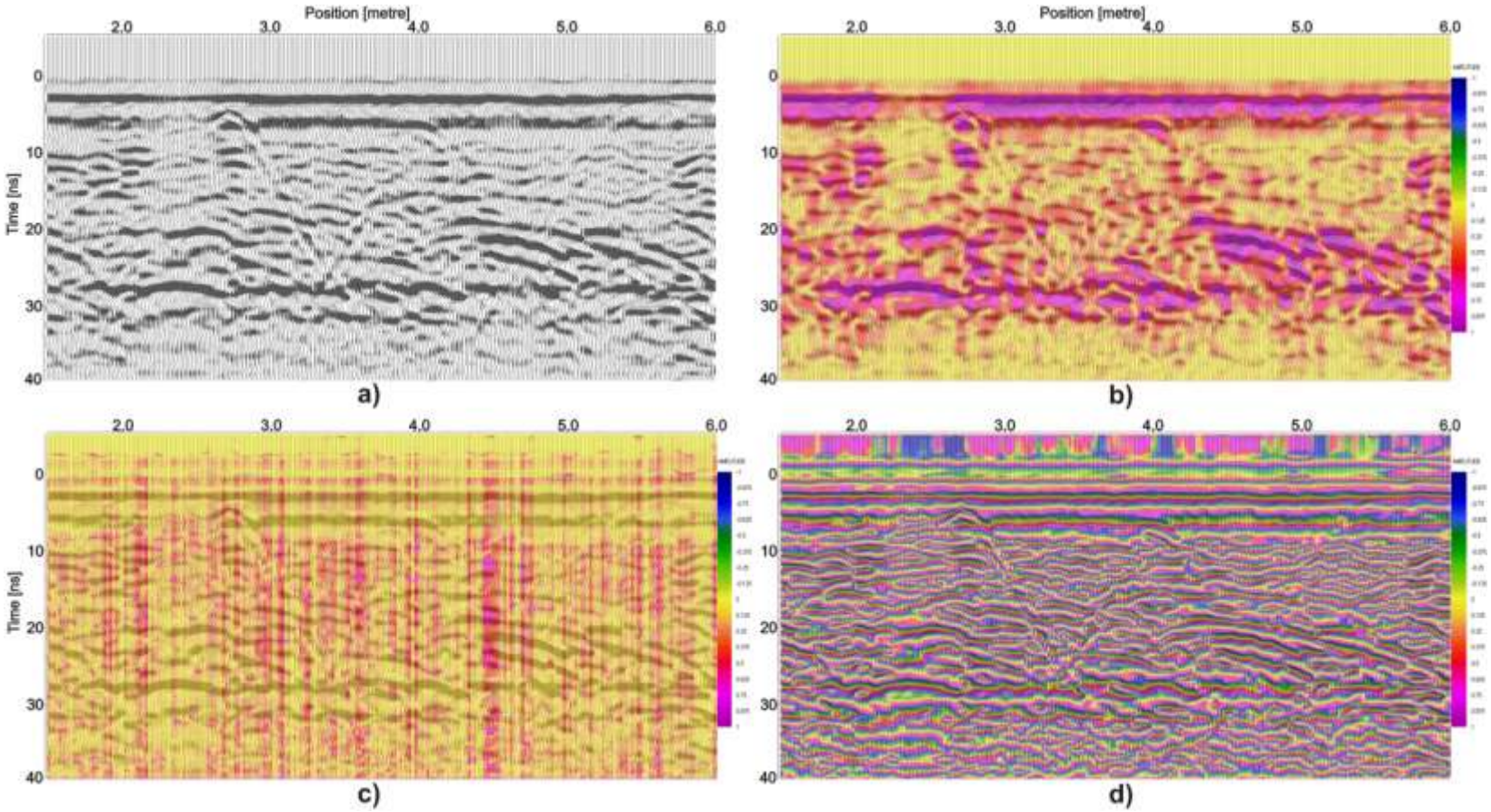

Figure 4.22 – Instantaneous attributes for Line B (Background-August 20) 900 MHz profile: a) Reflection profile, b) Instantaneous amplitude, c) Instantaneous frequency and d) Instantaneous phase. All of the instantaneous attribute results have a reflection profile overlay.

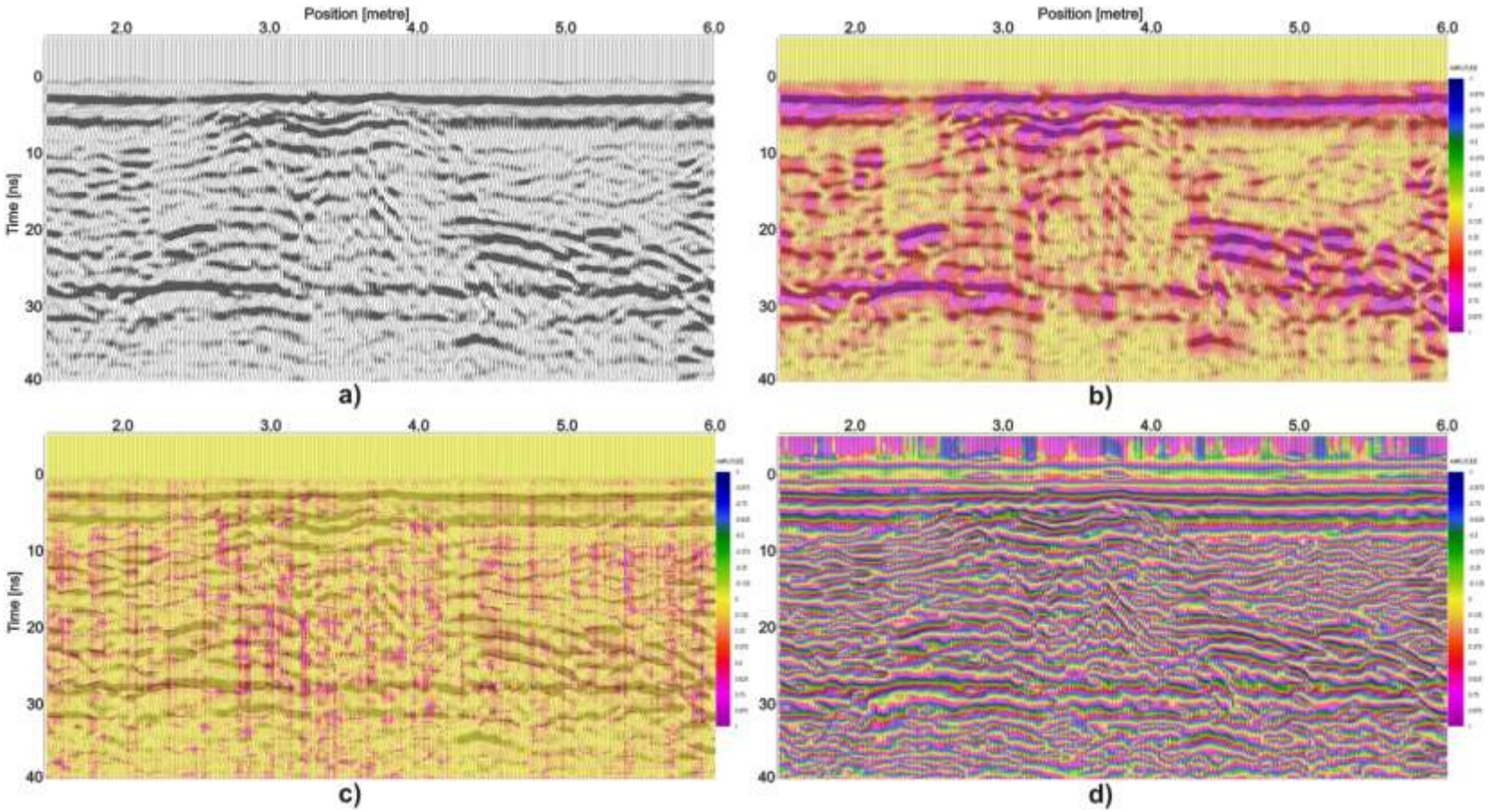

Figure 4.23 – Instantaneous attributes for Line B (Day 26-Septmeber 17) 900 MHz profile: a) Reflection profile, b) Instantaneous amplitude, c) Instantaneous frequency and d) Instantaneous phase. All of the instantaneous attribute results have a reflection profile overlay.

5.0 Traveltime and Amplitude Analysis

In an attempt to quantify the temporal and spatial variation in the GPR response due to the LNAPL release and its subsequent evolution, analyses of the traveltime changes in the 450 MHz profiling of the deep stratigraphic reflection and shallow reflection amplitude variations in 900 MHz profiling were done. This information was extracted from processed reflection profiles for selected events using ReflexW software.

5.1 Traveltime Differences from 450 MHz Profile

The 450 MHz reflection profiling data were used to determine the variations in two-way traveltime to the deep stratigraphic reflection between 40 ns – 50 ns that is continuous over the entire study area. Since this interface is fixed in location, variations in traveltime are due to changes in the EM wave velocity of the overlying medium. These velocity changes are most likely the result of variations on water content; caused by water table fluctuations and displacement of water by the immiscible LNAPL. To monitor velocity changes in the overlying medium, the traveltime measurements obtained after the gasoline release differenced with those obtained from the background data set given by the traveltime difference:

$$=$$ (19)

A positive traveltime difference indicates that medium overlying the stratigraphic reflection has a higher velocity than the background. Conversely, a negative traveltime difference shows that the medium has a lower velocity than the background. The direct ground wave is used as a reference in the traveltime determination to account for zero time variations between traces in the profile data set as well as between different monitoring dates.

Graphs of the traveltime difference for the 450 MHz profiles for Lines A, B, C, 2, 3 and 4 are given in Figures 5.1 – 5.6, respectively. Absence of high amplitude shallow reflections on the 900 MHz profiles after the release indicate that the immiscible gasoline pool did not extend

beneath Lines A and 4. The traveltime difference measurements performed on the 450 MHz Lines A and 4 are consistent with this finding (Figures 5.1 and 5.6). In particular, the 450 MHz traveltime difference profiles along each of these lines on any given date exhibit relative small amplitude spatial variations, indicating that the overlying medium is laterally uniform. The 450 MHz traveltime difference profiles for subsequent monitoring dates appear to be bulk shifted; this type of response would be expected from water table fluctuations that impact the entire cell.

In comparison, the appearance of high amplitude shallow reflections on the 900 MHz profiles after the release indicates the presence of the immiscible gasoline pool along Lines B, C, 2 and 3. The 450 MHz traveltime difference measurements for these lines given in Figures 5.2, 5.3, 5.4 and 5.5, respectively, support this interpretation. For each of these lines, the 450 MHz traveltime difference profiles exhibit a region of significantly large positive traveltime difference that correlates with the position of the gasoline pool imaged on corresponding 900 MHz profiles. This positive traveltime difference is due to the displacement of lower velocity water by higher velocity LNAPL, which resulted in what is commonly referred to in seismic reflection profiling as a "velocity pull-up" feature. Velocity pull-up features have been documented by previous Borden DNAPL (Brewster and Annan, 1994) and LNAPL (DeRyck 1994) experiments. Further, it can be qualitatively observed that the magnitude of these velocity pull-up features exhibit general decreasing trend over the long term. While this progressive reduction in the pull-up magnitude could indicate removal of the immiscible gasoline phase from the original impacted zone, these traveltime differences could also reflect EM wave velocity of the gasoline impacted zone due to water table fluctuations.

To examine the spatial variability of the traveltime differences for the deep stratigraphic reflection, planviews of the data set were generated using Surfer version 8 (Golden Software Incorporated). The Inverse Distance to a Power was the method used to contour the data. The locations of the profile lines with the planview area are shown in Figure 5.7. The planview for selected monitoring dates are given in Figures 5.8-5.14.

The planviews for the initial period after the release during fall water table condition (Figures 5.8-5.10) show progressively increasing traveltime differences. The planeviews during unfrozen conditions for the remainder of monitoring period (Figures 5.11, 5.12 and 5.14) show

much lower values and become similar in magnitude to the variations in the unimpacted areas. All of these unfrozen planviews of the traveltime difference data suggest that the gasoline pool initially formed in the vicinity of the release trench and did not significantly spread during the experiment. The plan view for the frozen conditions (Figure 5.13) clearly illustrates the presence of the velocity pull-up is dependent on the large dielectric contrast between gasoline and water. When water freezes into ice, its dielectric permittivity decreases from κ ~80 to κ = 3.2, a value that is very close to those of LNAPLs (i.e., κ = 2-5).

5.2 Reflection Amplitude from 900 MHz Profile

In an attempt to quantify and examine the spatial pattern of the increased reflectivity associated with the LNAPL release, three time slices at 8 ns, 10 ns and 12 ns were constructed using the 900 MHz reflection profiling data. These three time levels were selected to avoid the effects of the superposition of the ground waves .The background amplitude for each line has been subtracted to remove the effects of pre-existing events (i.e., stratigraphic reflections, scattering from sampling wells).

The results for selected monitoring dates are given in Figures 5.15-5.20. The 10 ns and 12 ns time slices (i.e., Panels b and c on Figures 5.15-5.20) show little, if any, consistent pattern in reflectivity changes. The 8 ns time slices (i.e., Panel a on Figures 5.15-5.20) exhibits significant amplitude changes in the vicinity of the release trench; however, there is no consistent spatial pattern discernable in the results. These results show the shortcomings of a simple time slicing technique given the complexity of the reflection events from LNAPL impacted zone.

5.3 Complex Refractive Index (CRI) Model Analysis

The CRI model described in Section 2.4 can be used to obtain an estimate of the thickness of the LNAPL impacted zone from the velocity pull-up measurements. This analysis was done using a simple two-layer case. Both layers have the porosity value ϕ = 0.33 given by MacKay et al. (1986) for Borden sand. The first layer represents LNAPL impacted Borden sand at residual water saturation (θ_r = 0.06) with the remainder of pore space occupied by the released

gasoline (θ_{NAPL} = 0.27). The second layer represents clean Borden sand that is totally saturated with water (θ = 0.33).

Using the component dielectric permittivities from Table 2.2, one obtains following effective permitivities for each layer: ε_{c1} = 6 for Layer 1 and ε_{c2} = 20 for Layer 2. These permittivity values correspond to EM wave velocities of v_1 = 0.125 m/ns for Layer 1 and v_2 = 0.067 m/ns for Layer 2.

From the pull-up we observe in the 450 MHz profile over the gasoline release, we see an increase in the two-way traveltime to a horizontal reflector. Using the traveltime difference analysis from Section 5.1, the pull-up caused by the LNAPL directly over the release appears to have shifted the direct ground wave an average of approximately 6 ns sooner; than observed in the background data (Figures 5.2, 5.3 and 5.5). Using these values, we can obtain the thickness of released gasoline in residually saturated Borden sand from Equation (18), for this case we find z_{NAPL} = 0.17 m. This estimate represents a minimum thickness since we are assuming gasoline completely replaces water in the pore spaces until residual water saturation. The calculated z_{NAPL} compares with soil cores taken by Freitas (2009) within the LNAPL release that estimate the height of gasoline at 0.3 m above the water table.

5.4 Comparison of GPR data to other field observations

Freitas (2009) took cores within the cell near the release zone (Figure 4.3) and found that ethanol and some gasoline components were retained in the variably saturated zone above the capillary fringe. The cores were collected within 0.5 m of the release zone. The results reported by Freitas (2009) are shown in Figure 5.21. It can be seen that substantial amounts of ethanol and LNAPL are present in these cores. These results correlate with the presence of high reflectivity and velocity pull-up observed on the 900 MHz and 450 MHz reflection profiling data, respectively, at the coring locations.

The surface expression of the red dyed LNAPL (Figure 3.1) observed after the September 2009 water table rise can be can be presumed to represent the areal extent of the released LNAPL since the mobile free phase LNAPL floats on the water table. This large upward fluctuation in the water table forced the dyed LNAPL to the surface during this event. The high reflectivity

and velocity pull-up observed in the GPR profiling on the September 11 and 17 monitoring dates along Lines B, C, 2 and 3 correlate well with the areal extent of the stained area at surface.

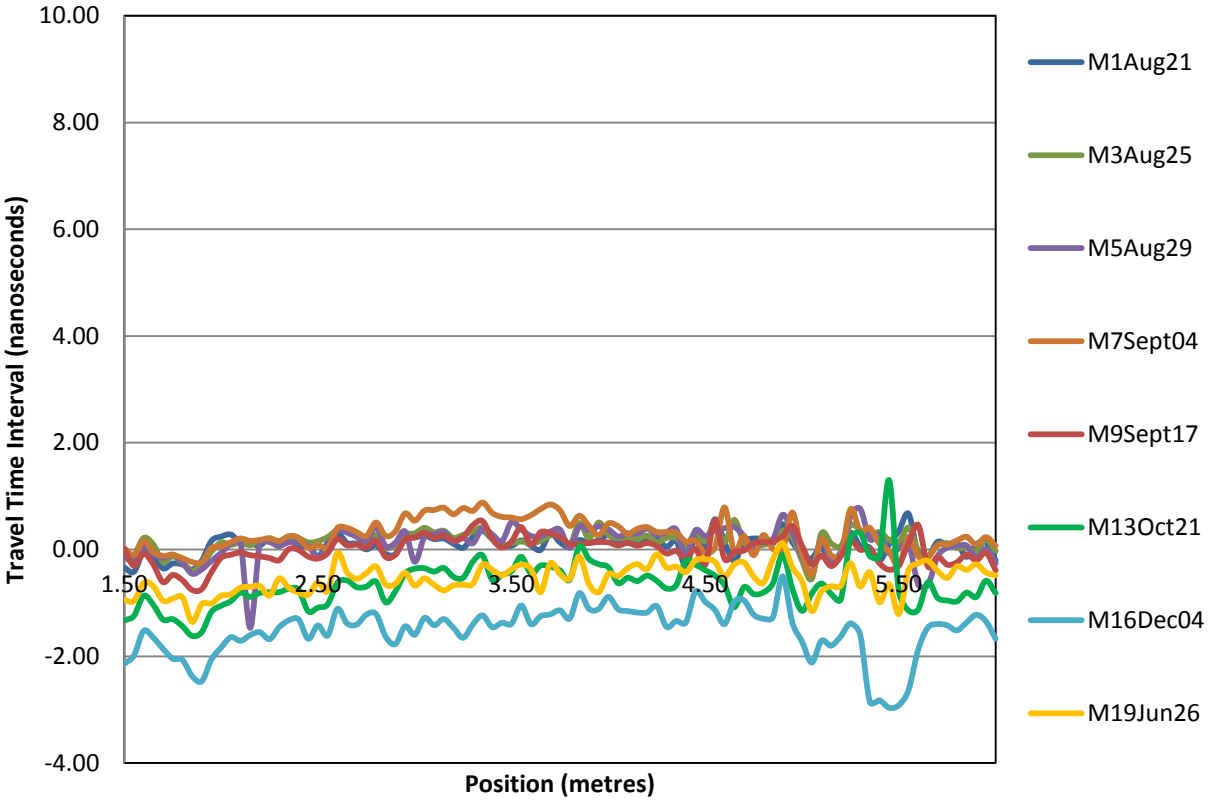

Figure 5.1 – Traveltime difference for the deep stratigraphic reflection obtained from the 450 MHz profiling along Line A.

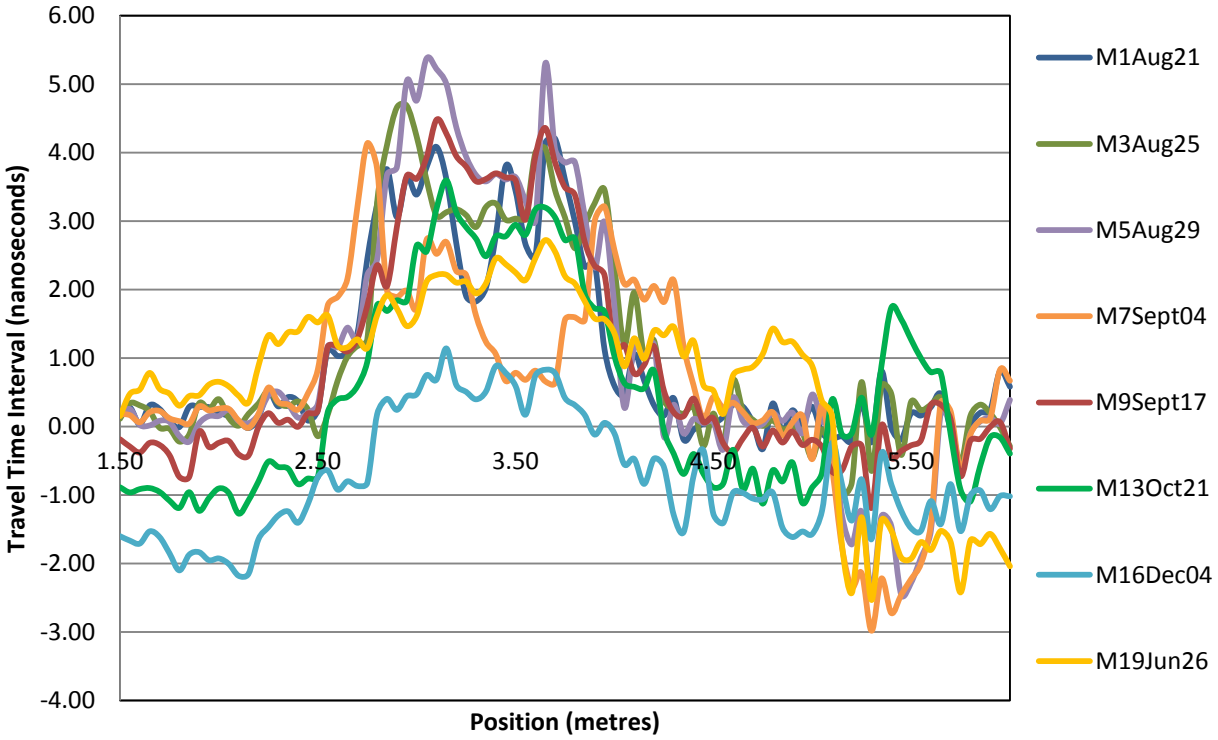

Figure 5.2 – Traveltime difference for the deep stratigraphic reflection obtained from the 450 MHz profiling along Line B.

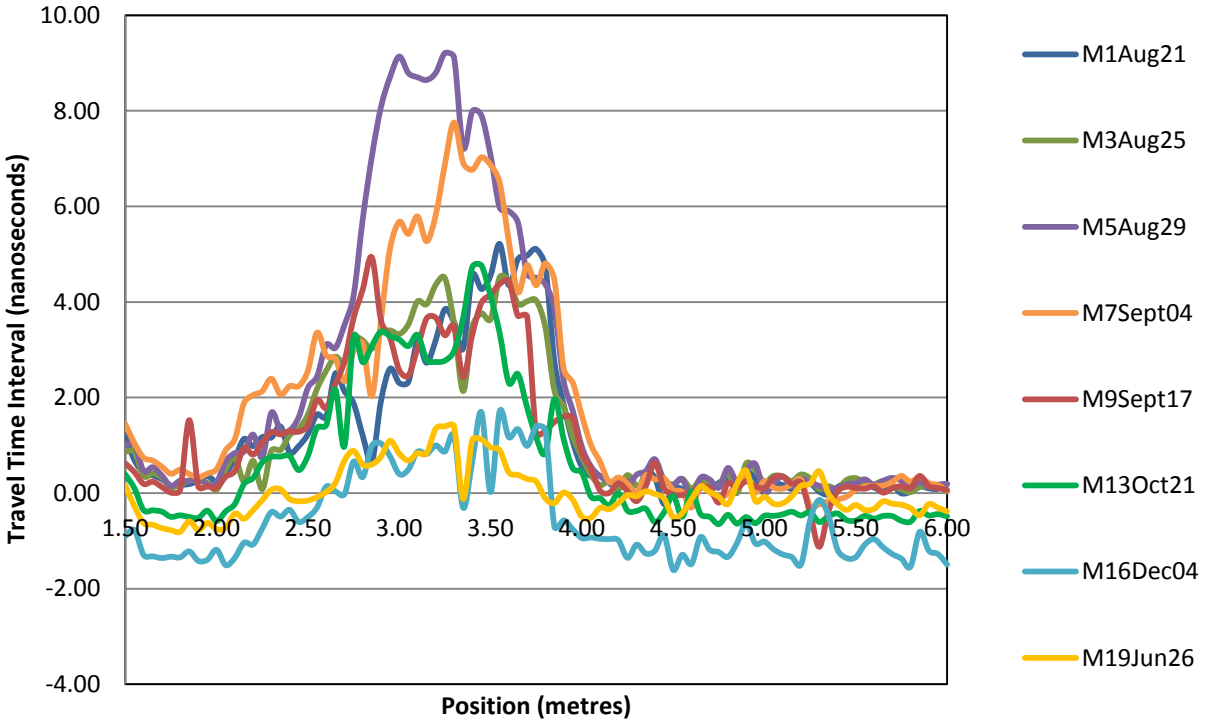

Figure 5.3 – Traveltime difference for the deep stratigraphic reflection obtained from the 450 MHz profiling along Line C.

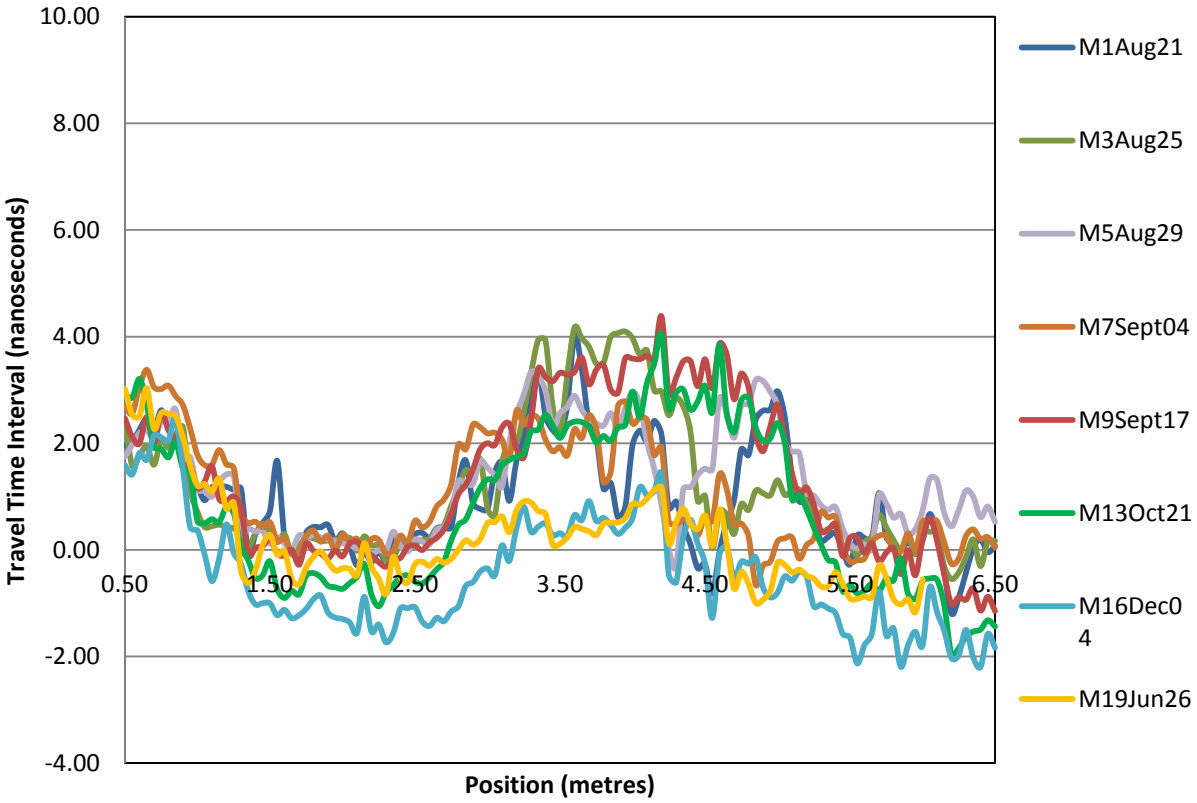

Figure 5.4 – Traveltime difference for the deep stratigraphic reflection obtained from the 450 MHz profiling along Line 2.

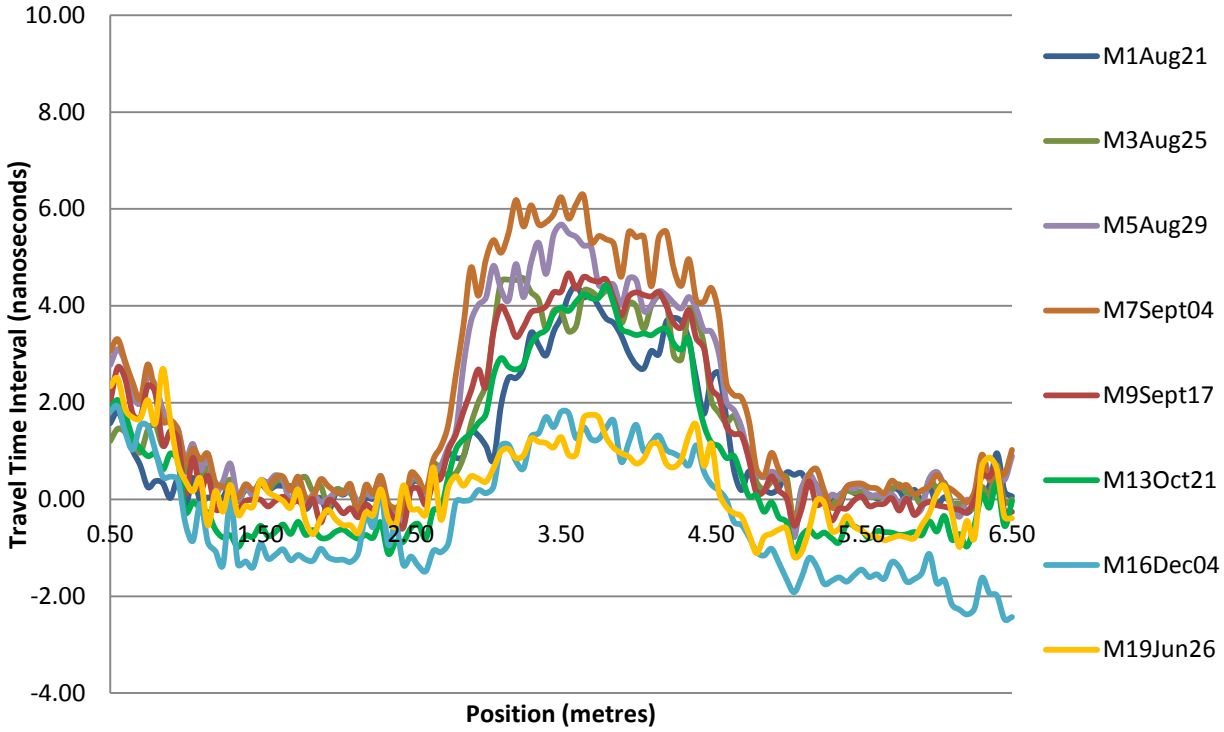

Figure 5.5 – Traveltime difference for the deep stratigraphic reflection obtained from the 450 MHz profiling along Line 3.

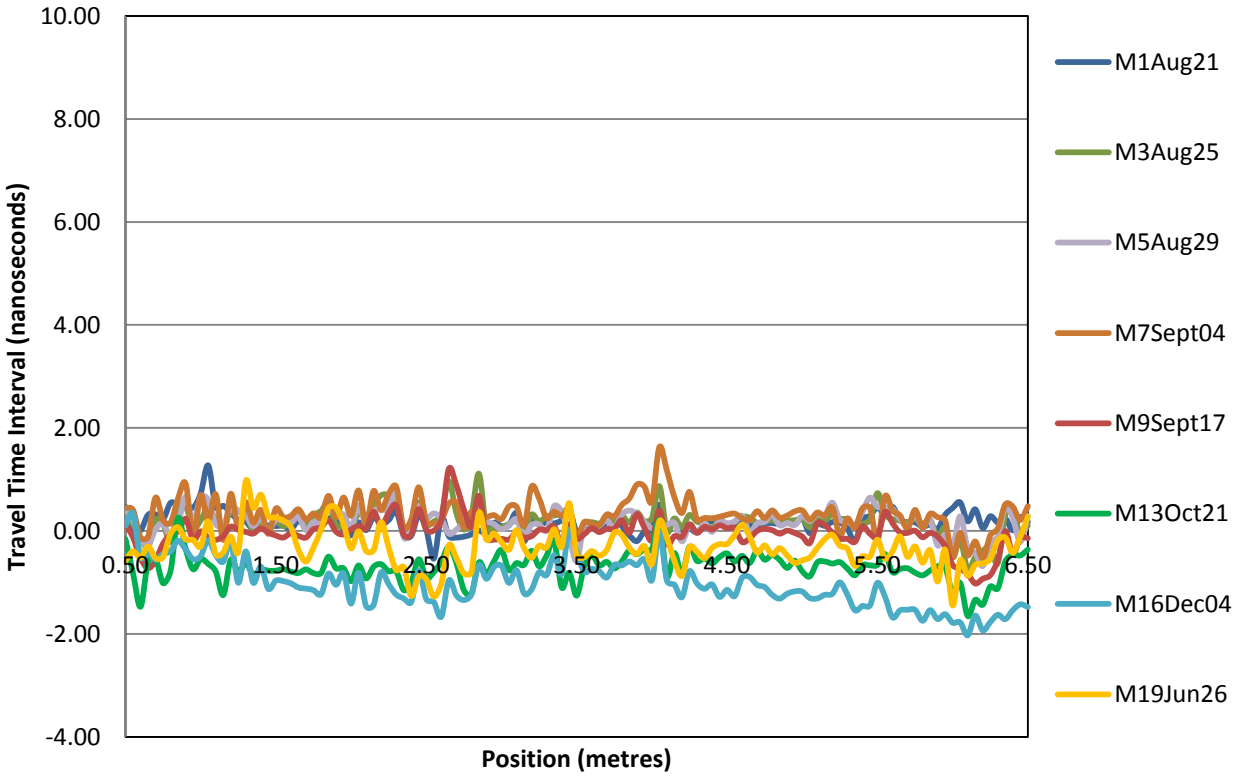

Figure 5.6 – Traveltime difference for the deep stratigraphic reflection obtained from the 450 MHz profiling along Line 4.

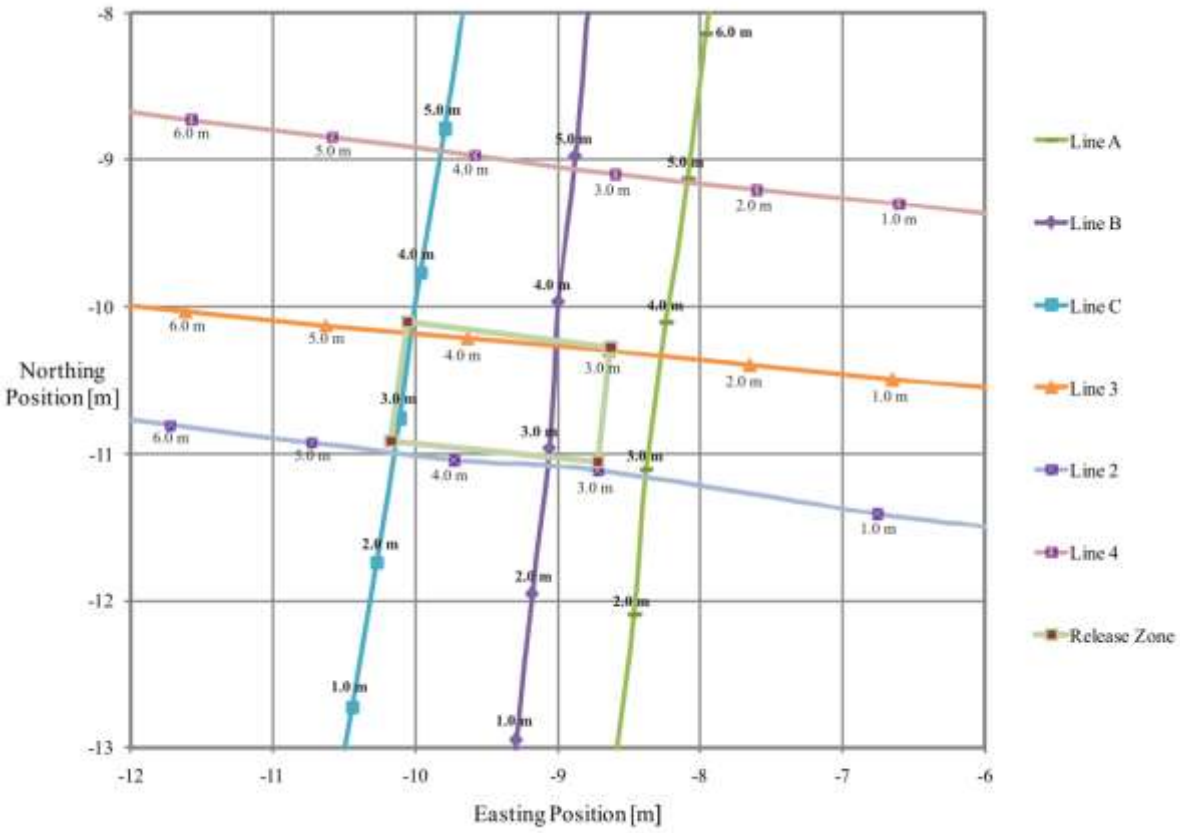

Figure 5.7 – Surveyed positions of GPR profile lines used to construct planviews. Dark grey grid lines and axis are northings and eastings from a benchmark; GPR profile lines appear skewed since they are aligned with the experimental cell. Bold numbers above marker indication metre position on Lines A, B and C. Regular number below marker indication metre position on Lines 2, 3 and 4 for GPR grid.

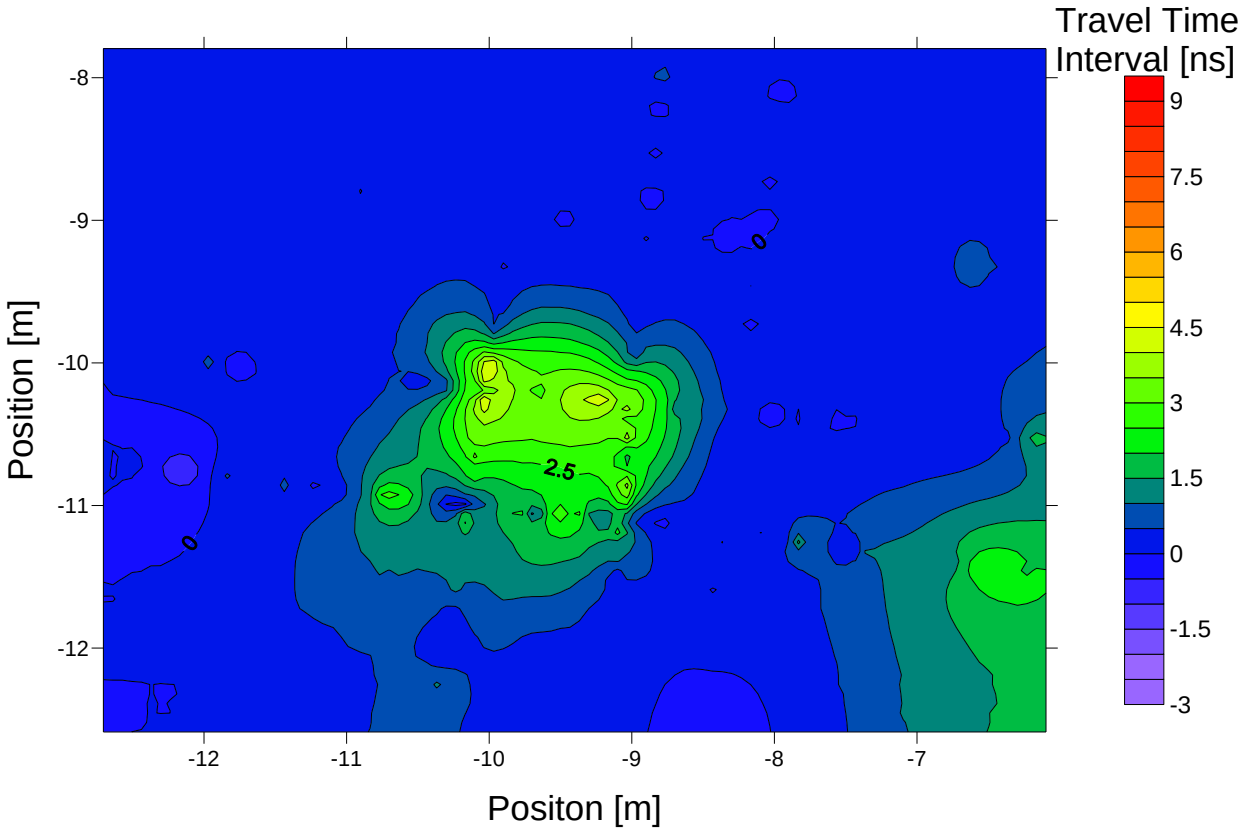

Figure 5.8 – Planview of the deep stratigraphic reflection traveltime differences obtained from the 450 MHz profiling for Day 0 (August 21 2008). Contour interval = 0.5 nanoseconds (ns).

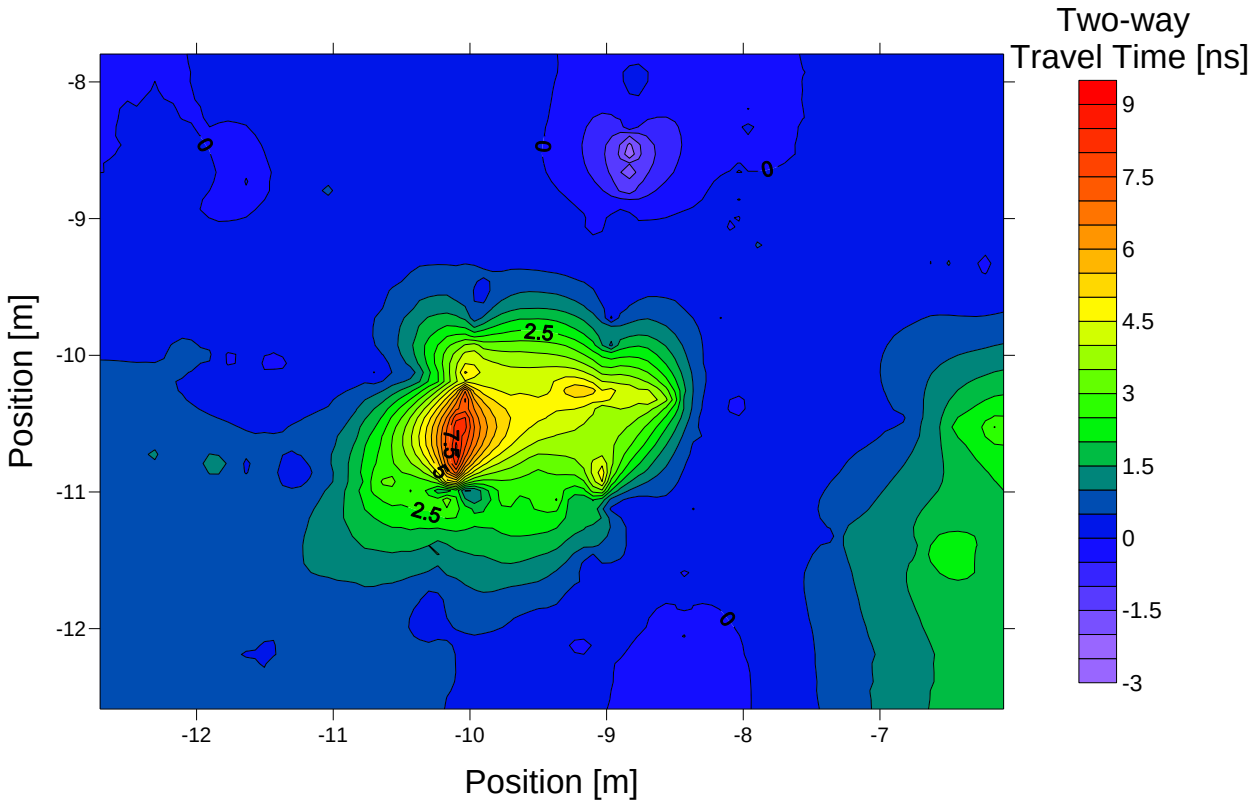

Figure 5.9 – Planview of the deep stratigraphic reflection traveltime differences obtained from the 450 MHz profiling for Day 7 (August 29 2008). Contour interval = 0.5 nanoseconds (ns).

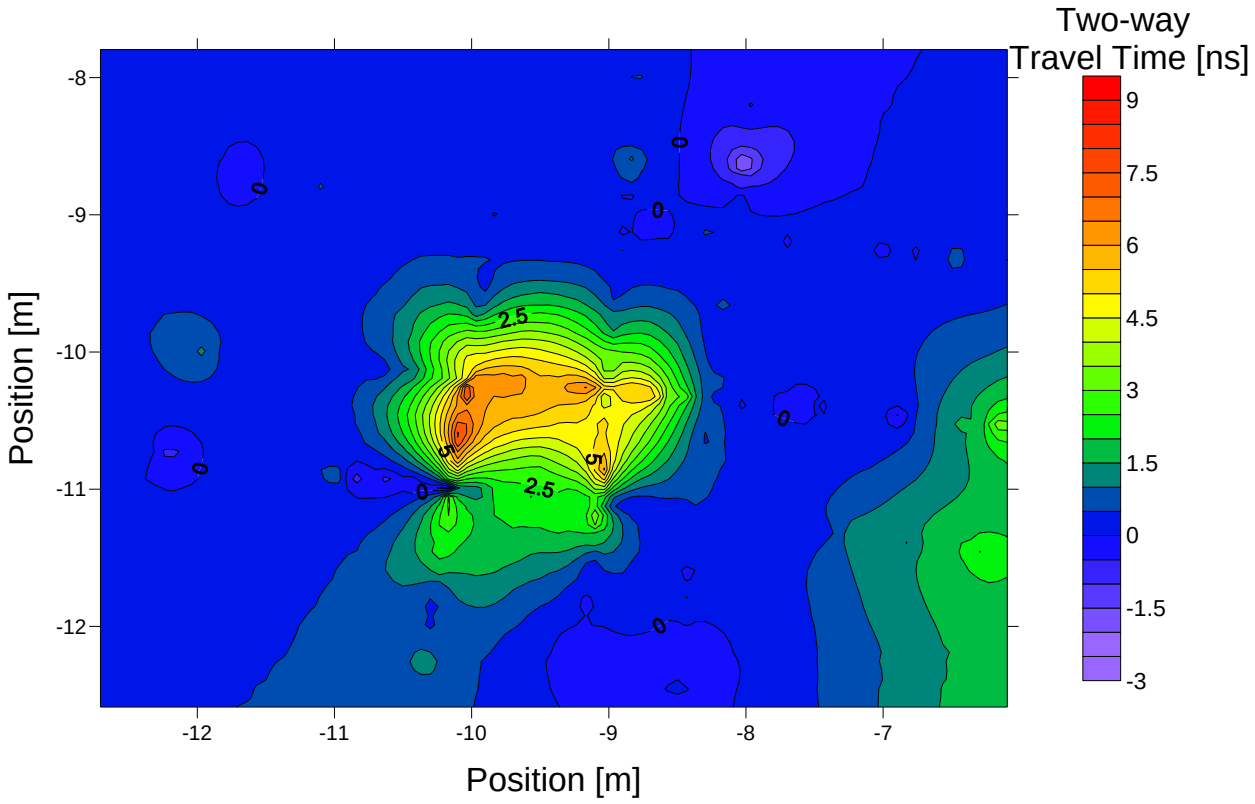

Figure 5.10 – Planview of the deep stratigraphic reflection traveltime differences obtained from the 450 MHz profiling for Day 20 (September 11 2008). Contour interval = 0.5 nanoseconds (ns).

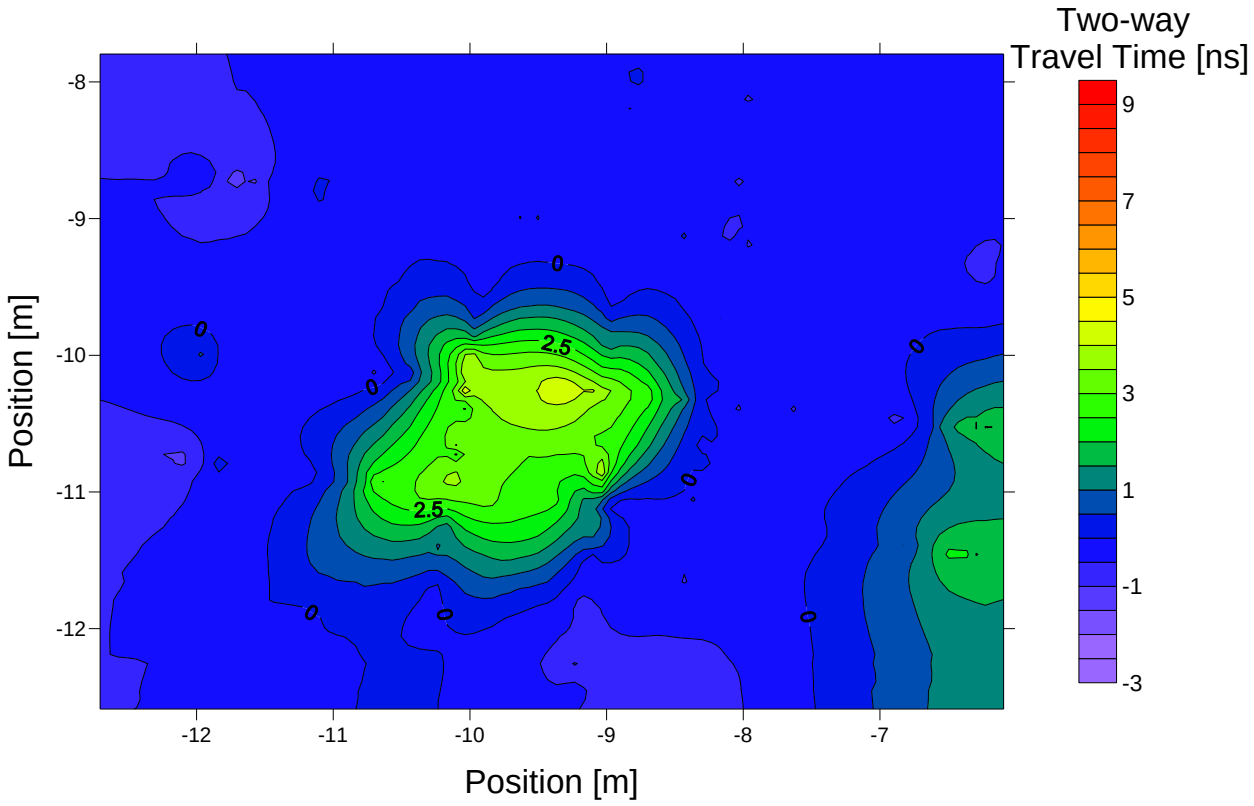

Figure 5.11 – Planview of the deep stratigraphic reflection traveltime differences obtained from the 450 MHz profiling for Day 73 (November 3 2008). Contour interval = 0.5 nanoseconds (ns).

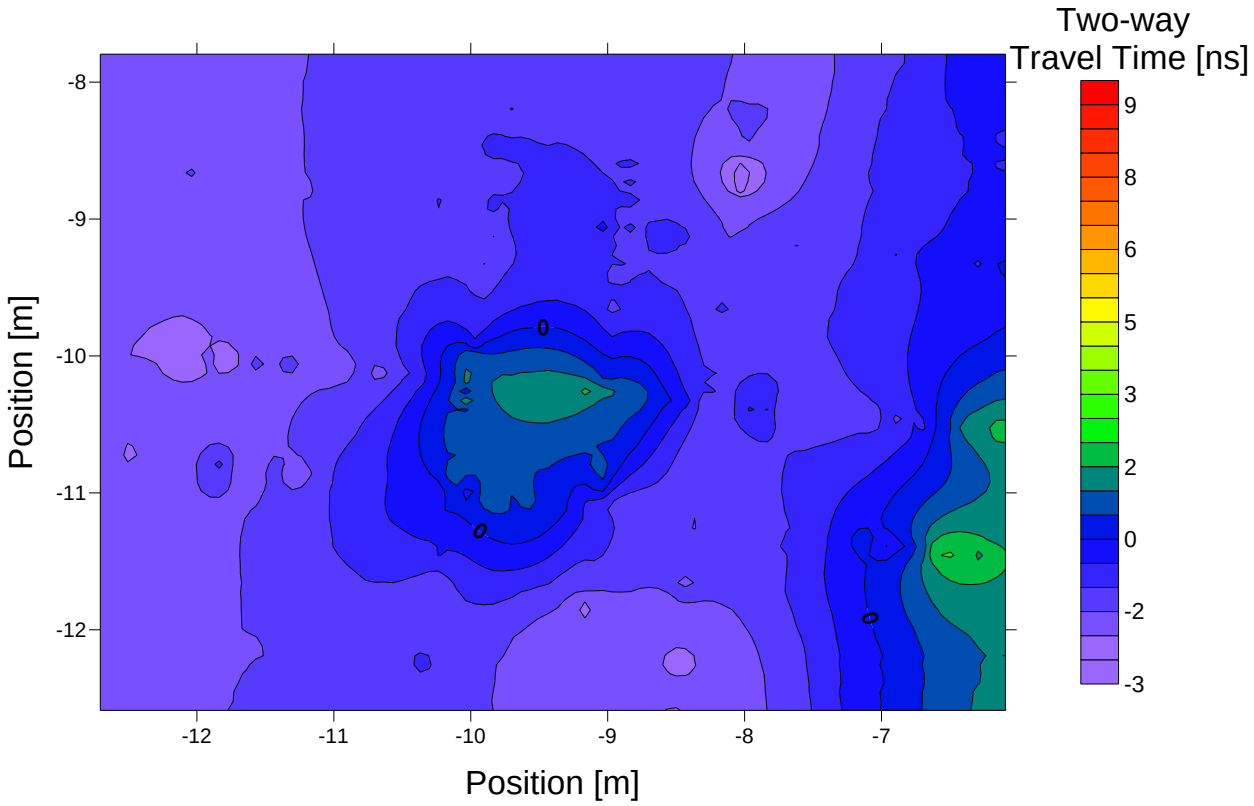

Figure 5.12 – Planview of the deep stratigraphic reflection traveltime differences obtained from the 450 MHz profiling for Day 116 (December 16 2008). Contour interval = 0.5 nanoseconds (ns).

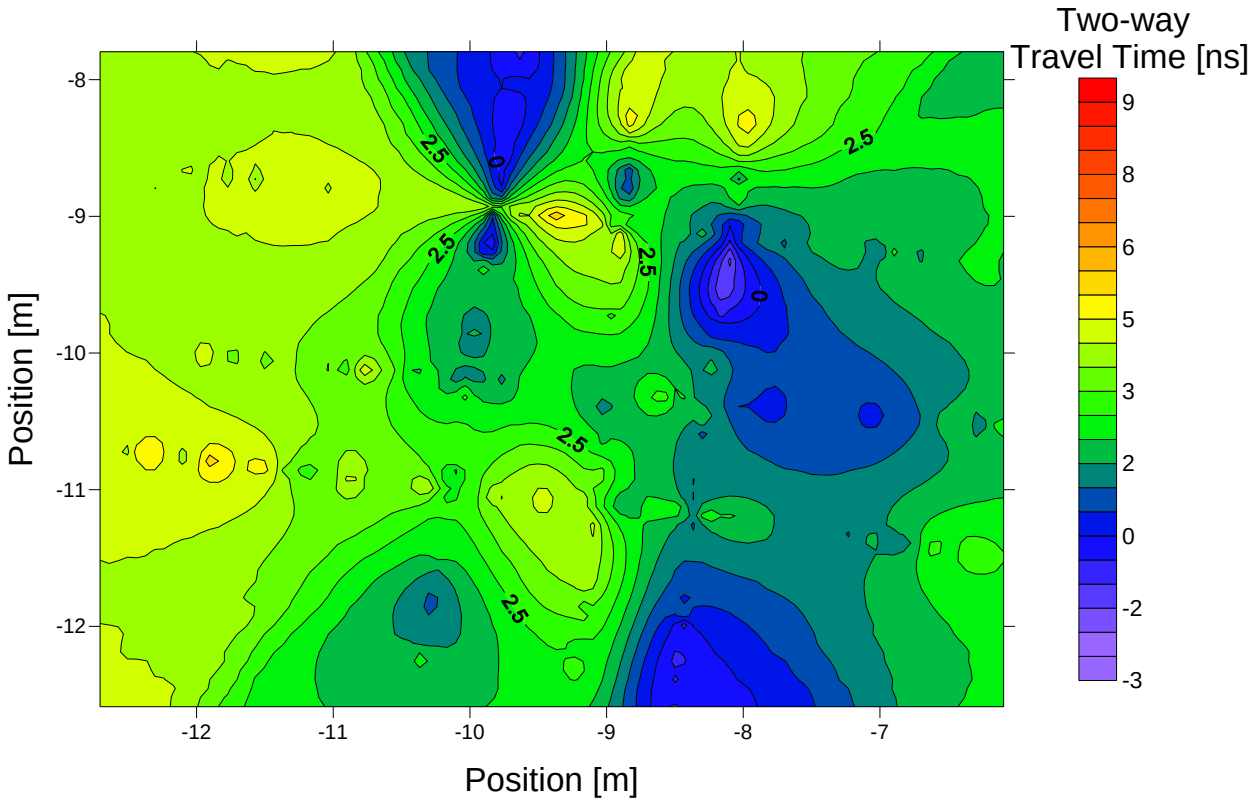

Figure 5.13 – Planview of the deep stratigraphic reflection traveltime differences obtained from the 450 MHz profiling for Day 153 (January 22 2009). Contour interval = 0.5 nanoseconds (ns).

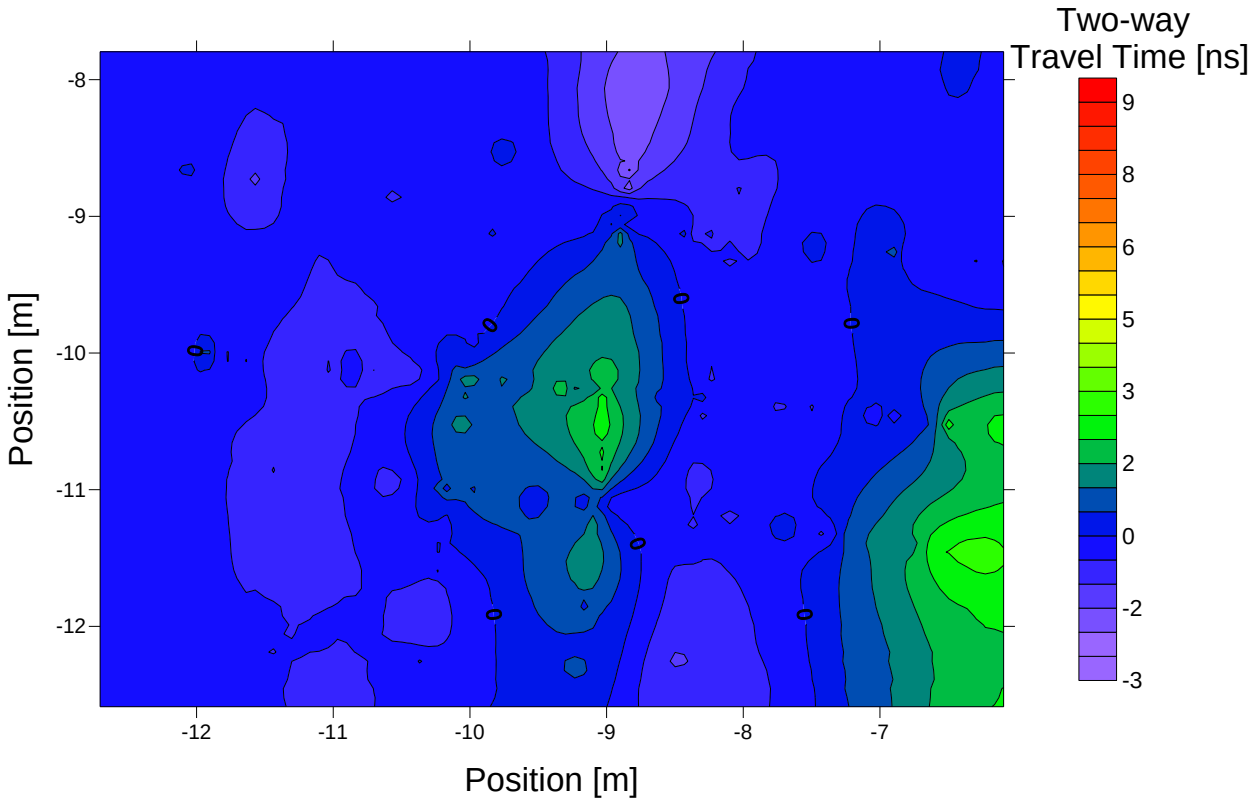

Figure 5.14 – Planview of the deep stratigraphic reflection traveltime differences obtained from the 450 MHz profiling for Day 308 (June 26 2009). Contour interval = 0.5 nanoseconds (ns).

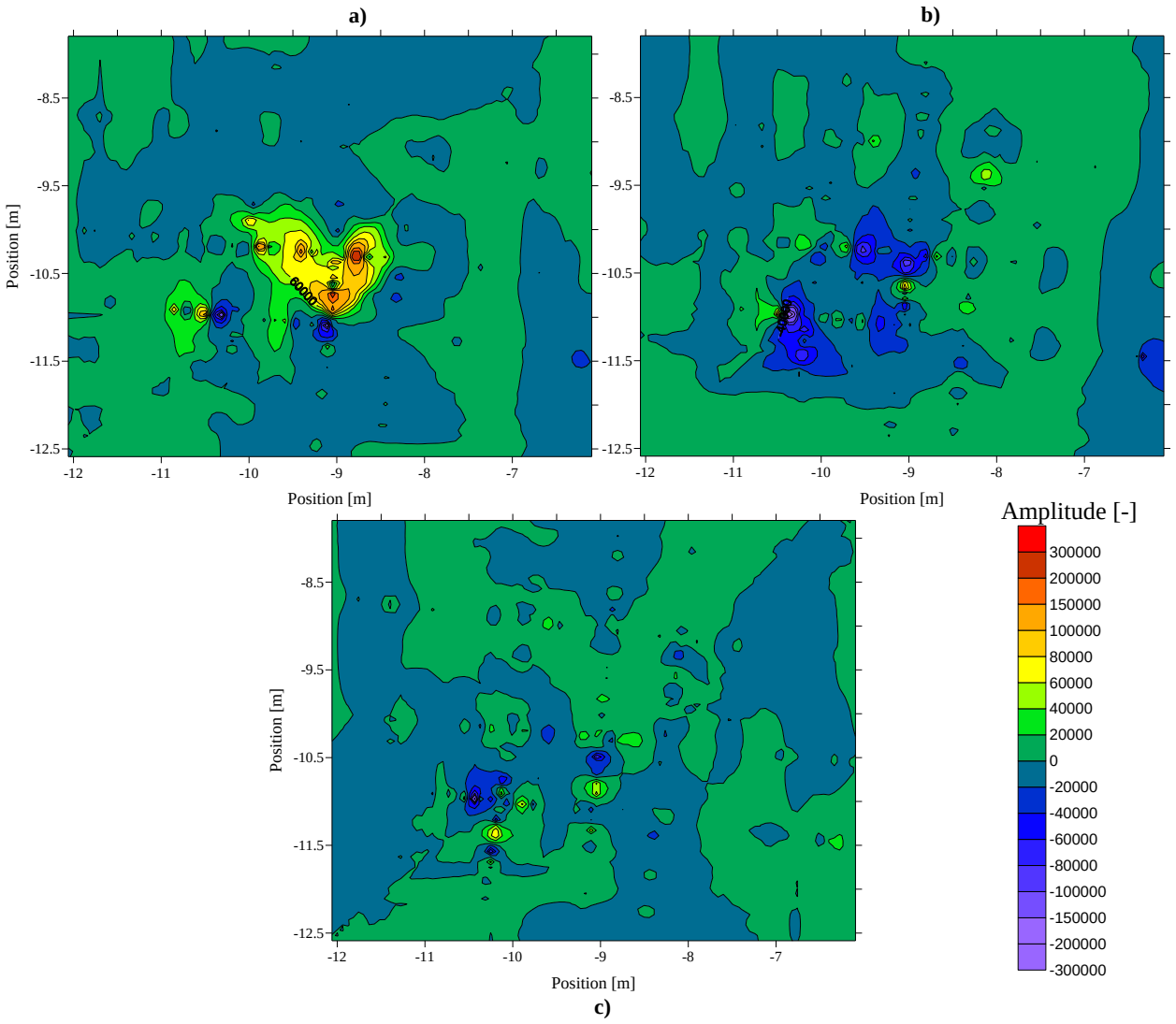

Figure 5.15 – Contoured amplitude from 900 MHz reflection profile data for Day 0 (August 21 2008). Amplitude is dimensionless. a) 8 ns time slice, b) 10 ns time slice and c) 12 ns time slice.

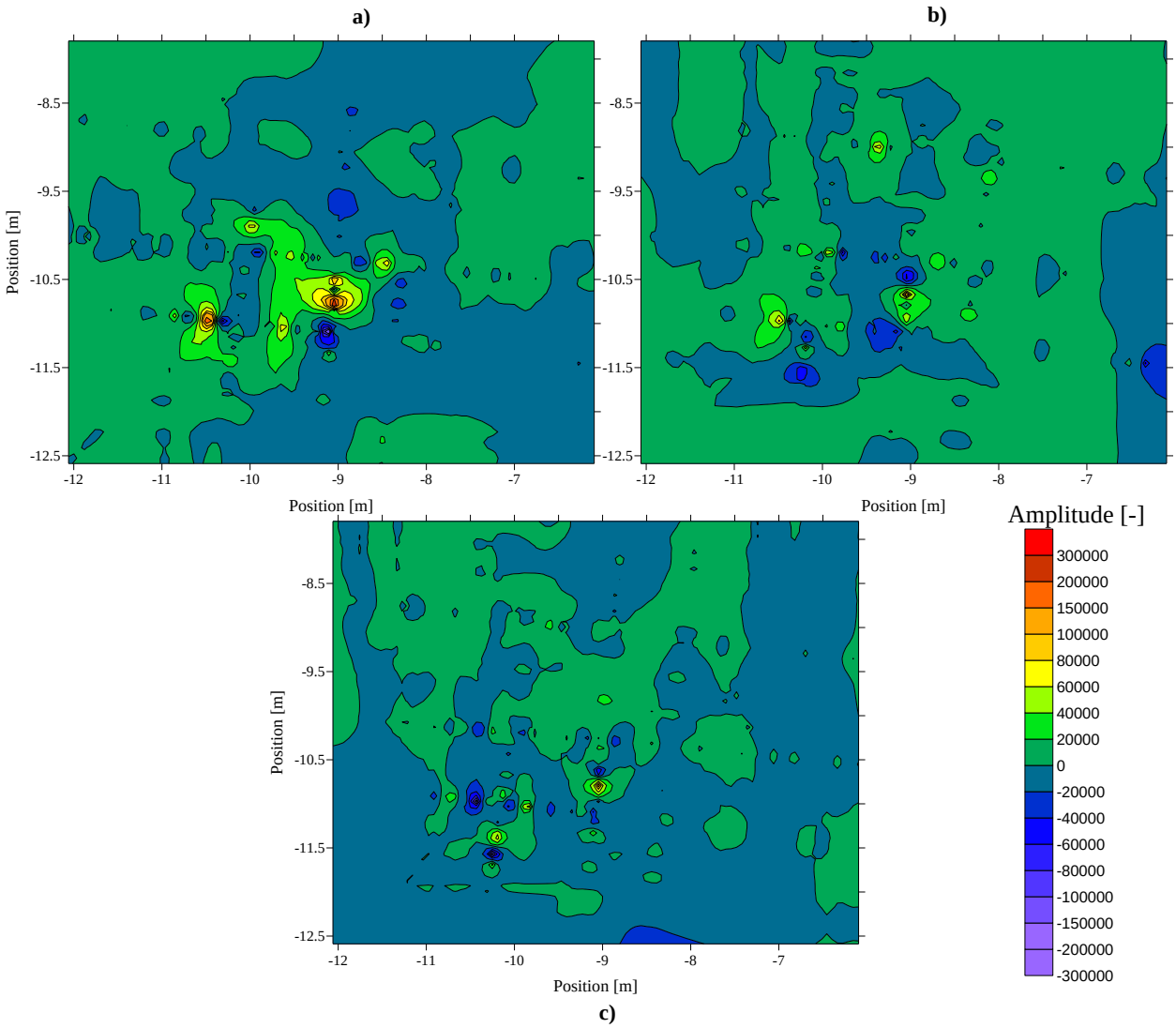

Figure 5.16 – Contoured amplitude from 900 MHz reflection profile data for Day 3 (August 25 2008). Amplitude is dimensionless. a) 8 ns time slice, b) 10 ns time slice and c) 12 ns time slice.

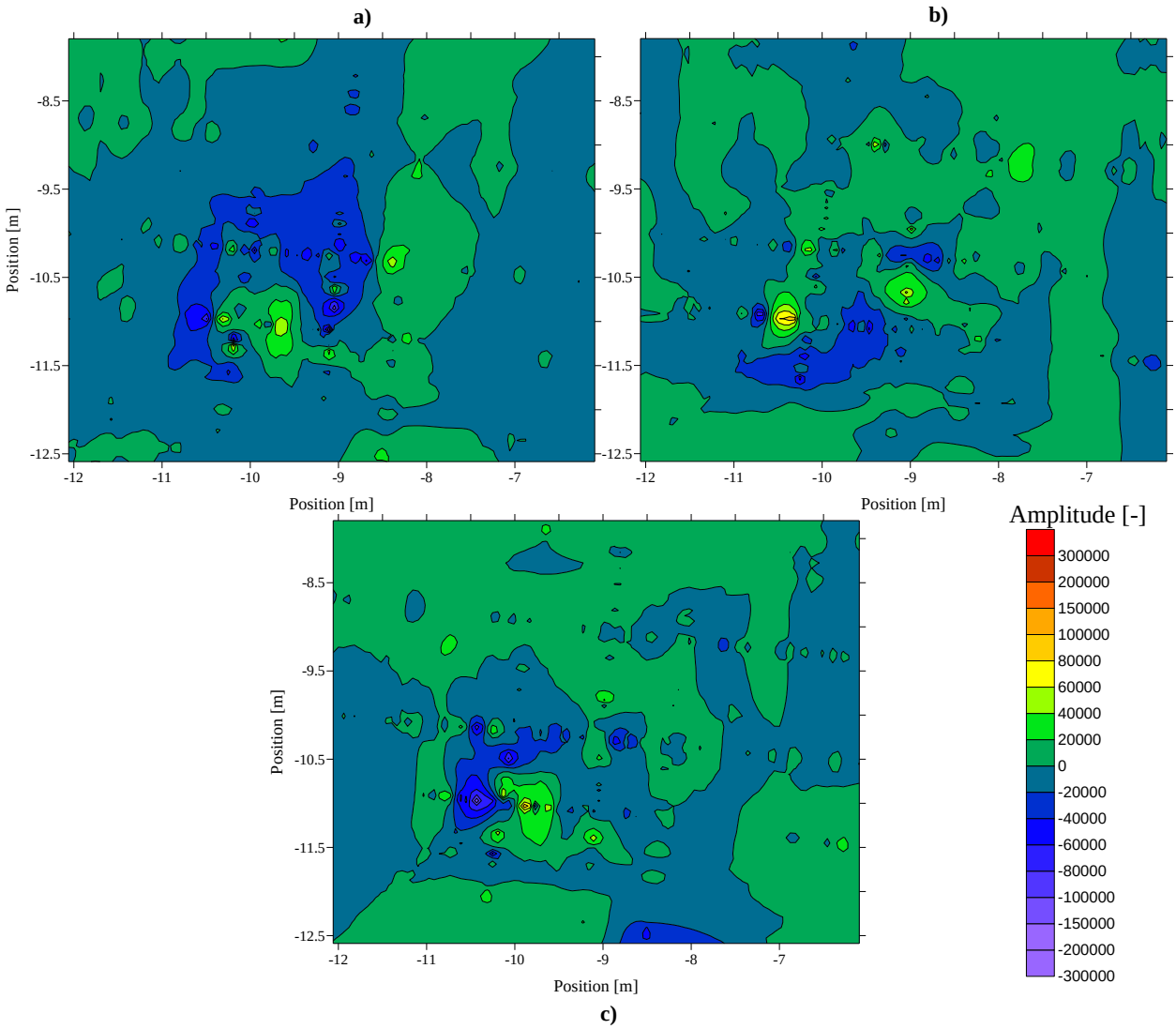

Figure 5.17 – Contoured amplitude from 900 MHz reflection profile data for Day 26 (September 17 2008). Amplitude is dimensionless. a) 8 ns time slice, b) 10 ns time slice and c) 12 ns time slice.

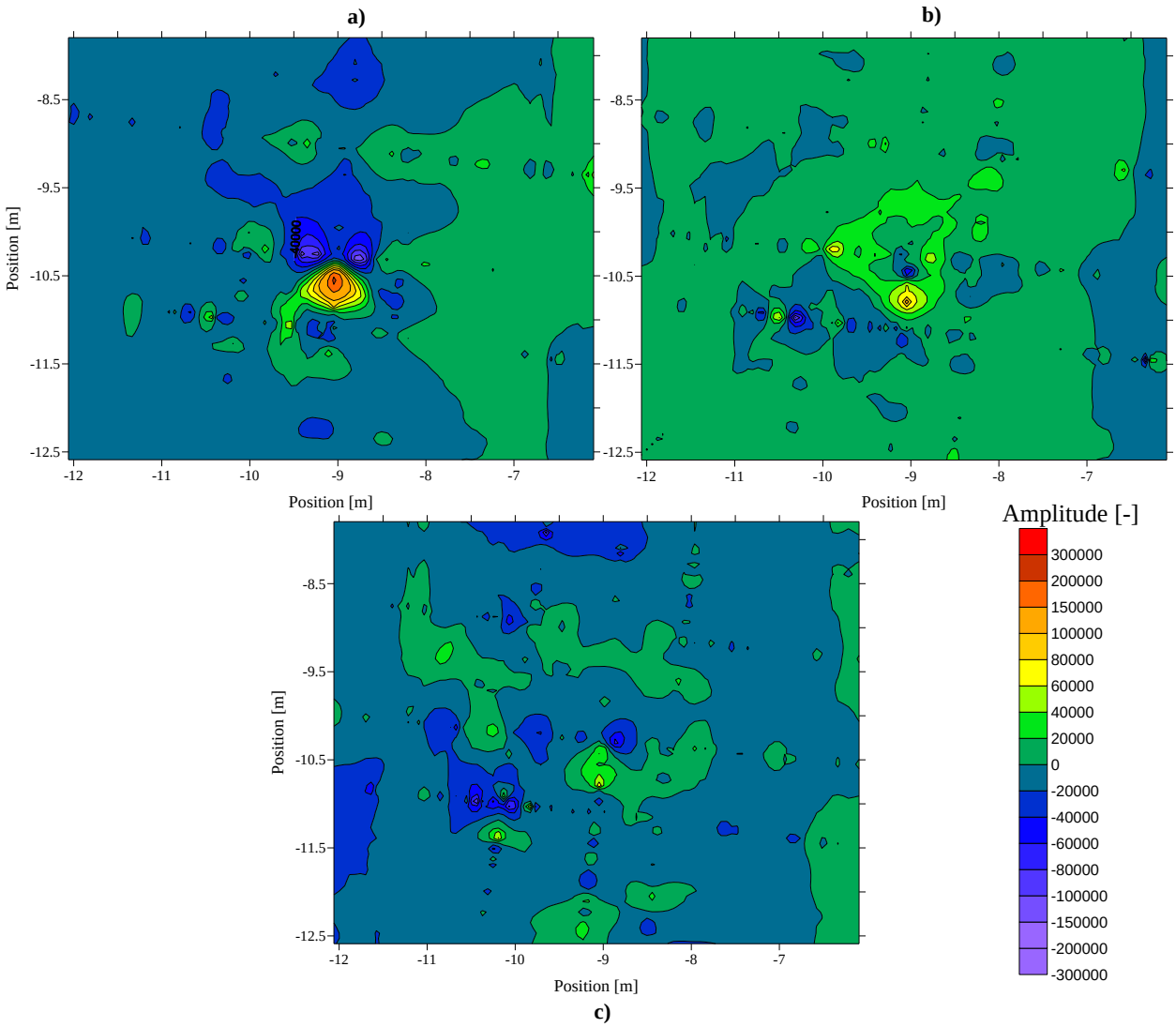

Figure 5.18 – Contoured amplitude from 900 MHz reflection profile data Day 116 (December 161 2008). Amplitude is dimensionless. a) 8 ns time slice, b) 10 ns time slice and c) 12 ns time slice.

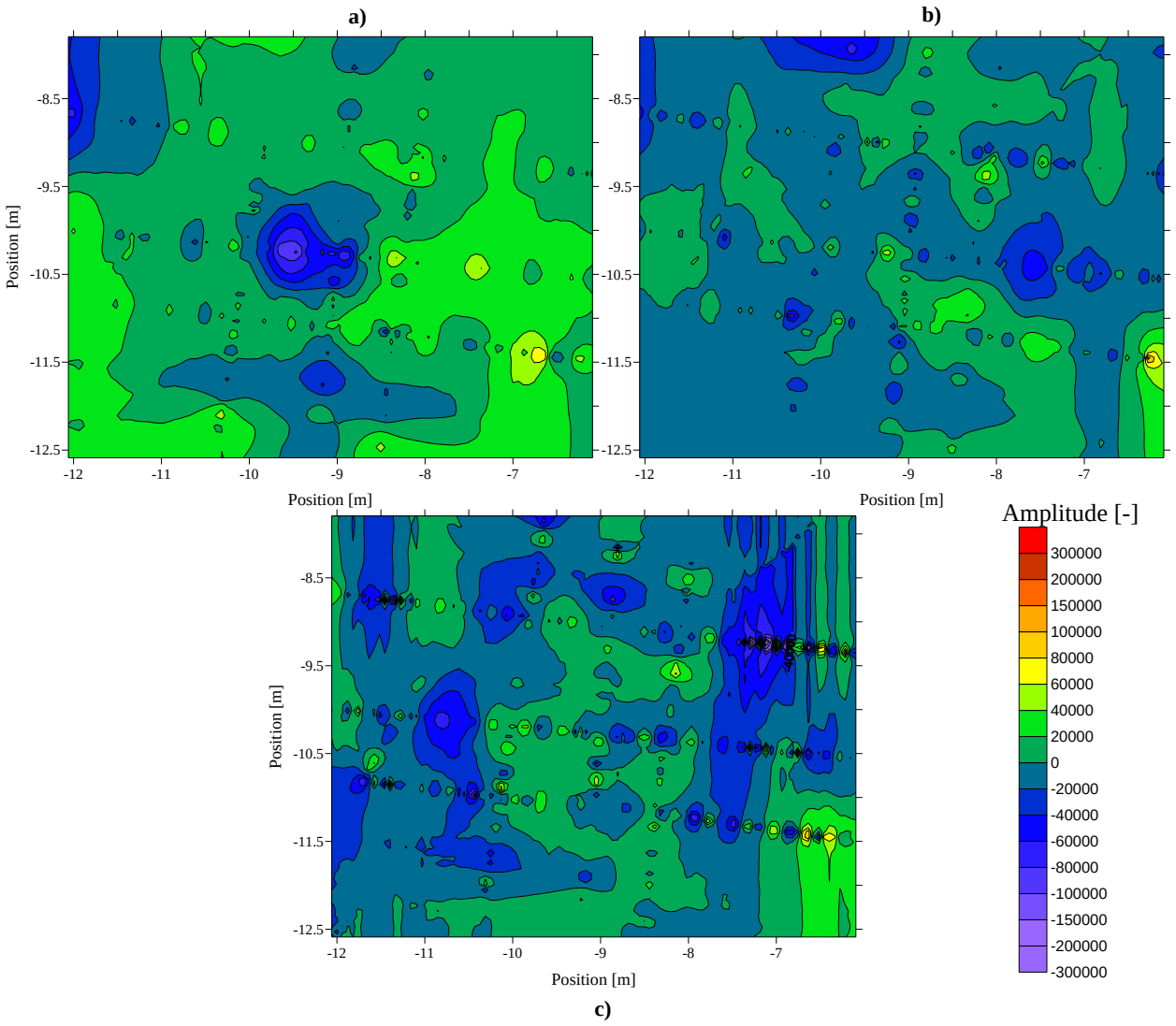

Figure 5.19 – Contoured amplitude from 900 MHz reflection profile data for Day 153 (January 22 2009). Amplitude is dimensionless. a) 8 ns time slice, b) 10 ns time slice and c) 12 ns time slice.

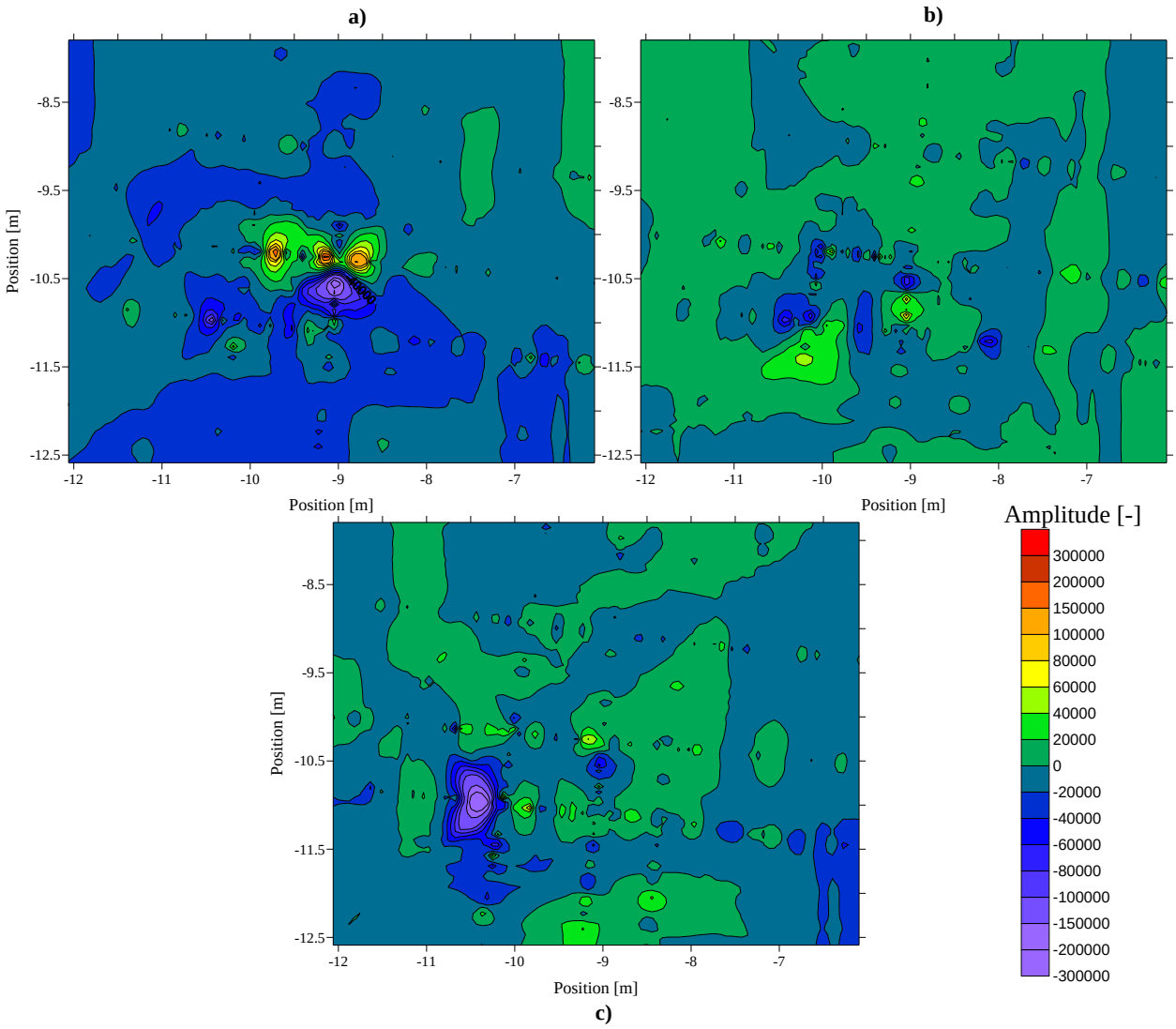

Figure 5.20 – Contoured amplitude from 900 MHz reflection profile data for Day 308 (June 26 2009). Amplitude is dimensionless. a) 8 ns time slice, b) 10 ns time slice and c) 12 ns time slice.

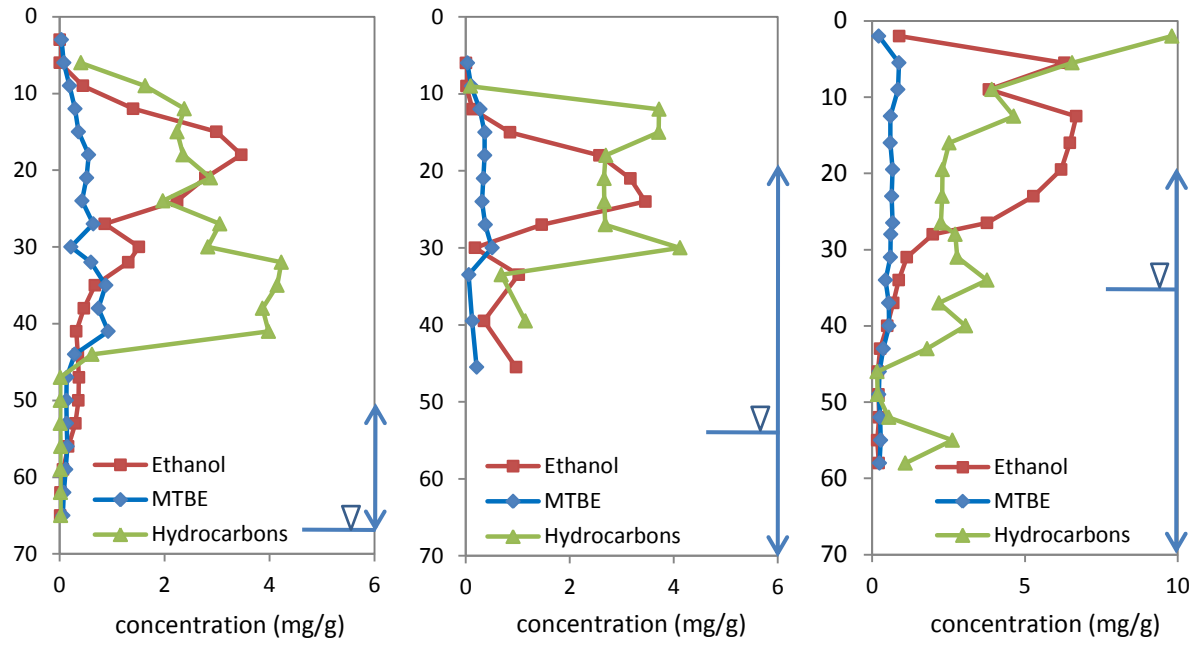

Core 1 – day 14 (04-Sep-08) Core 2 - day 47 (07-Oct-08) Core 3 - day 117 (16-Dec-08)

Figure 5.21 – Main LNAPL components concentration as mg/g of wet soil from Freitas (2009). Y-axis is depth below ground surface in cm. Blue vertical arrows are fluctuations in water table up to coring date. Location of cores is indicated in Figure 4.1.

6.0 Conclusions

This experiment has assessed the capacity of high frequency ground penetrating to detect and monitor very shallow (i.e., less than 0.5 meter depth) LNAPL impacted zones. This work is unique in that the controlled release was done in a natural aquifer. Previous studies have examined the ability of GPR to characterize controlled releases in repacked test cells, only accidental releases have been investigated in natural aquifers. In addition, the experiment was contained within a cell that was hydraulically connected to the surrounding aquifer; this design permitted naturally occurring horizontal flow through the cell. Hence, we were able to observe the potential effects of ground water flow and water table fluctuations on the GPR response of the LNAPL pool. These conditions are difficult, if not impossible, to accurately simulate in the test cell used by other researchers.

Because of the very shallow depth of the LNAPL impacted zone and the presence of the direct air and ground wave arrivals, the high resolution capacity of the 900 MHz antennas was better for directly image the impacted zone. The high amplitude reflection events developed immediately after the release in the vicinity of the trench. The scattering and reverberations that appear in the profiling are probably due to initial heterogeneity within the release zone and their dissipation likely indicate the re-distribution of the LNAPL. These high reflectivity events expanded lateral during the initial water table lowering until the seasonal low stand occurred. Afterwards, no additional lateral extension of these reflections was observed through the remainder of the monitoring; minor reflectivity variations observed during this period are thought to be connected with the effects of water table fluctuation.

While the 450 MHz antennas produced less well-defined direct imaging of the impacted zone due to its lower resolution, its better depth of penetration allowed us to evaluate the effects of gasoline induced velocity changes on the imaging of an underlying stratigraphic reflecting boundary (i.e., a velocity pull-up feature). The velocity pull-up is due to the displacement of low velocity water by high velocity gasoline in the LNAPL impacted zone. The resulting change in velocity within this shallow zone affects the traveltime of deeper events whose raypaths traverse the LNAPL impacted zone. Comparison of the reflection profiles shows that the locations of the shallow high amplitude reflection events on the 900 MHz data and the

velocity pull-up of the deeper stratigraphic on the 450 MHz data coincide, supporting the our interpretation that they are both the result of the LNAPL release.

The magnitude of the velocity pull-up was quantified by determine the two-way traveltime change of the stratigraphic reflection relative to its pre-release/background values at each position along the reflection profiles. The magnitude of the pull-up increased until the occurrence of the seasonal water table low in mid-September and generally decreased throughout the remainder of the monitoring during unfrozen conditions. While these changes likely reflect changes in the distribution and/or mass of immiscible gasoline phase, the interpretation of these results are complicated by to the impact of fluctuating water table and its effects on soil moisture. The plan-views of the velocity pull-up measurements indicate that the gasoline pool initially formed in the vicinity of the release trench and did not significantly spread during the experiment.

GPR profiling during the winter period of frozen soil conditions clear show that presence of the gasoline impacted zone affects the freezing process. Further, changes in the direct air-ground wave amplitude suggest that the contaminant phase brought to the surface has affected the near-surface freezing process. These are the first documented geophysical observations of these effects.

In conclusion, the results presented in this thesis clearly demonstrate the capacity of high frequency ground penetrating to detect and monitor very shallow (i.e., less than 0.5 meter depth) LNAPL impacted zones. However, it also apparent that further work is required to improve the extraction of quantitative information concerning LNAPL distribution and saturation in this natural system. It is hoped that this experiment provides the data and impetus for this work.

References

Abdel Aal, G.Z., L.D. Slater and E.A. Atkewana, 2006. Induced-Polarization Measurements on Unconsolidated Sediments from a site of Active Hydrocarbon Bioremediation. *Geophysics*. **71**(2): H13 – H24.

Akindunni, F.F. and R.W. Gillham, 1992. Unsaturated and Saturated Flow in Response to Pumping of an Unconfined Aquifer: Numerical Investigation of Delayed Drainage. *Groundwater*. **30**(6): 873 – 884.

Annan, A.P., 2005a. Chapter 11: Ground Penetrating Radar, *in* Butler D.K. (editor), Near-Surface Geophysics. Society of Exploration Geophysicists, Tulsa, OK. pp: 357 – 438.

Annan, A.P., 2005b. Chapter 7: Ground Penetrating Radar Methods in Hydrogeological Studies, *in* Rubin Y. and Hubbard S.S. (editors), Hydrogeophysics. Springer, Dordrecht, NL. pp 185 – 213.

Annan, A.P., 2009. Chapter 1: Electromagnetic Principles of Ground Penetrating Radar, *in* Jol H.M. (editor), Ground Penetrating Radar: Theory and Applications. Elsevier, Amsterdam, NL. pp 3 – 40.

Atekwana, E.A and E.A Atekwana, 2009. Geophysical Signatures of Microbial Activity at Hydrocarbon Contaminated Sites: A Review. *Surveys in Geophysics*. doi: 10.1007/s10712-009-9089-8

Atekwana, E.S., W.A. Sauck and D.D. Werkema, 2000. Investigations of Geoelectrical Signatures at a Hydrocarbon Contaminated Site. *Journal of Applied Geophysics*. **44**(2-3): 167 – 180.

Atekwana, E. A. and L. D. Slater, 2009. Biogeophysics: A new frontier in Earth science research. *Reviews in Geophysics*. **47** (RG4004). doi: 10.1029/2009RG000285

Baker, G.S., 1998. Applying AVO analysis to GPR data. *Geophysical Research Letters*. **25**: 397– 400.

Baker G.S., T.E. Jordan and J. Pardy, 2007. An Introduction to Ground Penetrating Radar, in Baker G.S. and Jol H.M. (editors), Stratigraphic Analyses using Ground Penetrating Radar: Geological Society of America Special Paper 432, pp 1 – 18. doi: 10.1130/2007.2432(01)

Bano, M., O. Loeffler and J. F. Girard, 2009. Ground penetrating radar imaging and time-domain modelling of the infiltration of diesel fuel in a sandbox experiment. *Comptes Rendus Geoscience*. **341**: 846-858.

Barnes, A.E., 2007. A Tutorial on Complex Seismic Trace Analysis. *Geophysics*. 72(6): PW33 – PW43.

Bauman P. 1989. A Detailed Geophysical Investigation of a Shallow Sandy Aquifer. M.Sc. thesis, Department of Earth and Environmental Science, University of Waterloo, Waterloo, ON.

Bermejo, J.L., W.A. Sauck and E.A. Atekwana, 1997. Geophysical discovery of a new LNAPL plume at the former Wurtsmith AFB, Oscoda, Michigan. *Ground Water Monitoring and Remediation*. **17**(4): 131 – 137.

Bevan, M.J., A.L. Endres, D.L. Rudolph and G. Parkin, 2003. The non-Invasive Characterization of Pumping-induced Dewatering using Ground Penetrating Radar. *Journal of Hydrology*. **281**: 55 – 69.

Bevan, M.J., A.L. Endres, D.L. Rudolph and G. Parkin, 2005. A Field Scale Study of Pumping-induced Drainage and Recovery in an Unconfined Aquifer. *Journal of Hydrology*. **315**: 52 – 70.

Bolha, J. Jr., 1986. A Sedimentological Investigation of a Progradational Foreshore Sequence: C.F.B. Borden. M.Sc. thesis, Department of Earth and Environmental Science, University of Waterloo, Waterloo, ON.

Brewster M.A., Annan A.P., Greenhouse J.P., Kueper B.H., Olhoeft G.R., Redman J.D. and Sander K.A. 1995. Observed Migration of a Controlled DNAPL Release by Geophysical Methods. *Groundwater*. **33**(6): 977 – 987.

Brewster, M.A. and A.P. Annan, 1994. Ground-penetrating Radar Monitoring of a Controlled DNAPL Release: 200 MHz radar. *Geophysics*. **59**(8): 1211 – 1221.

Brovelli, A. and G. Cassiani, 2008. Effective Permittivity of Porous Media: A Critical Analysis of the Complex Refractive Index Model. *Geophysical Prospecting*. **56**: 715 – 727.

Cassidy, N.J., 2007. Evaluating LNAPL Contamination using GPR Signal Attenuation Analysis and Dielectric Property Measurements: Practical Implications for Hydrological Studies. *Journal of Contaminant Hydrology*. **94**(1-2): 49 – 75.

Cassidy, N.J., 2009. Chapter 5: Ground Penetrating Radar Data Processing, Modelling and Analysis, *in* Jol H.M. (editor), Ground Penetrating Radar: Theory and Applications. Elsevier, Amsterdam, NL. pp 141 – 176.

Che-Alota, V., E.A. Atekwana, E.A. Atekwana, W.A. Sauck and D.D. Werkema, 2009. Temporal Geophysical Signatures from Contaminant-mass Remediation. *Geophysics*. **74**(4): B113 – B123.

Daniels, D.J. (editor), 2004. Ground Penetrating Radar – 2nd Edition. The Institution of Electrical Engineers, London, UK.

Daniels, J.J., R. Roberts and M. Vendl, 1995. Ground Penetrating Radar for the Detection of Liquid Contaminants. *Journal of Applied Geophysics*. **33**(1-3): 195 – 207.

Davis, J.L. and A.P. Annan, 1989. Ground Penetrating Radar for High Resolution Mapping of Soil and Rock Stratigraphy. *Geophysical Prospecting*. **37**: 531 – 551.

DeRyck, S.M., 1994. Monitoring a Controlled LNAPL Spill. M.Sc. thesis, Department of Earth and Environmental Science, University of Waterloo, Waterloo, ON.

Endres, A.L., W.P. Clement and D.L. Rudolph, 2000. Ground Penetrating Radar Imaging of an Aquifer During a Pumping Test. *Groundwater*. **38**(4): 566 – 576.

Endres, A.L. and J.P. Greenhouse, 1996. Detection and Monitoring of Chlorinated Solvent Contamination by Thermal Neutron Logging. *Groundwater*. **34**(2): 283 – 292.

Fetter, C.W., 1993. Contaminant Hydrogeology. MacMillan, NewYork.

Freitas, J. de Gardenalli, 2009. Impacts of Ethanol in Gasoline on Subsurface Contamination. PhD dissertation, Department of Earth and Environmental Science, University of Waterloo, Waterloo, ON.

Freitas, J.G. and J.F. Barker, 2008. Sampling VOC's with Porous Suction Samplers in the Presence of Ethanol: How Much are we Losing? *Ground Water Monitoring & Remdiation*. **28**(3): 83 – 92.

Freitas, J.G. and S.D. Piggott, 2006. GPR tracking disturbed sand at CFB Borden using 450 MHz, 225 MHz and 200 MHz antennas. Unpublished data and internal report for environmental geophysics group at University of Waterloo. Department of Earth and Environmental Science, University of Waterloo, Waterloo, ON.

Greenhouse, J.P., M.A. Brewster, G.W. Schneider, J.D. Redman, A.P. Annan, G.R. Olhoeft, J. Lucious, K.A. Sander and A. Mazzella, 1993. Geophysics and Solvents: The Borden experiment. *The Leading Edge*. **12**: 261-267.

Hwang, Y.K., A.L. Endres, S.D. Piggott and B.L. Parker, 2008. Long-term ground penetrating radar monitoring of a small volume DNAPL release in a natural groundwater flow field. *Journal of Contaminant Hydrology*. **97**(1-2): 1 – 12.

Hwang, Y.K., 2006. Long Term Monitoring of a Small Volume Chlorinated Solvent Release. M.Sc. thesis, Department of Earth and Environmental Science, University of Waterloo, Waterloo, ON.

Jordan, T. E. and G. S. Baker, 2003. Recommendation for New Terminology for Linearly Polarized Components of Ground Penetrating Radar Waves. *Journal of Environmental and Engineering Geophysics*. **8**(1): 39 – 42.

Jordan, T. E., G. S. Baker, K. Henn and J. P. Messier, 2004. Using amplitude variation with offset and normalized residual polarization analysis of ground penetrating radar data to differentiate an NAPL release from stratigraphic changes. *Journal of Applied Geophysics*. **56**: 41-58.

Jordan, T.E. and G.S. Baker, 2004. Reprocessing Ground Penetrating Radar data from the CFB Borden experiment using AVO/GPR Techniques. Proceedings from the Symposium on the Application of Geophysics to Engineering and Environmental Problems (SAGEEP). Colorado Springs, CO. February, 2004. pp: 506 – 513.

Kim, C., J.J. Daniels, E.D. Guy, S.J. Radzevicius and J. Holt, 2000. Residual hydrocarbons in a water saturated medium: a detection strategy using ground penetrating radar. *Environmental Geosciences*. **7**: 169-176.

Knight, R., 2001. Ground Penetrating Radar for Environmental Applications. *Annual Review of Earth and Planetary Sciences*. **29**: 229 – 255.

Lambert, J.M., 2008. Pulsed Biosparging of the E10 gasoline Source in the Borden Aquifer. M.Sc. thesis, Department of Earth and Environmental Science, University of Waterloo, Waterloo, ON.

Laukonen, K.A., 2001. Long-Term Natural Gradient Experiments in the Borden Sand Aquifer: A Bromide Slug and a Chloroform Plume from a Three-Component DNAPL Source. M.Sc. thesis, Department of Earth and Environmental Science, University of Waterloo, Waterloo, ON.

Lopes de Castro, D. and R.M.G. Castelo Branco, 2003. 4-D ground penetrating radar monitoring of a hydrocarbon leakage site in Fortaleza (Brazil) during its remediation process: a case history. *Journal of Applied Geophysics*. **54**: 127-144.

MacFarlane, D.S., J.A. Cherry, R.W. Gillham and E.A. Sudicky, 1983. Migration of Contaminants in Groundwater at al Landfill: A Case Study 1. Groundwater Flow and Plume Delineation. *Journal of Hydrology*. **63**: 1 – 29.

MacKay, D.M., D.L. Freyberg, P.V. Roberts and J.A. Cherry, 1986. A Natural Gradient Experiment on Solute Transport in a Sand Aquifer: 1. Approach and Overview of Plume Movement. *Water Resources Research*. **22**(13): 2017 – 2029.

Mocanu, M.T., 2007. Behaviour or Oxygenates and Aromatic Hydrocarbons in Groundwater from Gasoline Residuals. M.Sc. thesis, Department of Earth and Environmental Science, University of Waterloo, Waterloo, ON.

Molson, J., M.T. Mocanu and J.F. Barker, 2008. Numerical Analysis of Buoyancy Effects During the Dissolution and Transport of Oxygenated Gasoline in Groundwater. *Water Resources Research*. **44**: W07418, doi:10.1029/2007WR006337.

Naudet, V., A. Revil, E. Rizzo, J.-Y. Bottero and P. Begassat, 2004. Groundwater Redox Conditions and Conductivity in a Contaminant Plume from Geoelectrical Investigations. *Hydrology and Earth Science Systems*. **8**(1): 8 – 22.

Nwankwor, G.I., 1985. Delayed Yield Processes and Specific Yield in a Shallow Sand Aquifer. PhD dissertation, Department of Earth and Environmental Science, University of Waterloo, Waterloo, ON.

Nwankwor, G.I., J.A. Cherry and R.W. Gillham, 1984. A Comparative-study of Specific Yield Determinations for a Shallow Sand Aquifer. *Groundwater*. **22**(6): 764 – 772.

Nwankwor, G.I., R.W. Gillham, G. van der Kamp and F.F. Akindunni, 1992. Unsaturated and Saturated Flow in Response to Pumping of an Unconfined Aquifer: Field Evidence of Delayed Drainage. *Groundwater*. **30**(5): 690 – 700.

Orlando, L., 2002. Detection and Analysis of LNAPL using the Instantaneous Amplitude and Frequency of Ground-Penetrating Radar data. *Geophysical Prospecting*. **50**: 27 – 41.

Roth, K., R. Schulin, H. Flühler and W. Attinger, 1990. Calibration of Time Domain Reflectometry for Water Content Measurement using a Composite Dielectric Approach. *Water Resources Research*. **26**(10): 2267 – 2273.

Redman, J. D., S.M. DeRyck and A. P. Annan, 1994. Detection of LNAPL pools with GPR: theoretical modeling and surveys of a controlled spill. Proceedings of the International Conference on Ground Penetrating Radar. pp: 1283-1294.

Redman, J. D., 2009. Chapter 8: Contaminant Mapping, *in* Jol H.M (editor), Ground Penetrating Radar: Theory and Applications. Elsevier, Amsterdam, NL. pp 3 – 40.

Sauck, W.A., E.A. Atekwana and M.S. Nash, 1998. High conductivities associated with an LNAPL plume imaged by integrated geophysical techniques. *Journal of Environmental and Engineering Geophysics*. **2**(3): 203–212.

Schneider, G.W. and J.P. Greenhouse, 1992. Geophysical detective of perchloroethylene in a sandy aquifer using resistivity and nuclear logging techniques. Proceedings of the Symposium on the Application of Geophysics to Engineering and Environmental Problems. pp: 619 – 628.

Schwartz, F.W. and H. Zhang, 2003. Fundamentals of Ground Water. John Wiley & Sons Inc., New York.

Sudicky, E.A., 1986. A Natural Gradient Experiment on Solute Transport in a Sand Aquifer: Spatial Variabilty of Hydraulic Conductivity and its Role in the Dispersion Process. *Water Resources Research*. **22**(13): 2069 – 2082.

Telford, W.M., L.P. Geldart, R.E. Sheriff and D.A. Keys, 1976. Applied Geophysics. Cambridge University Press, N.Y.

Tomlinson D.W., N.R. Thomson, R.L. Johnson and J.D. Redman, 2003. Air Distribution in the Borden Aquifer during In-situ Air Sparging. *Journal of Contaminant Hydrology*. **67**: 113 – 132.

Vakili, F., 2008. High Resolution Geophysical Characterization of a Gasoline Release into a Sand Column. M.Sc. thesis, Department of Earth and Environmental Science, University of Waterloo, Waterloo, ON.

van Loon, W.K.P., E. Perfect, P.H. Groenevelt and B.D. Kay, 1991. Application of Dispersion Theory to Time Domain Reflectometry in Soils. *Transport in Porous Media*. **6**: 391 – 406.

Weast, R.C., M.J. Astle and W.H. Beyer (Editors), 1985. CRC Handbook of Chemistry and Physics, 66th edn, CRC Press, Boca Raton, FL. pp: E53 – E56.

Werkema, D.D., E.S. Atekwana, A.L. Endres, W.A. Sauck and D.P. Cassidy, 2003. Investigating the Geophysical Response of Hydrocarbon Contamination undergoing Biodegradation. *Geophysical Research Letters*. **30**(12): 49-1 – 49-4.

Yang, T., 2008. Investigation of Residual Gasoline in the GMT and E10 Sources in Borden Aquifer. M.Sc. thesis, Department of Earth and Environmental Science, University of Waterloo, Waterloo, ON.

Yilmaz, O., 2001. Seismic Data Analysis: Processing, Inversion and Interpretation of Seismic Data. Society of Exploration Geophysicists, Tulsa, OK.

Yu, S., J.G. Freitas, A.J.A. Unger, J.F. Barker and J. Chatzis, 2009. Simulating the Evolution of an Ethanol and Gasoline Source Zone within the Capillary Fringe. *Journal of Contaminant Hydrology*. **105**: 1 – 17, doi:10.1016/j.jconhyd.2008.11.006.

Appendices

Appendix A: Line A 900 MHz Profile Sequence

Appendix B: Line B 900 MHz Profile Sequence

Appendix C: Line C 900 MHz Profile Sequence

Appendix D: Line 2 900 MHz Profile Sequence

Appendix E: Line 3 900 MHz Profile Sequence

Appendix F: Line 4 900 MHz Profile Sequence

Appendix G: Line A 450 MHz Profile Sequence

Appendix H: Line B 450 MHz Profile Sequence

Appendix I: Line C 450 MHz Profile Sequence

Appendix J: Line 2 450 MHz Profile Sequence

Appendix K: Line 3 450 MHz Profile Sequence

Appendix L: Line 4 450 MHz Profile Sequence

Appendix M: Line C 900 MHz CMP Centred at 1.0 m Sequence

Appendix N: Line C 900 MHz CMP Centred at 3.2 m Sequence

Appendix O: Line A 900 MHz CMP Centred at 3.2 m Sequence

Appendix P: Line 4 900 MHz CMP Centred at 3.6 m Sequence

Appendix Q: Line C 450 MHz CMP Centred at 1.0 m Sequence

Appendix R: Line C 450 MHz CMP Centred at 3.2 m Sequence

Appendix S: Line A 450 MHz CMP Centred at 3.2 m Sequence

Appendix T: Line 4 450 MHz CMP Centred at 3.6 m Sequence

Appendix U: 450 MHz Profile Traveltime contours

Appendix V: 900 MHz Profile Amplitude time slices

Appendix W: Pictures From Field Activities

Appendix X: Scanned Field Notes

Appendix Y: Unprocessed Ground Penetrating Radar Data

Appendices Addendum

Appendices included in attached data disk with hard copies of this work.

For electronic versions of this thesis, unprocessed ground penetrating radar data and other raw data collected in the field from this work are available in electronic format upon request from Professor A.L. Endres (alendres@uwaterloo.ca) or the author (chmcnaug@uwaterloo.ca or alternatively Cameron.McNaughton@gmail.com). Please refer to list of appendices on previous page for information available.